January 2013

Towards Interference-Immune and Channel-Aware Multicarrier Schemes: Filters, Lattices, and Interference Issues

Alphan Sahin
University of South Florida, alphan@mail.usf.edu

Towards Interference-Immune and Channel-Aware Multicarrier Schemes:

Filters, Lattices, and Interference Issues

by

Alphan Şahin

A dissertation submitted in partial fulfillment
of the requirements for the degree of
Doctor of Philosophy
Department of Electrical Engineering
College of Engineering
University of South Florida

Major Professor: Hüseyin Arslan, Ph.D.
Richard D. Gitlin, Sc.D.
Thomas Weller, Ph.D.
Ken Christensen, Ph.D.
Zafer Şahinoğlu, Ph.D.

Date of Approval:
November 3, 2013

Keywords: Edge windowing, partially overlapping tones, sidelobe suppression,
time-frequency analysis, uncoordinated networks

DEDICATION

To my family

ACKNOWLEDGMENTS

First and foremost, I would like to thank my advisor Dr. Hüseyin Arslan for his guidance, encouragement, trust, and support throughout my studies. I have learnt a lot from him; how to approach the challenges in research, how to write technical papers in good flow, how to present an idea, and most important of all; how to study hard. His continuous pushing, high expectations, his patience on immediate discussions made this dissertation possible. For me, it has been a privilege to have the opportunity to do research as a member of Wireless Communications and Signal Processing (WCSP) research group.

I would also like to thank Dr. Richard D. Gitlin, Dr. Thomas Weller, Dr. Kenneth Christensen, and Dr. Zafer Şahinoğlu for serving in my committee, for reviewing my dissertation, and their valuable time and suggestions; and to Dr. Yu Sun for chairing my defense. Definitely, Irene Wiley, Cherie Dilley, Jessica Procko, Becky Brenner, Gayla Montgomery and Sheila Kay Jackson deserve many thanks for helping out in numerous issues over past years.

I would especially like to thank Dr. İsmail Güvenç. I am grateful to him for his valuable collaboration and persistent encouragement. I have enjoyed the discussions with him. I have tried to benefit from his invaluable knowledge and experience as much as I can. It is an honor for me to work with such an outstanding researcher.

I owe a lot to my colleagues at USF. First of all, I am grateful to my friend Mehmet Bahadır Çelebi with whom I have begun this journey together. Many thanks go to Anas Tom (thank you for many enjoyable and fruitful discussions during the lunches!), Murat Karabacak, Emre Seyyal, Sabih Güzelgöz, Ertugrul Güvenkaya, Zekeriyya Esad Ankaralı, Ali Görçin, Mustafa Cenk Ertürk, Ahmad Gheethan, Amar Amouri, Mustafa Harun Yılmaz, Jamal Haque, Sadia Ahmed, Ali Fatih Demir, Osman Şaylı, Salih Erdem, Gabriel Arrobo, Thomas P. Ketterl, and Dr. Gökhan Mumcu. We shared many things together. I have learned the importance of diversity with you. I wish all of you the best in your future lives.

I would also like to thank my friends who experience the Ph.D. years at different parts of the world: Çağdaş Tuna with University of Illinois at Urbana-Champaign, Çağla Taşdemir with Stony Brook University, Çağıl Taşdemir with City University of New York, and Selda Yıldız with University of California, San Diego. You were the unseen part of the Ph.D. years in Tampa.

My deepest gratitude go to Laura Maria Warriner and Lizzie DeJesus whom I have shared beautiful things during the years in Tampa. You were the moments from different worlds and different words. You were there to share joy and disappointments, and to provide hope and motivations at times I started losing them.

Last, but by no means least, I would like to express my utmost appreciation to my parents Meliha Şahin and Ali Şahin, my dear sister Pinar Şahin, her husband Ediz Gizlier, and my nephew Can Batu Gizlier for their immense sacrifice and their unconditional support throughout the years. It is not possible to thank them enough. I will be forever indebted to them for all they have done.

TABLE OF CONTENTS

LIST OF TABLES

LIST OF FIGURES

ABSTRACT

In this dissertation, multicarrier schemes are reviewed within the framework of Gabor Systems. Their fundamental elements; what to transmit, i.e., *symbols*, how to transmit, i.e., *filters* or *pulse shape*, and where/when to transmit, i.e., *lattices* are investigated extensively. The relations between different types of multicarrier schemes are discussed.

Within the framework of Gabor systems, a new windowing approach, *edge windowing*, is developed to address the out-of-band (OOB) radiation problem of orthogonal frequency division multiplexing (OFDM) based multicarrier schemes. To the best of our knowledge, for the first time, the diversity on the range of the users is exploited to suppress the sidelobes of OFDM. In addition to that, the concept of using different filters in OFDM structure is proposed. Besides the improvement on the OOB radiation performance of OFDM via edge windowing, conventional lattice structure of OFDM frame is enhanced considering the diversity in the network. The lattice structure of an OFDM frame is designed based on the statistical characteristics of the range of the users and the mobility. The concept of *channel-aware frame structure* is developed, which allows more efficient and reliable transmission.

In addition to the aforementioned improvements on OFDM, interference issues in uncoordinated networks are addressed in this dissertation considering different multicarrier schemes. It is stressed that the interference from other links in the network sharing the same spectrum might degrade the link performance between the devices in an uncoordinated network, significantly. Considering the degradation due to other-user interference, the concept of *partially overlapping tones (POT)* is proposed. With the concept of partially overlapping tones, the interference energy observed at the victim receiver is mitigated via an intentional frequency offset between the links. The usefulness of intentional frequency offset to combat with the asynchronous nature of other-user interference without any timing constraint between interfering signals is emphasized. To the best of our knowledge, for the first time, the efficacy of non-orthogonal schemes are shown along with POT to address the other-user interference, which relies on the fact that self-interference problem is easier than other-user interference problem in an uncoordinated network.

In the last part of this dissertation, *required number of equalizer taps for multicarrier schemes* is investigated to address the potential self-interference problems (e.g. due to the non-orthogonal multicarrier schemes with the concept of POT). Composite impact of transmit pulse shape, communication medium, and receive filter on the charac-

teristics of the interference among the symbols in time and frequency is analyzed. It is emphasized that while taking less number of taps into account for the channel estimation causes lack of description of the composite effect, using more number of taps folds the noise into the estimated channel. The number of interfering symbols and their locations are obtained in both time and frequency for a given multicarrier scheme and signal-to-noise ratio. It is shown that correct number of taps yields not only improvement on BER performance but also less complex equalizer structures in practice.

CHAPTER 1

INTRODUCTION

1.1 Introduction

There are two fundamental issues that come into the prominence along with the communication over wireless channels: *dispersion* and *interference*. A transmitted signal is dispersed in time and frequency due to the existence of the multiple paths and the mobility in wireless communication channels. The amount of the dispersion depends on the properties of the communication systems, e.g., communication range, operating frequency, and physical characteristics of operation environment. Besides the dispersion, the signals might be interfered by the signals of other users or other networks that access the same spectrum. The amount of interference and the type of the interference are related to many factors, e.g., density of the network, path loss, and availability of the coordination mechanisms. Dealing with the dispersion and the interference constitutes the main subject for the design of wireless communications systems [1].

In communications, waveform corresponds to the formations of the resources in time and frequency, based on a specific structure. Conventionally, basic parameters related to the waveform structure, e.g., symbol rate, modulation order, and modulation type, are optimized to increase the effective utilization of the resources in dispersive channels. From the view point of waveform design, this approach has its own merits since the impact of dispersion is inherently related to the waveform structure. Potential interference issues due to the other users or the other systems are mainly managed via proper interference management strategies such as interference coordination mechanisms, scheduling, interference cancellation/mitigation/alignment methods, and smart antennas, rather than the manipulations on waveform structure. However, waveform structure is also able to address the potential interference issues in the network, which constitutes the theme of this dissertation.

Main motivation of this dissertation is to provide solutions considering potential interference issues in next generation wireless communication systems and dispersion due the wireless communication channel by using the waveform structure. To this end, conventional waveform-based methodologies are investigated, extended, and improved by taking both dispersion and interference into account. The main difference of this investigation compared to the existing techniques along the same line is the *utilization of waveform structure* itself, rather than developing methods excluding the impact of waveform structure.

In this introductory chapter, the challenges for waveform design based on interference and channel conditions are outlined. Potential benefits of dealing with these problems are emphasized. Then, a brief outline of the dissertation is presented.

1.2 Motivations for Waveform-Based Methodologies

First motivation for considering waveform-based approaches is to exploit the potential benefits emerging from the diversity by using the waveform structure. The current transmission in point-to-multipoint links are based on a single waveform with fixed parameters. Generally, the selection of these parameters is based on the statistics that are obtained through the offline measurements. Most of the time, the worst-case statistics are used to ensure the desired performance, at the expense of reduced spectral efficiency. Wireless communication standards often employ adaptive modulation and coding, adaptive power control, adaptive resource scheduling, adaptive antenna parameters configuration. In all these techniques, the physical layer parameters are adjusted accordingly for each communicating node, based on the channel and radio parameters between the transmitter and receiver. However, waveform and its related parameters are still fixed for each node. When waveform structure is design based on the individual physical signatures of the communicating nodes, e.g. location, mobility, channel condition, signal-to-noise ratio (SNR), additional gains in the systems can be obtained.

Second motivation for taking waveform-based methodologies into account emerges from the trends toward the network sharing the same electrospace. Orthogonal frequency division multiplexing (OFDM) offers a simple receiver architecture with fast Fourier transformation (FFT) and single-tap frequency domain equalization (FDE), which is one of the reason of being a dominating multicarrier structure for many wireless standards, such as 802.11a/b/g under WiFi alliance, 802.16 (WiMax), DVB-T/DAB-T, WRAN 802.22, and Long Term Evolution (LTE) of cellular radio. However, OFDM is not designed to address the coexistence issues. Hence, it might not be the most efficient method to access the spectrum for the networks sharing the same electrospace. Unfortunately, coexistence appeared later in the game. If we know that coexistence will be there in the future, would orthogonal frequency division multiple accessing (OFDMA) be the best choice? To answer this question, the suitability of OFDM to coexisting scenarios is discussed in the dissertation. As it is investigated in Chapter 5, orthogonal waveform structures cannot address *interference mitigation* without losing their spectral efficiencies. However, non-orthogonal waveform structures are able to address the constraints of uncoordinated networks without losing their efficiencies at the expense of attainable receiver complexity.

Third motivation for waveform-based approach is to control the localizations of resources in time and frequency. A pulse shape is one of the main factor that determines the localization of waveforms. With the proper of waveform structure, it is possible to control the concentration of a pulse shape in time and frequency. This adaptation allows interference management in waveform domain. Therefore, waveform-based approaches exploits the degree-of-freedoms due to the waveform structure to deal with the interference scenarios.

Another supporting motivation for developing waveform-based methodologies is the simple implementation of different types of waveform structures by using poly phase networks (PPN). It is worth noting that discrete Fourier transformation (DFT) is the core block for OFDM. The simple implementation of DFT via FFT makes OFDM an appealing multicarrier scheme. However, it is also possible to synthesize or analyze other types of multicarrier schemes with PPN which is also rely on FFT implementation. Besides, it is always possible to generate OFDM symbols via PPN, considering the back-compatibility issues.

1.3 Potential Challenges for Waveform Design

Most of the challenging issues on waveform design arise due to the tendency of various sizes of networks to coexist over the same electrospace. This trend is mainly because of the excessive demands for the throughput over limited resources, wide variety of wireless communication applications, and increasing number of communicating devices. In order to increase efficient utilization of time-frequency resources, while one path of the researches investigates the solutions to obtain more spectral efficient structures considering self-interference issues, i.e., inter-symbol interference (ISI) and inter-carrier interference (ICI), the other path examines the cross-relation between the waveform structures in terms of adjacent-channel interference (ACI) and co-channel interference (CCI). Based on these two paths, potential challenges for waveform design are provided in the following subsections.

1.3.1 Channel-Aware Waveform Structures

Conventionally, waveform structure is designed based on the worst-case dispersion characteristics. While this approach ensures the reliability in the network, it also limits the potential benefits arising from the diversity. It is worth noting that networks get smarter day by day and they collect significant of amount information on physical signatures of the communicating nodes. It is important to relate this information to the waveform structure. This issue is addressed with the concept of *multi-user aware frame structures* in Chapter 4.

1.3.2 Adjacent Channel Interference Mitigation with Waveform Structure

ACI becomes a significant problem when two asynchronous or distinct networks access the adjacent bands. If sufficient precaution for out-of-band (OOB) radiation is not taken, the performance of the both networks might degrade significantly. While OFDM offers nice features such as simple equalization, it also introduces large sidelobes due to its pulse shape which is rectangular. Hence, OFDM without additional manipulation for sidelobe suppression might decrease the spectrum utilization. This issue is addressed with a new type of sidelobe suppression method, *edge windowing*, in Chapter 3.

1.3.3 Other-user Interference Mitigation with Waveform Structure

In next generation wireless communication systems, the network performance might be limited due to the significant amount of other-user interference. In the literature, the interference between the nodes is often elaborated with the approaches which question the amount of the interference power at the receiver location, excluding the impact of the waveform itself. This is mainly due to the fact that orthogonal structure does not provide immunity against asynchronous nature of uncoordinated networks without spectral efficiency loss, which is discussed with the concept of *partially overlapping tones (POT)* in Chapter 5.

1.3.4 Self-Interference Mitigation Based on Waveform Structure

Next generation wireless communication systems might allow distinct networks accessing the same spectrum. In such co-existing scenarios, controlling the time-frequency resources in a compact manner is critical to handle the interference issues due to the other users. However, orthogonal structures, e.g., OFDM, cannot accommodate concentrated pulse shapes in both time and frequency without losing their spectral efficiencies, based on Balian-Low theorem discussed in Chapter 2. When non-orthogonal schemes are utilized in the network instead of orthogonal schemes, it is possible to control the localization of the resources at expense of self-interference, i.e., ICI and ISI. Hence, it is important to re-consider self-interference cancellation methods, e.g., equalization and waveform structure, jointly. This issue is addressed by obtaining *required number of equalizer taps for multicarrier schemes* in Chapter 6.

1.4 Fundamental Approach for Waveform Design: Lattices and Filters

In this dissertation, waveform design issues are investigated based on a specific structure: *multicarrier schemes*. When the resources in time and frequency rely on multiple simultaneously operating subcarriers, the waveform structure corresponds to a multicarrier scheme. Without loss of generality, a multicarrier scheme consists of three basic elements: what to transmit, i.e., *symbols*, how to transmit, i.e., *filter* or *pulse shape*, and where/when to transmit,

i.e., *lattices*. For example, OFDM is a multicarrier scheme based on rectangular filter and rectangular lattice structure and symbols can be generated based quadrature amplitude modulation (QAM).

Throughout this dissertation, the time-frequency structure of a multicarrier scheme is discussed within the framework of *Gabor systems*. A Gabor system essentially generates a signal space based on a prototype filter and its translation in time and frequency, which fundamentally changes the understanding of multicarrier schemes, especially, within the two last decades. This is mainly because of the fact that the synthesis of a signal with a Gabor system also corresponds to generation of multicarrier signal. A comprehensive discussion that relates Gabor systems to multicarrier schemes are provided in Chapter 2. Relying on this framework, the approaches followed in this dissertation are based on the degree-of-freedom provided by Gabor systems, i.e., lattice and filter. In addition, multicarrier schemes are represented via time-frequency plane, e.g. Figure 3.1, Figure 2.1, Figure 4.1, Figure 5.4, and Figure 6.1, where time and frequency constitute its dimensions, which is a well-known notation for representing one dimensional signals in two dimensions [2, 3]. This notation provides intuitive explanations on multicarrier schemes.

1.5 Dissertation Outline

1.5.1 Chapter 2: A Survey on Multicarrier Schemes: Filters and Lattices

The goal of Chapter 2 is not only to provide a unified review of waveform design options for multicarrier schemes, but also to pave the way for the evolution of the multicarrier schemes from the current state of the art to future technologies. In particular, a generalized framework on multicarrier schemes is presented, based on symbols, filters, and lattices. Capitalizing on this framework, different variations of orthogonal, bi-orthogonal, and non-orthogonal multicarrier schemes are discussed. In addition, filter design for various multicarrier systems is reviewed considering four different design perspectives: energy concentration, rapid decay, spectrum nulling, and channel/hardware characteristics. Finally, evaluation tools which may be used to compare different filters in multicarrier schemes are studied.

1.5.2 Chapter 3: A Filter Adaptation: Edge Windowing

In Chapter 3, we propose a new sidelobe suppression method for OFDM-based schemes. Unlike the conventional windowing techniques where the same windowing is used for all the subcarriers within an OFDM symbol, in the proposed approach, windowing is heavily applied to the subcarriers located at the edges of the band; shorter windowing sizes are used for the inner subcarriers compared to edge subcarriers. This approach essentially correspond to use different types of pulse shapes for each subcarriers. Instead of introducing additional windowing interval, in the proposed approach, the windowing time is stolen from cyclic prefix (CP) duration. Therefore, with the proposed

approach, sidelobe suppression is achieved while maintaining the spectral efficiency. The proposed technique brings about a trade-off between achieving spectrally efficient multicarrier scheme and introducing controllable ISI and ICI. Then, this trade-off is exploited along with multi-user environment to overcome ISI and ICI without introducing complexity at the physical layer, which is a unique approach for sidelobe suppression methods known in the literature.

1.5.3 Chapter 4: A Lattice Adaptation: Channel-Aware Frame Structures

In Chapter 4, we propose a channel-aware frame structure for doubly dispersive channels in order to increase both spectral efficiency and frequency spread immunity of OFDMA based accessing schemes. Unlike the conventional OFDMA based system where the fixed CP duration and subcarrier spacing are utilized within the frame structure considering the worst case communication channel, in the proposed approach, multiple CP durations and subcarrier spacings are employed. In order to build the proposed frame structure, the statistics of the mobility and the range of the users are mapped to inter-carrier-interference and maximum excess delay to obtain multiple subcarrier spacings and CP durations. Therefore, the lattice structure of OFDMA frame is modified based on the channel characteristics in the network. Better immunity against frequency dispersion is achieved while increasing the spectral efficiency by exploiting the doubly dispersive channel characteristics of the communicating nodes.

1.5.4 Chapter 5: Partial Overlapping Tones for Uncoordinated Networks

In an uncoordinated network, the link performance between the devices might degrade significantly due to the interference from other links in the network sharing the same spectrum. As a solution, the concept of *partial overlapping tones (POT)* is introduced in Chapter 5. The interference energy observed at the victim receiver is mitigated by partially overlapping the individual subcarriers via an intentional frequency offset between the links. Also, it is shown that while orthogonal transformations at the receiver cannot mitigate the other-user interference without losing spectral efficiency, non-orthogonal transformations are able to mitigate the other-user interference without any spectral efficiency loss at the expense of self-interference. Using spatial Poisson point process, a tractable bit error rate analysis is provided to demonstrate potential benefits emerging from partially overlapping tones (POT).

1.5.5 Chapter 6: Number of Required Equalizer Taps for Multicarrier Schemes

In a multicarrier scheme, transmit filter, communication medium, and receive filter result in a *composite effect* that determines the characteristics of the interference among the symbols in time and frequency. However, precise information to handle the interference is not available at the receiver due to the uncertain noise and the random nature of the communication medium. While taking a smaller number of taps into account for channel estimation causes lack

of description of the composite effect, using a larger number of taps folds noise into the channel estimation. Hence, using fewer or more taps than the required ones degrades the bit error rate (BER) performance of the receiver. In this chapter, this issue is theoretically investigated for multicarrier schemes. The number of interfering symbols and their locations in both time and frequency are obtained for a given multicarrier structure. Considering practical scenarios, the number of required equalizer taps is also extracted via Akaike information criterion. It is shown that considering correct number of taps yields not only improvement on BER performance, but also less complex equalizer structures in practice.

CHAPTER 2

A SURVEY ON MULTICARRIER SCHEMES: FILTERS AND LATTICES

2.1 Introduction

The explosion of mobile applications and data usage in the recent years necessitate the development of adaptive, flexible, and efficient radio access technologies. To this end, multicarrier techniques have been extensively used over the last decade for broadband wireless communications. This wide interest is primarily due to their appealing characteristics, such as the support for multiuser diversity, simpler equalization, and adaptive modulation and coding techniques.

Among many other multicarrier techniques, orthogonal frequency division multiplexing (OFDM) dominates the current broadband wireless communication systems. On the other hand, OFDM also suffers from several shortcomings such as high spectral leakage, stringent synchronization requirements, and susceptibility to frequency dispersion. Transition from the existing OFDM-based multicarrier systems to the next generation radio access technologies may follow two paths. In the first approach, existing OFDM structure is preserved, and its shortcomings are addressed through appropriate solutions [4]. Considering backward compatibility advantages with existing technologies, this approach has its own merits. The second approach follows a different rationale based on a generalized framework for multicarrier schemes [5, 6], which may lead to different techniques than OFDM. In this chapter, we choose to go after the second approach since it provides a wider perspective for multicarrier schemes, with OFDM being a special case. Based on this strategy, the goals of the chapter are listed as follows:

- To provide a unified framework for multicarrier schemes along with Gabor systems by emphasizing their basic elements: what to transmit, i.e., symbols, how to transmit, i.e., filters, and where/when to transmit, i.e., lattices;
- To extend the understanding of existing multicarrier schemes by identifying the relations to each other;
- To review the existing prototype filters in the literature considering their utilizations in multicarrier schemes;
- To understand the trade-offs between different multicarrier schemes;

- To pave the way for the further developments by providing a wider perspective on multicarrier schemes.

This chapter is organized as follows: First, preliminary concepts and the terminology are presented in Section 2.2. Various multicarrier schemes are provided in Section 2.3, referring to the concepts introduced in Section 2.2. Then, known prototype filters are identified and their trade-offs are discussed in Section 2.4. Useful tools and metrics to evaluate the filter performances are investigated in Section 2.5, and, finally, the investigation is concluded in Section 2.6.

2.2 Preliminary Concepts: Symbols, Lattices, and Filters

The purpose of this section is to provide preliminary concepts related to multicarrier schemes along with the notations used throughout the chapter. Starting from the basics, symbols, lattices, and filters are discussed in detail within the framework of Gabor systems. For a comprehensive treatment on the same subject, we refer the reader to the books by I. Daubechies [7], H.G. Feichtinger and T. Strohmer [8], and O. Christensen [9]. Also, the reader who wants to reach the development of Gabor systems from the mathematical point of view may refer to the surveys in [6, 10–13]. Besides, it is worth noting [2, 3, 14–25] constitute the key research papers which construct a bridge between the Gabor theory and its applications on communications. These studies also reveal how the Gabor theory changes the understanding of multicarrier schemes, especially, within the two last decades. Additionally, [26–29] are the recent complete reports and theses based on Gabor systems.

2.2.1 Fundamentals

In the classical paper by C. Shannon [30], a geometrical representation of communication systems is presented. According to this representation, messages and corresponding signals are points in two function spaces: message space and signal space. While a transmitter maps every point in the message space into the signal space, a receiver does the reverse operation. As long as the mapping is one-to-one from the message space to the signal space, a message is always recoverable at the receiver. Based on this framework, a waveform corresponds to a specific structure in the signal space and identifies the locations of the signals in the signal space. Throughout this survey, the signal space is considered as a time-frequency plane where time and frequency constitute its coordinates, which is a well-known notation for representing one dimensional signals in two dimensions [2, 3].

When the structure in signal space relies on multiple simultaneously-transmitted subcarriers, the waveform structure corresponds to a multicarrier scheme. It is represented by

$$x(t) = \sum_{m=-\infty}^{\infty} \sum_{k=0}^{N-1} X_{mk} g_{mk}(t) \,, \tag{2.1}$$

where m is the time index, k is the subcarrier index, X_{mk} is the symbol (message) being transmitted, N is the number of subcarriers, and $g_{mk}(t)$ is the synthesis function which maps X_{mk} into the signal space. The family of $g_{mk}(t)$ is referred to as a *Gabor system*, when it is given by

$$g_{mk}(t) = p_{\text{tx}}\left(t - m\tau_0\right) e^{j2\pi k\nu_0 t} \,, \tag{2.2}$$

where $p_{\text{tx}}(t)$ is the prototype filter (also known as pulse shape, Gabor atom), τ_0 is the symbol spacing in time, and ν_0 is the subcarrier spacing. A Gabor system implies that a single pulse shape is considered as a prototype and others are derived from the prototype filter via some translations in time and modulations in frequency, as given in (2.2). The coordinates of the filters form a two dimensional structure in the time-frequency plane, known as lattice. Assuming a linear time-varying multipath channel $h(\tau, t)$, the received signal is obtained as

$$y(t) = \int_{\tau} h(\tau, t) x(t - \tau) \mathrm{d}\tau + w(t), \tag{2.3}$$

where $w(t)$ is the additive white Gaussian noise (AWGN). Then, the symbol $\tilde{X}_{nl}$ located on time index n and subcarrier index l is obtained by the projection of the received signal onto the analysis function $\gamma_{nl}(t)$ as

$$\tilde{X}_{nl} = \langle y(t), \gamma_{nl}(t) \rangle \triangleq \int_{t} y(t) \gamma_{nl}^{*}(t) \mathrm{d}t \,, \tag{2.4}$$

where

$$\gamma_{nl}(t) = p_{\text{rx}}\left(t - n\tau_0\right) e^{j2\pi l\nu_0 t} \,. \tag{2.5}$$

Similar to (2.1), $\gamma_{nl}(t)$ given in (2.5) is obtained by a prototype filter $p_{\text{rx}}(t)$ translated in both time and frequency, constructing another Gabor system at the receiver.

The equations (2.1)-(2.5) correspond to basic model for multicarrier schemes illustrated in Figure 2.1(a), without stressing the variables in the equations. In a crude form, a multicarrier scheme can be represented by a

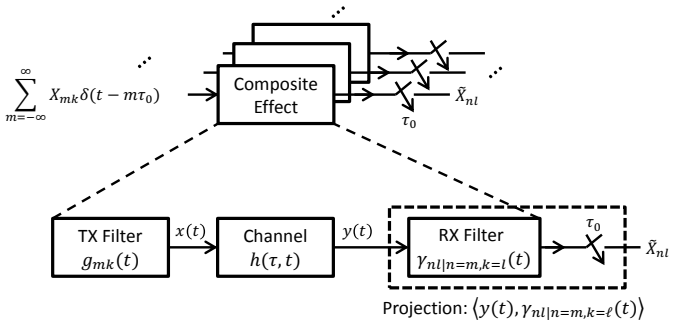

(a) A block diagram for communications via multicarrier schemes. Both the transmitter and the receiver construct Gabor systems.

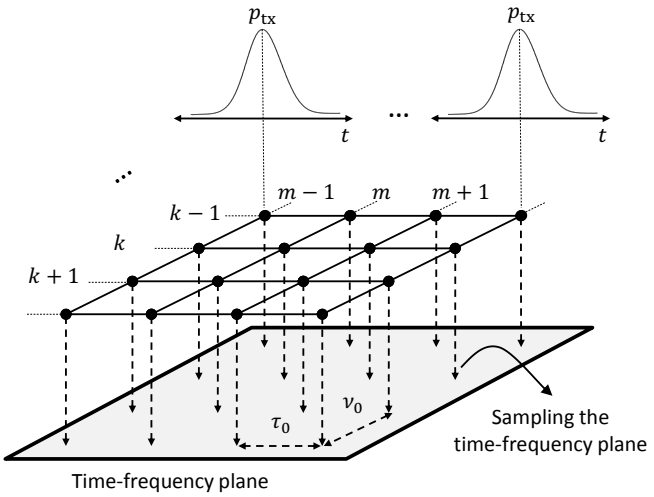

(b) Sampling the time-frequency plane. Modulated pulses are placed into the time-frequency plane, based on the locations of samples. In the illustration, the product of $1/\tau_0\nu_0$ corresponds to the lattice density.

Figure 2.1 Utilization of the prototype filters at the transmitter and the receiver.

specific set of equations constructed in the time-frequency plane, i.e., these equations are synthesized at the transmitter and analyzed at the receiver. In the following subsections, symbols, filters, and lattices in a multicarrier system are discussed in detail.

2.2.2 Symbols

Without loss of generality, the transmitted symbols are denoted by $X_{mk} \in \mathbb{C}$, where $\mathbb{C}$ is the set of all complex numbers. As a special case, it is possible to limit the set of X_{mk} to real numbers, i.e. $X_{mk} \in \mathbb{R}$, where $\mathbb{R}$ is the set of all real numbers. One may choose X_{mk} as a modulation symbol or a part of the modulation symbol, e.g. its real or imaginary part or a partition after a spreading operation. In addition, it is reasonable to consider finite number of elements in the set, based on the limited number of modulation symbols in digital communications. Note

that the set of the symbols may be important for the perfect reconstruction of the symbols since its properties may lead one-to-one mapping from message space to the signal space [30], as in signaling over Weyl-Heisenberg frames, faster-than-Nyquist signaling, or partial-response signaling [24, 25, 31, 32].

2.2.3 Filters

In digital communication, symbols are always associated with pulse shapes (also known as filters). A pulse shape essentially corresponds to an energy distribution which indicates the density of the symbol energy (in time, frequency, or any other domain). Hence, it is one of the determining factors for the dispersion characteristics of the signal. At the receiver side, the dispersed energy due to the transmit pulse shape is coherently combined via receive filters. Thus, the transmit and receive filters jointly determine the amount of the energy transfered from the transmitter to the receiver. Also, they determine the correlation between the points in the lattice, which identify the structure of the multicarrier scheme, i.e., orthogonal, bi-orthogonal, or non-orthogonal.

2.2.3.1 Matched Filtering

If the prototype filter employed at the receiver is the same as the one that the transmitter utilizes, i.e., $p_{\text{tx}}(t) = p_{\text{rx}}(t)$, this approach corresponds to matched filtering, which maximizes signal-to-noise ratio (SNR). As opposed to matched filtering, one may also use different prototype filters at the transmitter and receiver, i.e., $p_{\text{tx}}(t) \neq p_{\text{rx}}(t)$ [17].

2.2.3.2 Orthogonality of Scheme

If the synthesis functions and the analysis functions do not produce any correlation between the different points in the lattice, i.e., $\langle g_{mk}(t), \gamma_{nl}(t) \rangle = \delta_{mn}\delta_{kl}$, where δ is the Kronecker delta function, the scheme is either orthogonal or bi-orthogonal. Otherwise, the scheme is said to be non-orthogonal, i.e., $\langle g_{mk}(t), \gamma_{nl}(t) \rangle \neq \delta_{mn}\delta_{kl}$. While orthogonal schemes dictate to the use of the same prototype filters at the transmitter and receiver, bi-orthogonal schemes allow to use different prototype filters at the transmitter and the receiver.

A nice interpretation on orthogonality and bi-orthogonality is provided in [19]. Let R be a Gram matrix given by $R \triangleq QQ^{\text{H}}$ where Q^{H} is a block-circulant matrix in which the columns consist of the modulated-translated vectors generated by an initial filter $p(t)$. Then, the relation between the filters at the transmitter and the receiver for orthogonal and bi-orthogonal schemes can be investigated by

$$X_{mk} = RR^{-1}X_{mk} = R^{-\rho}RR^{-(1-\rho)}X_{mk} = R^{-\rho}QQ^{\text{H}}R^{-(1-\rho)}X_{mk} = \underbrace{R^{-\rho}Q \times \overbrace{(R^{-(1-\rho)}Q)^{\text{H}}X_{mk}}^{\text{Transmitted signal}}}_{\text{Received symbol}} \tag{2.6}$$

where $[\cdot]^H$ is the Hermitian operator and ρ is the weighting parameter to characterize orthogonality and bi-orthogonality. Using (2.6), the prototype filters at the transmitter and the receiver can be obtained from the first rows of $R^{-\rho}Q$ and $R^{-(1-\rho)}Q$, respectively, which yields

$$p_{\text{rx}} = \sum_{m,k} R^{-\rho} p_{mk} \tag{2.7}$$

and

$$p_{\text{tx}} = \sum_{m,k} R^{-(1-\rho)} p_{mk} \,, \tag{2.8}$$

where p_{mk} is the column vector generated by modulating and translating p. As a simpler approach, it is also possible to calculate (2.7) and (2.8) as

$$p_{\text{rx}} = S^{-\rho} p \tag{2.9}$$

and

$$p_{\text{tx}} = S^{-(1-\rho)} p \tag{2.10}$$

respectively, where $S = Q^{\text{H}}Q$. While the choice $\rho = 1/2$ leads to an orthogonal scheme, $\rho \to 0$ or $\rho \to 1$ result in bi-orthogonal schemes [19]. When $\rho = 1$, minimum-norm dual pulse shape is obtained.

Note that orthogonal schemes maximize SNR for AWGN channel [19] since they assure matched filtering. On the contrary, bi-orthogonal schemes may offer better performance for dispersive channels, as stated in [17]. In addition, when the scheme has receive filters which are not orthogonal to each other, i.e., $\langle \gamma_{n'l'}(t), \gamma_{nl}(t) \rangle \neq \delta_{n'n}\delta_{l'l}$, the noise samples becomes correlated, as in non-orthogonal and bi-orthogonal schemes [17].

2.2.3.3 Localization

The localization of a prototype filter characterizes the variances of the energy in time and frequency. While the localization in time is measured by $\|tp(t)\|^2$, the localization in frequency is obtained as $\|fP(f)\|^2$, where $\|\cdot\|$ is the L^2-norm and $P(f)$ is the Fourier transformation of $p(t)$. The functions where $\|fP(f)\|\|tp(t)\| \to \infty$ are referred as non-localized filters; otherwise, they are referred as localized filters.

2.2.4 Lattices

A lattice corresponds to an algebraic set which contains the coordinates of the filters in the time-frequency plane [19, 21, 22, 24, 26]. In other words, it is a set generated by sampling the time-frequency plane as illustrated in Figure 2.1(b). It determines the bandwidth efficiency and the reconstruction properties of a multicarrier scheme. Without loss of generality, a lattice Λ can be described by a non-unique generator matrix L as,

$$L = \begin{bmatrix} x & y \\ 0 & z \end{bmatrix}, \tag{2.11}$$

where $x, z \neq 0$. The generator matrix contains the coordinates of the first two identifying points of the lattice in its column vectors, i.e., $(0, x)$ and (y, z) [19]. The locations of other points are calculated by applying L to $[m\ k]^T$, where $[\cdot]^T$ is the transpose operation.

2.2.4.1 Lattice Geometry

Generator matrix L determines the lattice geometry. For example, the choice

$$L = \begin{bmatrix} T & 0 \\ 0 & F \end{bmatrix}, \tag{2.12}$$

yields a rectangular structure as in (2.2) and (2.5), with a symbol duration of T and subcarrier width F. Similarly, a hexagonal (or quincunx) pattern [19, 24, 26] is obtained when

$$L = \begin{bmatrix} T & 0.5T \\ 0 & F \end{bmatrix}. \tag{2.13}$$

Lattice geometry identifies the distances between the points indexed by the integers m and k. For example, assuming that $F = 1/T$, while the minimum distance between the points is 1 for the rectangular lattice in (2.12), it is $\sqrt{1.25}$ for the quincunx lattice in (2.13) [26].

2.2.4.2 Lattice Density/Volume

Lattice density can be obtained as

$$\delta(\Lambda) = \frac{1}{\mathrm{vol}(\Lambda)} = \frac{1}{|\det(L)|}, \tag{2.14}$$

where $|\cdot|$ is the absolute value of its argument and vol(Λ) is the volume of the lattice Λ calculated via determinant operation $\det(\cdot)$. It identifies not only the bandwidth efficiency of the scheme as

$$\epsilon = \beta\delta(\Lambda), \tag{2.15}$$

where β is the bit per volume, but also the perfect reconstruction of the symbols at the receiver. In order to clarify the impact of the lattices on the perfect reconstruction of the symbols, the concept of basis is needed to be investigated along with Gabor systems.

A set of linearly independent vectors is called a basis if these vectors are able to represent all other vectors for a given space. While including an extra vector to the basis spoils the linear independency, discarding one from the set destroys the completeness. From communications point of view, having linearly independent basis functions is a conservative condition since it allows one-to-one mapping from symbols to constructed signal without introducing any constraints on the symbols. Representability of the space with the set of $\{g_{mk}(t)\}$ is equivalent to the completeness property, which is important in the sense of reaching Shannon's capacity [16, 17]. Gabor systems provide an elegant relation between the linear independence and the completeness properties based on the lattice density. This relation for Gabor systems is given as follows [17, 23, 27, 33]:

- Undersampled case ($\delta(\Lambda) < 1$): Gabor system cannot be a complete basis since the time-frequency plane is not sampled sufficiently. However, this case gives linearly independent basis functions. Well-localized prototype filters can be utilized, but the bandwidth efficiency of the Gabor system degrades with decreasing $\delta(\Lambda)$.

- Critically-sampled case ($\delta(\Lambda) = 1$): It results in a complete Gabor System. Bases exist, but they cannot utilize well-localized prototype filters according to the Balian-Low theorem [3]. This theorem states that there is no well-localized function in both time and frequency for a Gabor basis where $\delta(\Lambda) = 1$. It dictates the use of non-localized functions, e.g., rectangular and sinc functions. A consequence of Balian-Low theorem can also be observed when the dual filters are calculated as in (2.7) and (2.8). If one attempts to utilize a well-localized function, e.g., Gaussian, when $\delta(\Lambda) = 1$, the Gram matrix R in (2.6) becomes ill-conditioned. Hence, the calculation of the dual pulse shape becomes difficult. The degree of ill-conditioning can be measured via the condition number of R. As stated in [19], the condition number of R approaches to infinity for Gaussian pulses when $\delta(\Lambda) \to 1$.

- Oversampled case ($\delta(\Lambda) > 1$): It yields an overcomplete set of functions. Gabor system cannot be a basis, but it may be a *frame*[1] with well-localized pulse shapes. However, since the Gabor system is overcomplete, representation of a signal might not be unique. Note that non-unique representations do not always imply loss of one-to-one mapping from modulation symbols to signal constructed. For example, a finite number of modulation symbols may be useful to preserve the one-to-one relation between the signal space and the message space [25].

2.2.5 A Combined Approach: Lattice Staggering

It is possible to circumvent the restriction of Balian-Low theorem on the filter design with lattice staggering[2] [14, 16, 33, 36, 37]. It is a methodology that generates inherent orthogonality between the points in the lattice for real domain through mandating symmetry conditions on the prototype filter. Since the inherent orthogonality does not rely on the cross-correlation between the filters, it relaxes the conditions for the filter design. It is worth noting that the real domain may be either the imaginary portion or the real portion of the complex domain. Thus, in lattice staggering, the real and imaginary parts of the scheme are treated separately. However, processing in real domain does not imply that the real and imaginary parts do not contaminate each other. Indeed, they interfere, but the contamination is orthogonal to the desired part.

The concept of lattice staggering is illustrated in detail in Figure 2.2. The lattices on real and imaginary parts of the scheme are given in Figure 2.2(a) and Figure 2.2(b), respectively. They also correspond to the lattices on in-phase and quadrature branches in baseband. While the filled circles represent the locations of the filters on the cosine plane, the empty circles show the locations of the filters on the sine plane. Cosine and sine planes indicate that the filters on those planes are modulated with either cosine or sine functions. First, consider the lattice given in the cosine plane of Figure 2.2(a). According to the Euler's formula, a pulse modulated with a complex exponential function includes components on both cosine and sine planes. Hence, when the filters on this lattice are modulated with complex exponential functions, there will be same lattice on the cosine and sine planes, as illustrated in Figure 2.2(a) and Figure 2.2(b). It is important to observe that the cross-correlation among the points indicated by arrows in the cosine plane of Figure 2.2(a) is always zero, when the filters are even-symmetric and the symbol spacing is selected as $\tau_0 = 1/2\nu_0$. This is because of the fact that the integration of a function which contains a cosine function multiplied with a symmetric function about the cosine's zero-crossings yields zero, as illustrated in Figure 2.2(c). From the communications point of view, this structure allows to carry only one real symbol without interference. Considering

[1] *Frames* are introduced in 1952 by Duffin and Schaeffer [34], as an extension of the concept of a basis. They can include more than the required elements to span a space. This issue corresponds to an overcomplete system, which causes non-unique representations [9, 35].

[2] In the literature, this approach appears with different names, e.g. offset quadrature amplitude modulation (OQAM), staggered modulation. Rather than indicating a specific modulation, it is referred as *lattice staggering* throughout the study.

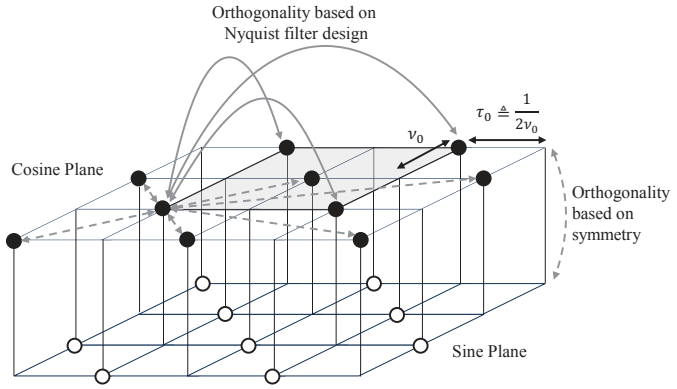

(a) Real part of the multicarrier signal (in-phase component).

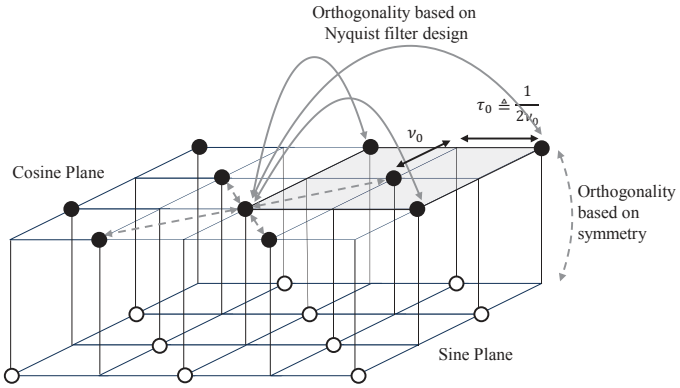

(b) Imaginary part of the multicarrier signal (quadrature component)

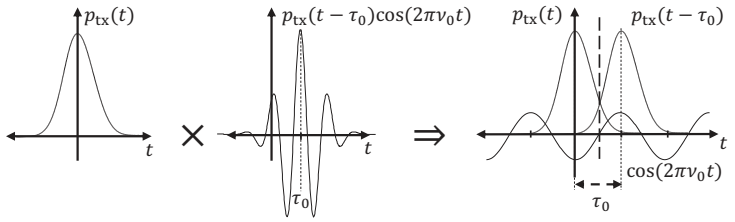

(c) Illustration for the orthogonality based on even-symmetric filters. Inner product of three functions is zero when τ_0 is set to $1/2\nu_0$.

Figure 2.2 Lattice staggering.

the same structure on the imaginary part by staggering the same lattice, illustrated in Figure 2.2(b), another real symbol could be transmitted. Although transmitting on the imaginary and real parts leads to contaminations on the sine planes, these contaminations are always orthogonal to the corresponding cosine planes when the filter is an even-symmetric function.

Lattice staggering induces an important result for the filter design: In order to obtain an orthogonal or biorthogonal scheme using lattice staggering, the correlation of the transmit filter and the receive filter should pro-

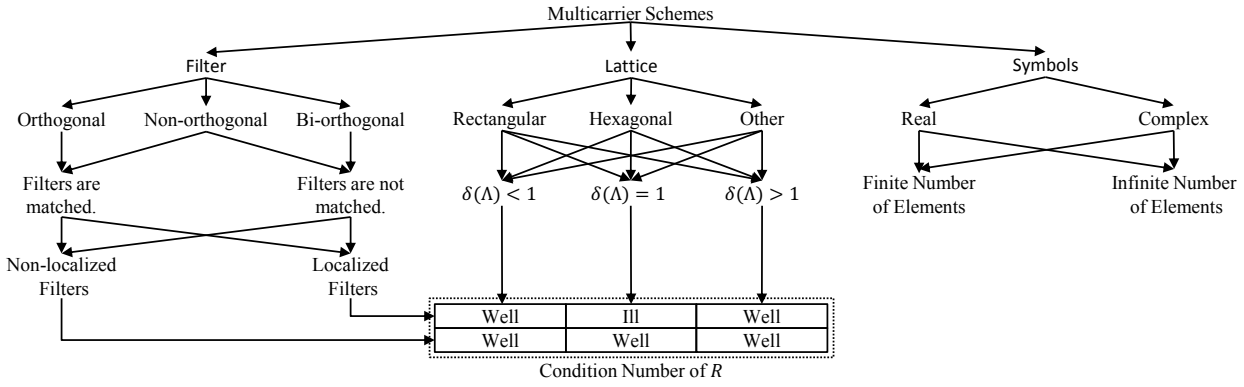

Figure 2.3 Multicarrier schemes based on lattices, filters, and symbols.

vide nulls in time and frequency at the multiples of $2\tau_0$ and $2\nu_0$. In other words, the unit area between the locations of the nulls in time-frequency plane is $2\tau_0 \times 2\nu_0$, which is equal to 2 since τ_0 is set to $1/2\nu_0$. This is because of the fact that even-symmetrical filters provide inherent orthogonality between some of the diagonal points in lattice when $\tau_0 = 1/2\nu_0$ even though the filters do not satisfy Nyquist criterion, as illustrated in Figure 2.2. Also, this approach circumvents the Balian-Low theorem since $\delta(\Lambda) = 1/\tau_0\nu_0 = 2$. Hence, lattice staggering allows orthogonal and bi-orthogonal schemes with well-localized filters while maintaining bandwidth efficiency as $\epsilon = \beta$. From the mathematical point of view, lattice staggering corresponds to utilizing Wilson bases on each real and imaginary parts of the scheme, which is equivalent to the linear combinations of two Gabor systems where $\delta(\Lambda) = 2$ [10, 12, 18, 19].

2.2.6 Summary

As a summary, the relations between the fundamental elements of a multicarrier scheme, i.e. symbols, lattice, and filter are given in Figure 2.3. One can determine these elements based on Gabor theory, considering the needs of the communication system. For example, let the signaling be an orthogonal scheme which is based on a rectangular lattice geometry without lattice staggering. Then, the localization of the filter is determined according to the statements of Gabor theory. For instance, equipping this system with well-localized filters yields an ill-conditioned R when $\delta(\Lambda) = 1$. Other inferences can also be obtained by following Figure 2.3.

2.3 Multicarrier Schemes

In this section, the concepts introduced in Section 2.2 are harnessed and they are associated with known multicarrier schemes. Rather than discussing the superiorities of schemes to each other, the relations between the orthogonal, bi-orthogonal, and non-orthogonal schemes within the framework of Gabor theory are emphasized. An

interpretation of the spreading operation in multicarrier systems (e.g., as in single carrier frequency division multiple accessing (SC-FDMA)) is also provided in the context of Gabor systems. Finally, milestones for multicarrier schemes reviewed for completeness.

2.3.1 Orthogonal Schemes

The schemes that fall into this category have orthogonal basis functions at both the transmitter and the receiver and follow matched filtering approach. The phrase of *orthogonal frequency division multiplexing* is often used for a specific scheme that is based on rectangular filters. However, there are other multicarrier schemes which provide orthogonality. We begin by describing the orthogonal schemes which do not consider lattice staggering:

- *Plain & Zero-padding OFDM:* Plain OFDM is an orthogonal scheme which is equipped with rectangular filters at the transmitter and the receiver when $\delta(\Lambda) = 1$. In order to combat with multipath channel, one can provide guard interval between OFDM symbols, known as zero-padding OFDM (ZP-OFDM) [38]. It corresponds to stretching the lattice in time domain, which yields $\delta(\Lambda) < 1$.

- *Filtered multitone (FMT):* Filtered multitone (FMT) is an orthogonal scheme where the filters do not overlap in frequency domain. There is no specific filter associated with FMT. Instead of the guard intervals in ZP-OFDM, guard bands between the subcarriers can be utilized in order to obtain more room for the filter localization in frequency domain. Hence, it is based on a lattice where $\delta(\Lambda) \leq 1$. For more details we refer the reader to the studies in [5, 39–43].

- *Lattice-OFDM:* Lattice-OFDM is the optimum orthogonal scheme for time- and frequency- dispersive channels in the sense of minimizing interference between the symbols in the lattice [19]. It relies on different lattice geometries and orthogonalized Gaussian pulses, depending on the channel dispersion characteristics.

The orthogonal schemes which consider lattice staggering are given as follows:

- *Staggered multitone (SMT) and Cosine-modulated multitone (CMT):* Both schemes exploit the lattice staggering approach to obtain flexibility on the filter design when $\epsilon = \beta$ [5, 37], where ϵ is the bandwidth efficiency and β is the bit per volume, introduced in (2.15). In these schemes, the symbols are real numbers due to the lattice staggering, however, as a special case, they are either real or imaginary part of the modulation symbols. The main difference between the staggered multitone (SMT) and the cosine-modulated multitone (CMT) is the modulation type. While SMT uses quadrature amplitude modulation (QAM) type

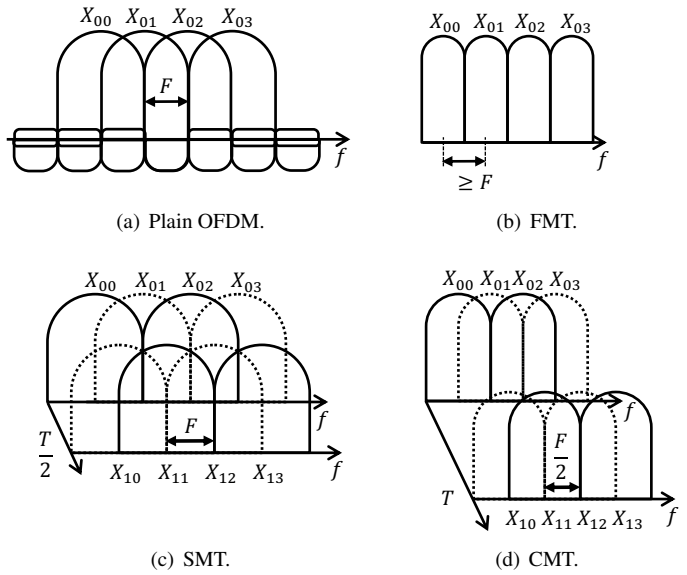

(a) Plain OFDM. (b) FMT.

(c) SMT. (d) CMT.

Figure 2.4 Illustrations of various orthogonal multicarrier schemes.

signals, CMT is dedicated to vestigial side-band modulation (VSB). Yet, SMT and CMT are structurally identical; it is possible to synthesize one from another by applying a frequency shift operation and proper symbol placement [37].

Illustrations for plain/zero-padding OFDM (ZP-OFDM), filtered multitone (FMT), staggered multitone (SMT), and cosine-modulated multitone (CMT) in time and frequency are provided in Figure 2.4.

2.3.2 Bi-orthogonal Schemes

These schemes do not follow matched filtering approach and do not have to contain orthogonal basis functions at the transmitter and the receiver. However, transmit and receive filters are mutually orthogonal to each other.

- *Cyclic-prefix OFDM:* Plain OFDM is often utilized with cyclic prefix (CP) to combat with the multipath channels. CP induces a lattice where $\delta(\Lambda) > 1$. At the same time, it results in a longer rectangular filter at the transmitter, compared to one at the receiver. Therefore, cyclic-prefix OFDM (CP-OFDM) does not follow matched filtering and constructs a bi-orthogonal scheme [6, 22, 44]. Yet, it provides many benefits, e.g. single-tap equalization and simple synchronization.

- *Windowed-OFDM:* OFDM has high out-of-band (OOB) radiation due to the rectangular filter. In order mitigate the out-of-band radiation, one may consider to smooth the transition between OFDM symbols. This

operation smooths the edges of rectangular filter, and commonly referred as windowing. If the windowing is performed with an *additional* guard period, a bi-orthogonal scheme where $\delta(\Lambda) > 1$ is obtained.

- *Biorthogonal frequency division multiplexing (BFDM):* In [17], it is stated that extending the rectangular filter as in CP-OFDM is likely to be a suboptimal solution under doubly dispersive channels, since this approach does not treat the time and frequency dispersions equally. As an alternative to CP-OFDM, by allowing different filters at the transmitter and the receiver, biorthogonal frequency division multiplexing (BFDM) with properly designed filters can reduce the interference contribution from other symbols in doubly dispersive channels. In [17], the design is given based on a prototype filter constructed with Hermite-Gaussian function family and a rectangular lattice geometry when $\delta(\Lambda) = 1/2$. In order to maintain the bandwidth efficiency, one can utilize BFDM with lattice staggering, as investigated in [36, 45].

- *Signaling over Weyl-Heisenberg Frames:* Main motivation is to exploit overcomplete Gabor frames with well-localized pulses and finite number of symbols for digital signal transmission. It is a unique approach that allows a scheme where $\delta(\Lambda) > 1$ with the perfect reconstruction property, which exploits subspace classifications [25].

It is interesting to observe that bi-orthogonal schemes are closely related to the concept of equalization. For example, transmitting the symbols over a non-orthogonal basis and forcing the correlations between the symbols to be zero at the receiver is similar to zero-forcing equalization. Furthermore, one may harness bi-orthogonal schemes to obtain single-tap equalization. For example, cyclic prefix (CP)-OFDM benefits from the extension of the rectangular filter to yield a single-tap equalization in time-invariant multipath channels. A similar approach can also be obtained via FMT. Consider a Gabor system at the transmitter, which utilizes sinc function that has a bandwidth greater than F, e.g., $F + F_{\text{cp}}$. Also, assume that the subcarrier spacing is extended not to allow overlapping between the subcarriers, i.e., $\nu_0 = F + F_{\text{cp}}$ and $\tau_0 = T$. If the Gabor system at the receiver is equipped with another sinc function that has a bandwidth F, which is smaller than ν_0, a cyclic behavior within band of F_{cp} is obtained, similar to the one in time domain for CP-OFDM. Therefore, a single-tap equalization would be sufficient for this scheme to combat with time-selective channels (which only introduces frequency dispersion). This issue is also shown in Figure 2.9(e) using the ambiguity surface for the extended null regions.

2.3.3 Non-orthogonal Schemes

The schemes that fall into this category do not contain orthogonal basis functions at the transmitter or the receiver. Also, there is no bi-orthogonal relation between the filters at the transmitter and the filters at the receiver.

- *Generalized Frequency Division Multiplexing:* Without loss of generality, generalized frequency division multiplexing (GFDM) is a non-orthogonal scheme which allows correlation between the points in the lattice in order to be able to utilize well-localized filters when $\delta(\Lambda) = 1$ [46]. It utilizes complex symbols and CP along with tail biting in the pulse shape. While tail biting allows channel shortening and CP provides reliability against multipath channel. Main feature of GFDM is the fact that each subcarrier corresponds to a pulse shaped single carrier transmission with cyclic prefix. As this structure yields a circulant channel matrix (including transmit filter, multipath channel, and receive filter) for each subcarrier, it allows single tap frequency domain equalization (FDE). However, when there are multiple subcarriers and $\delta(\Lambda) = 1$, orthogonality between the adjacent subcarriers cannot be maintained for localized filters. In [47], at the receiver side, successive interference cancellation is suggested to remove the interference between the symbols in frequency.

- *Concentric Toroidal Pulses:* By exploiting the orthogonality between Hermite-Gaussian functions, concentric toroidal pulses are introduced to increase the bandwidth efficiency of the transmission [48]. Four Hermite pulses are combined on each point in the lattice and each Hermite pulse carries one symbol. Although Gaussian-Hermite functions are orthogonal among each other, the pulses between neighboring points are not orthogonal.

- *Faster-than-Nyquist & Partial Response Signaling:* When $\delta(\Lambda) > 1$, certain conditions may yield the reconstruction of the transmitted symbols. This issue firstly is investigated by Mazo in 1975 as faster-than-Nyquist by addressing the following question: to what extent can the symbols be packed more than the Nyquist rate without loss in bit error rate (BER) performance? It is shown that the symbol spacing can be reduced to $0.802T$ without suffering any loss in minimum Euclidean distance between the synthesized signals for binary modulation symbols and sinc pulse [32]. In other words, BER performance is still achievable with *optimal receivers* even when the symbols are transmitted at a rate greater than the Nyquist rate. The minimum symbol spacing that keeps the minimum Euclidean distance is later on referred as the *Mazo limit* in the literature. By generalizing faster-than-Nyquist approach to other pulses, various Mazo limits are obtained for root-raised-cosine (RRC) pulses with different roll-off factors in [49]. For example, when roll-off is set to 0, 0.1, 0.2, and, 0.3, Mazo limits are derived as 0.802, 0.779, 0.738, and, 0.703 respectively. The faster-than-Nyquist approach is extended to multicarrier schemes by allowing interference in time and frequency in [50–52], which show that two dimensional signaling is more bandwidth efficient than one dimensional signaling. Another way of developing a scheme where $\delta(\Lambda) > 1$ is to transmit correlated

symbols. This approach corresponds to partial-response signaling and introduced in [31]. Similar to the faster-than-Nyquist signaling and partial-response signaling, in [24], Weyl-Heisenberg frames ($\delta(\Lambda) > 1$) is examined considering a hexagonal lattice geometry and sequence detector is employed at the receiver for symbol detection.

2.3.4 Multicarrier Schemes with Spreading Approaches

Spreading operation is commonly used to reduce the peak-to-average-power ratio (PAPR) in multicarrier schemes, in which modulation symbols are mapped to the multiple points in the lattice. One way to interpret and generalize the spreading operation in multicarrier systems (e.g., as in SC-FDMA [53] and filter bank spread FBMC (FB-S-FBMC) [54]) is to consider another Gabor system that spreads the energy of the modulation symbols into multiple subcarriers. In other words, as opposed to using single Gabor system at the transmitter and receiver, two Gabor systems combined with serial-to-parallel conversions are employed at the transmitter and the receiver. For example, it can be said that SC-FDMA, which allows better PAPR characteristics and frequency domain equalization (FDE) along with CP utilization [55–58], employs an extra Gabor system equipped with a rectangular filter and $\delta(\Lambda) = 1$ to spread the modulation symbols at the transmitter (i.e., discrete Fourier transformation (DFT)) and de-spread them at the receiver (i.e., inverse DFT). On the contrary, in OFDM, since there is no spreading of the modulation symbols in frequency domain, employed prototype filter for spreading is a Dirac function.

2.3.5 Milestones for Orthogonal Schemes

Having discussed the different variations of multicarrier systems in the earlier subsections, this subsection provides a brief history on the development of aforementioned multicarrier systems. Earlier works related to orthogonal multicarrier schemes actually date back to 1960s [59, 60], which utilize a bank of filters for parallel data transmission. In [59], Chang presented the orthogonality condition for the multicarrier schemes considering band-limited filters. This condition basically indicates that the subcarriers can be spaced half of the symbol rate apart without any interference. This scheme has then been re-visited by Saltzberg in 1967 [60] by showing the fact that Chang's condition is also true when the time and frequency axes are interchanged, based on offset quadrature amplitude modulation (OQAM). Indeed, Chang and Saltzberg exploits the lattice staggering for their multicarrier schemes which includes the basics of CMT and SMT. However, the idea of parallel transmission suggested in [59] and [60] were *unreasonably expensive and complex* for large number of data channels at that time. In [61], through the use of DFTs, Weinstein and Ebert eliminated the banks of subcarrier oscillators to allow simpler implementation of the multicarrier schemes. This approach has been later named as OFDM, and it has become more and more popular after

1980s due to its efficient implementation through fast Fourier transformation (FFT) techniques and FDE along with CP utilization [62] compared to other multicarrier schemes. On the other hand, Weinstein's DFT method in [61] limits the flexibility on different baseband filter utilization while modulating or demodulating the subcarriers, but instead used a time windowing technique to cope with the spectral leakage. In [63], by extending Weinstein's method, Hirosaki showed that different baseband filters may also be digitally implemented through DFT processing by using a poly phase network (PPN) [64], [65]. Several other developments over the last two decades have demonstrated low complexity and efficient implementations of lattice staggering, paving the way for its consideration in the next generation wireless standards (see e.g., [5, 16, 66], and the references listed therein).

2.4 Filter Design

In a multicarrier scheme, a prototype filter determines the correlation between the symbols and the robustness of the scheme against dispersive channels. This issue induces to design prototype filters which are suitable for communications in time-selective and frequency-selective channels. The goal of this section is to review the filters available in the literature. In order to reveal the connections between the filters, we categorized the filters based on their design criteria: 1) energy concentration [19, 67–77], 2) rapid-decay [78–81], 3) spectrum-nulling, and 4) channel characteristics and hardware. Analytical expressions of the investigated filters are given in Table 2.1. For more detailed discussions on the discussed filters, we refer the reader to the review papers [5, 82, 83] and the books [35, 43].

2.4.1 Design Criterion: Energy Concentration

In practice, limiting a pulse shape in time decreases the computational complexity and reduces the communications latency, which are inversely proportional to the filter length. However, using shorter or truncated filter may cause high sidelobes in the frequency domain. prolate spheroidal wave functions (PSWF) address this energy-concentration trade-off problem through obtaining a time-limited pulse with minimum out-of-band leakage or a band-limited pulse with maximal concentration within given interval. There are severals ways to characterize PSWFs [76]. A convenient definition for the prototype filter design is that PSWFs, $\{\psi_{n,\tau,\sigma}(t)\}$, is a family that includes the orthogonal functions which are optimal in terms of the energy concentration of a σ-bandlimited function on the interval $[-\tau, \tau]$, where n is the function order. In the family, $\psi_{0,\tau,\sigma}(t)$ is the most concentrated pulse and the concentration of the functions decreases with the function order. In other words, $\psi_{n,\tau,\sigma}(t)$ is the most concentrated function after $\psi_{n-1,\tau,\sigma}(t)$ and it is also orthogonal to $\psi_{n-1,\tau,\sigma}(t)$. Hence, if one provides the filter length and the bandwidth (where the pulse should be concentrated) as the design constraints, the optimum pulse becomes $\psi_{0,\tau,\sigma}(t)$ constructed based on these constraints.

Table 2.1 Analytical expressions of known prototype filters in the literature.

Filter	Analytical Model	Comments
Rectangular	$p(t) = \begin{cases} 1\,, & \lvert t\rvert \le \frac{1}{2} \\ 0\,, & \text{otherwise} \end{cases}$	It distributes the symbol energy uniformly in time domain. It is the prototype filter for CP-OFDM scheme.
Hanning (Raised-cosine)	$p(t) = \begin{cases} \frac{1}{2} + \frac{1}{2}\cos(2\pi t)\,, & \lvert t\rvert \le \frac{1}{2} \\ 0\,, & \text{otherwise} \end{cases}$	The function itself and its first derivative are continuous. Hence, the power of the sidelobes fall at $1/\lvert\omega\rvert^3$ per octave.
Exact Hamming	$p(t) = \begin{cases} \frac{25}{46} + \frac{21}{46}\cos(2\pi t)\,, & \lvert t\rvert \le \frac{1}{2} \\ 0\,, & \text{otherwise} \end{cases}$	Exact Hamming filter places zero at the position of the first sidelobe.
Exact Blackman	$p(t) = \begin{cases} \frac{7938}{18608} + \frac{9240}{18608}\cos(2\pi t) + \frac{1430}{18608}\cos(4\pi t)\,, & \lvert t\rvert \le \frac{1}{2} \\ 0\,, & \text{otherwise} \end{cases}$	Exact Blackman filter places zeros at the positions of the the third and fourth sidelobes.
Tapered-cosine-in-time (Tukey)	$p(t) = \begin{cases} 1\,, & \lvert t\rvert \le \frac{1-\alpha}{2} \\ \frac{1}{2} + \frac{1}{2}\cos(\frac{\pi}{\alpha}(\lvert t\rvert - \frac{1-\alpha}{2}))\,, & \frac{1-\alpha}{2} < \lvert t\rvert \le \frac{1+\alpha}{2} \\ 0\,, & \text{otherwise} \end{cases}$	It is the rectangular filter where the edges are tapered by convolving a rectangular function with a cosine lobe. When $\alpha = 1$, it corresponds to Hanning filter.
Tapered-cosine-in-frequency (Tukey)	$p(t) = \frac{\sin(\pi t)}{\pi t}\frac{\cos(\pi\alpha t)}{1-4\alpha^2 t^2}$	It distributes the symbol energy uniformly in frequency domain when $\alpha = 0$.
Root-raised-cosine	$p(t) = \begin{cases} 1-\alpha+4\frac{\alpha}{\pi}, & t = 0 \\ \frac{\alpha}{\sqrt{2}}\Big[\Big(1+\frac{2}{\pi}\Big)\sin\big(\frac{\pi}{4\alpha}\big) + \Big(1-\frac{2}{\pi}\Big)\cos\big(\frac{\pi}{4\alpha}\big)\Big], & t = \pm\frac{1}{4\alpha} \\ \frac{\sin\Big((1-\alpha)\pi t\Big)+4\alpha t\cos\Big((1+\alpha)\pi t\Big)}{\pi t\Big(1-16\alpha^2 t^2\Big)}\,, & \text{otherwise} \end{cases}$	It corresponds to tapered-cosine-in-frequency after matched filtering.
Mirabbasi-Martin	$p(t) = \begin{cases} a_0 + 2\sum_{l=1}^{K-1} a_l\cos(2\pi l t)\,, & \lvert t\rvert \le \frac{1}{2}\,, \\ 0\,, & \text{otherwise} \end{cases}$ $k_l = (-1)^l a_l\,,\ k_0 = -1\,,\ k_l^2 + k_{K-l}^2 = 1\,,\ k_0 + 2\sum_{l=1}^{K-1} k_l = 0\,,$ $\sum_{l=1}^{K-1} l^q k_l = 0\,,\ q \ge 2\,,\ q \in \{2n \mid n \in \mathbb{Z}\}$	It provides rapid-decaying. Power of the sidelobes fall at $1/\lvert\omega\rvert^{(q+3)}$ per octave, where q is the derivation order. Last equation is utilized to construct a complete set of equations.
Prolate	$p(t) = \arg\min_{p(t)} \Big\{\int_{-\infty}^{\infty} \lvert P(f)\rvert^2 \mathrm{d}f - \int_{-\sigma}^{\sigma} \lvert P(f)\rvert^2 \mathrm{d}f\Big\}\,.$	It is the optimally-concentrated pulse in frequency for a given filter length and bandwidth.
Optimal finite duration pulses	$p(t) = \sum_{l=0}^{N} a_{2l}\psi_{2l,\tau,\sigma}(t)$	It is the optimally-concentrated pulse for a given duration and bandwidth, which also satisfies Nyquist criterion in both time and frequency.
Kaiser	$p(t) = \begin{cases} \frac{I_0\left(\beta\sqrt{1-4t^2}\right)}{I_0(\beta)}\,, & \lvert t\rvert \le \frac{1}{2} \\ 0\,, & \text{otherwise} \end{cases}$ $I_0(x) = 1 + \sum_{k=1}^{\infty}\Big[\frac{(x/2)^k}{k!}\Big]^2$	Kaiser filter has very similar time-frequency characteristics of prolate filter. Although it is suboptimum solution for concentration problem, its formulation is given in closed-from.
Modified Kaiser	$p(t) = \begin{cases} \frac{I_0\left(\beta\sqrt{1-4t^2}\right)-1}{I_0(\beta)-1}\,, & \lvert t\rvert \le \frac{1}{2} \\ 0\,, & \text{otherwise} \end{cases}$	In order to provide faster decaying, Kaiser window is modified to obtain zeros at $\lvert t\rvert = 1/2$.
Gaussian	$p(t) = (2\rho)^{1/4} e^{-\pi\rho t^2}\,,\ P(f) = p_{\text{gaussian}}(t, 1/\rho)$	It is the optimally-concentrated filter when there are no restrictions on filter length and bandwidth and $\rho = 1$.
IOTA	$p(t) = \mathcal{F}^{-1} O_{\tau_0}\mathcal{F} O_{\upsilon_0} p_{\text{gaussian}}(t)$ $O_a x(t) = \frac{x(t)}{\sqrt{a\sum_{k=-\infty}^{\infty}\lVert x(t-ka)\rVert^2}}\,,\ x(t) \in \mathbb{R}$ $\mathcal{F}^{-1}X(f) = \int X(f)e^{-j2\pi f t}\mathrm{d}f\,,\ \mathcal{F}x(t) = \int x(t)e^{j2\pi f t}\mathrm{d}t$	IOTA yields optimally-concentrated function when there are no restrictions on filter length and bandwidth. It also fulfills Nyquist criterion after matched filtering.
Hermite	$p(t) = \sum_{l=0}^{N} a_{4l}\psi_{4l,\infty,\infty}(t)\,,$ $\psi_{n,\infty,\infty}(t) = H_{\text{n}}\left(\sqrt{2\pi}t\right)e^{-\pi t^2}\,,\ H_{\text{n}}(t) = (-1)^n e^{t^2}\frac{d^n}{dt^n}e^{-t^2}$	By deforming the Gaussian filter with the high-order Hermite functions, it obtains zero-crossings to satisfy Nyquist criterion. It has similar characteristics with IOTA.
Extended Gaussian	$p(t) = \frac{1}{2}\Big[\sum_{k=0}^{\infty} d_{k,\rho,\upsilon_0}\big[p_{\text{gaussian}}(t + k/\upsilon_0, \rho) + p_{\text{gaussian}}(t - k\upsilon_0, \rho)\big]\Big]\times$ $\sum_{l=0}^{\infty} d_{l,1/\rho,\tau_0}\cos(2\pi l t/\tau_0)$	It is a generalized family based on Gaussian function which gives the closed-form expression of the filter derived via IOTA.

PSWFs have many appealing properties [68, 72]. For example, they are the eigenfunctions of the operation of *first-truncate-then-limit-the-bandwidth*. Therefore, these functions can pass through this operation without any distortion or filtering effect excluding the scaling with a real coefficient, i.e, eigenvalue, which also corresponds to the energy after this operation. Assuming that the energy of the pulse is 1, eigenvalues will always be less than 1. Also, PSWFs correspond to an important family when $\tau = \sigma \to \infty$, known as Hermite-Gaussian functions which are the eigenfunctions of Fourier transformation. Hermite-Gaussian functions provide optimum concentration in time and frequency at the same time. Hence, they are able to give isotropic (same) responses in time and frequency. We also refer the reader to the detailed discussions on the properties of PSWFs in [67, 69–71, 76, 77]

In the following subsections, the prototype filters that target time-frequency concentration are discussed. Their characteristics are inherently related to the PSWFs.

2.4.1.1 Prolate Window

Prolate window addresses the energy concentration in frequency for a given filter length and bandwidth. In time domain, its expression corresponds to $\psi_{0,\tau,\sigma}(f)$ or 0th order Slepian sequence in time for the discrete case [71]. This issue is explained as a sidelobe minimization problem in [5], as shown in Table 2.1. The time and frequency characteristics of prolate window are given in Figure 2.5.

2.4.1.2 Kaiser Function

An efficient solution for a filter with finite length is proposed by Jim Kaiser by employing Bessel functions to achieve an approximation to the prolate window [73, 82]. It offers a suboptimal solution for the out-of-band leakage. A favorable property of Kaiser filter is its flexibility to control the sidelobes and stop-band attenuation, through a single design parameter β with a closed-form expression. The expression is given in Table 2.1 where $I_0(x)$ denotes the zeroth order modified Bessel function of the first kind.

2.4.1.3 Optimal Finite Duration Pulses

Although prolate window is an optimally-concentrated filter in terms of minimum sidelobe energy for a given filter length and bandwidth, it does not satisfy the Nyquist criterion that ensures zero-interference between the points in the lattice. Considering this fact, Vahlin exploits PSWFs to realize a new family which is referred as optimal finite duration pulse (OFDP) [75] by generalizing the optimization procedure given for single carrier, presented in [74]. The aim is to achieve a Nyquist filter in both time and frequency with the maximum energy in the main lobe for a given bandwidth and filter length. In order to develop these pulses, as summarized in Table 2.1, Vahlin chooses the signal

representation of OFDPs as the linear combinations of the PSWFs and formulates the constraints as an optimization problem to find the weights a_l for lth PSWF for a given interval, using Lagrange multipliers and calculus of variations. Since only the even-indexed prolate functions are even-symmetrical, only a_{2l} are considered through the optimization procedure. By applying similar optimization procedure, OFDP has been utilized in [66]. Also, another optimization procedure which is based on deriving the composite matched filtering response of OFDP filter instead OFDP itself is suggested in [84] to reduce the optimization complexity.

2.4.1.4 Gaussian Function

It is a prolate window when $\tau = \sigma \to \infty$. It is utilized with a parameter ρ in [19, 26, 42, 85] to control the filter localization. Using the properties of Fourier transform, one may show that the frequency response of a Gaussian function is also another Gaussian function [26]. When $\rho = 1$, it yields identical responses in time and frequency and it corresponds to optimally-concentrated pulse among all functions. On the other hand, since it has no zero-crossings, Gaussian filter does not satisfy the Nyquist criterion. In other words, it introduces interference from one point to other points in the lattice.

2.4.1.5 Isotropic Orthogonal Transform Algorithm

Isotropic orthogonal transform algorithm (IOTA) targets to obtain a filter which preserves the optimum concentration property of Gaussian filter, and orthogonalizes it to prevent interference to neighboring points in the lattice [16]. Starting with the Gaussian function, orthogonalized pulse is obtained as shown in Table 2.1 where $\mathcal{F}$ and $\mathcal{F}^{-1}$ are the operators for Fourier transform and its inverse, respectively, and O_a is the orthogonalization operator. This operation also corresponds to the orthogonalization process in (2.9) and (2.10) [19]. The constructed prototype filter fulfills the Nyquist criterion and may yield isotropic response in time and frequency. For example, when $\rho = 1$, $\tau_0 = \sqrt{2}T/2$ and $\nu_0 = \sqrt{2}F/2$, the pulse shape becomes identical to its Fourier transform as shown in Figure 2.5.

2.4.1.6 Extended Gaussian Function

Extended Gaussian function (EGF) corresponds to the analytical expression of the function obtained via IOTA [86] as given in Table 2.1, where $0.528\nu_0^2 \leq \rho \leq 7.568\nu_0^2$ and d_{k,ρ,ν_0} are real valued coefficients. It is shown that these coefficients can be computed (for finite number of coefficients $b_{k,j}$) as

$$d_{k,\rho,\nu_0} = \sum_{j=0}^{j_k} b_{k,j} e^{-(\pi\rho/2\nu_0^2)(2j+k)} \ , \ 0 \leq k \leq K \ , \tag{2.16}$$

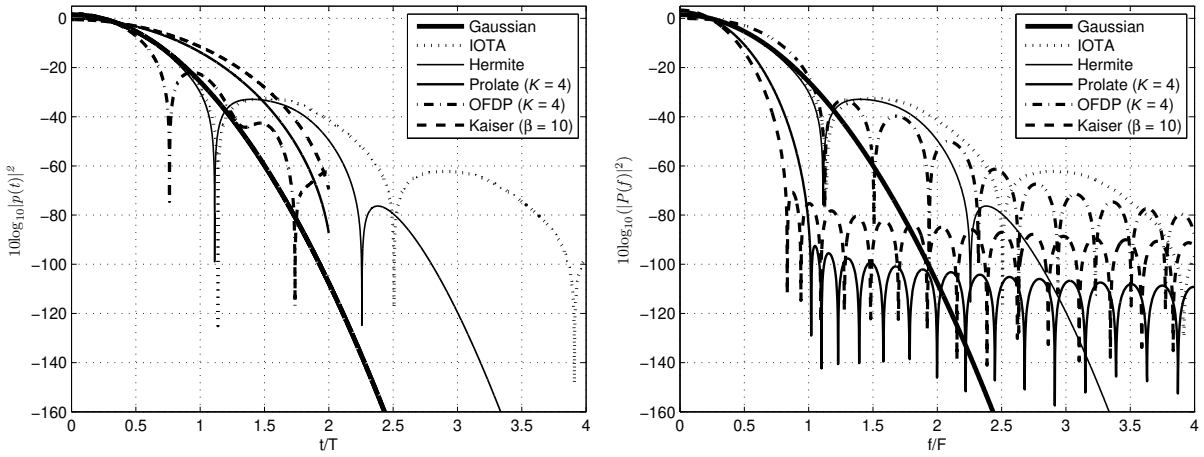

(a) Energy distribution in time.

(b) Energy distribution in frequency.

Figure 2.5 Time and frequency characteristics of the filters, designed based on energy concentration.

where [87] lists the coefficients $b_{k,j}$ for $0 \leq k \leq 14$ and $0 \leq j \leq 7$. For $\rho = 1$, $\tau_0 = \sqrt{2}T/2$ and $\nu_0 = \sqrt{2}F/2$, EGF gives the identical responses in time and frequency. In addition, one may truncate EGFs into one symbol duration to handle the latency drawback due to the filter length while maintaining filter localization through some optimization procedures [29, 66].

2.4.1.7 Hermite Filter

Hermite filter is obtained from the linear combinations of Hermite-Gaussian functions. By deforming the Gaussian filter with the high-order Hermite functions, zero-crossings are provided to satisfy Nyquist criterion [81]. It has similar characteristics with IOTA and yields isotropic response, which can be observed in Figure 2.5. Advanced forms of the Hermite-Gaussian combinations also consider the dispersion characteristics of communication medium, which is discussed in Section 2.4.4.2.

2.4.2 Design Criterion: Rapid-Decay

Even though PSWFs provide the optimum solution for the energy concentration problem, they do not address the rapid-decaying of the sidelobes, as can be seen in Figure 2.5. Decaying of the sidelobes is related to the smoothness of a filter. It is known that smoothness is measured by the number of continuous derivatives. If the mth derivative of a function is impulsive, the sidelobes of the function in frequency falls at $|\omega|^{-m}$ or $6m$ dB/octave, where ω is the angular frequency [80, 82, 88].

Table 2.2 Coefficients for Mirabbasi-Martin Filter.

	$K = 3$	$K = 4$	$K = 6$	$K = 8$
a_0	1	1	1	1
a_1	0.91143783	0.97195983	0.99818572	0.99932588
a_2	0.41143783	0.70710678	0.94838678	0.98203168
a_3		0.23514695	0.70710678	0.89425129
a_4			0.31711593	0.70710678
a_5			0.06021021	0.44756522
a_6				0.18871614
a_7				0.03671221

2.4.2.1 Raised-Cosine Function (Hanning Filter)

The Hanning filter whose shape is captured through a period of cosine function, is a smooth function in time. The zeroth and first order derivatives of the Hanning filter are continuous. Hence, sidelobes fall at $1/|\omega|^3$ per octave, which corresponds to 18 dB/octave.

2.4.2.2 Tapered-Cosine Function (Tukey Filter)

Tapered-cosine function is a filter where the time-frequency localization is controlled by the roll-off factor (α). While tapered-cosine function where $\alpha = 0$ results in rectangular shape, the shape becomes a raised-cosine function, i.e., Hanning filter, when $\alpha = 1$. Hence, it provides a function family where the decaying range is between 6 dB/octave to 18 dB/octave.

2.4.2.3 Root-Raised-Cosine Function

Root-raised-cosine (RRC) is typically utilized to satisfy Nyquist criterion after matched filtering. It is derived from the raised-cosine filter. RRC where $\alpha = 1$ is known as half-cosine function (HCF), which is employed in [5, 16, 37, 66, 85]. It provides a good compromise for time/frequency behavior; its relaxed transition bands allow approximation through a relatively short time-domain filter, while achieving high attenuation in the stop-band [5]. On the other hand, RRC filter with $\alpha = 0$ becomes a sinc function. While sinc function results in minimal bandwidth, it is very susceptible to truncation in time.

2.4.2.4 Mirabbasi-Martin Filter

Mirabbasi-Martin function is a filter where its coefficients are calculated by ensuring that the derivatives of the function is continuous [78, 80]. Obtained filter coefficients are also specified for different K in Table 2.2. While

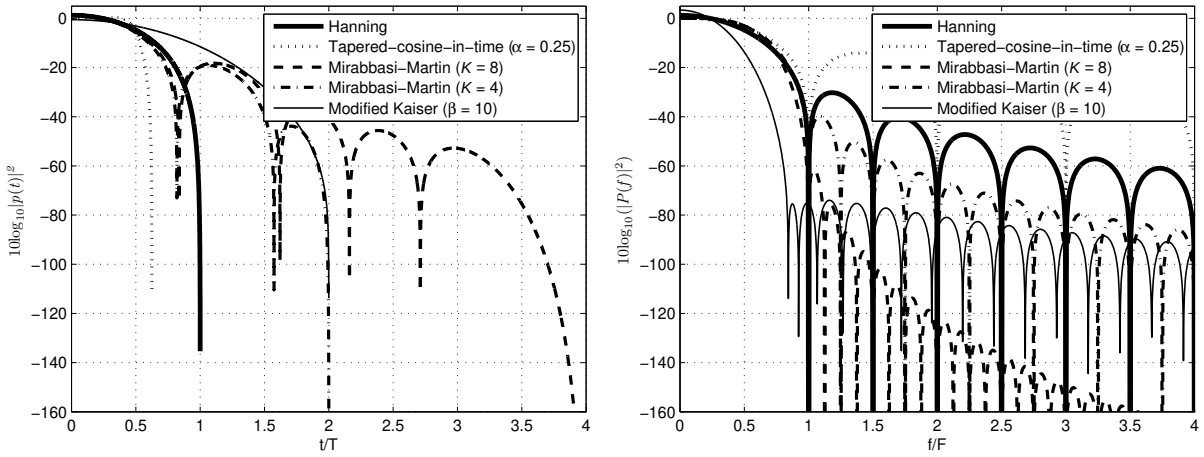

(a) Energy distribution in time.

(b) Energy distribution in frequency.

Figure 2.6 Time and frequency characteristics of the filters, designed based on rapid-decaying property.

the decaying rate is $1/|\omega|^5$ per octave when $K = 6$, it is $1/|\omega|^7$ per octave when $K = 8$ [80]. Its efficacy on decaying can be observed in Figure 2.6. It has been investigated further in [79, 89] for multicarrier schemes, and was then subsequently adopted to be used in the European Physical layer for dynamic access (PHYDYAS) project on filter bank multicarrier (FBMC) [90, 91]. A similar approach based on polynomial functions is also proposed in [88].

2.4.2.5 Modified Kaiser Function

Since Kaiser window is not a continuous function, it decays at the rate of $1/|\omega|$. In order to provide faster decaying, Kaiser window is modified to obtain zeros at $|t| = 1/2$ [83].

2.4.3 Design Criterion: Spectrum-nulling

As it can be realized, some of the functions in Table 2.1 follow a general form of the low-pass filters as

$$p(t) = \begin{cases} a_0 + 2\sum_{l=1}^{K-1} a_l \cos(2\pi l t) \ , & |t| \leq \frac{1}{2} \ , \\ 0 \ , & \text{otherwise} \end{cases} \tag{2.17}$$

where K is the number of bins in frequency and a_l is the lth filter coefficient. The form given in (2.17) is a generalized characterization to fulfill the spectrum-nulling criteria, since it corresponds to summation of sinc functions in the frequency domain. By exploiting the coherent cancellation of the tails of the sinc functions, one may systematically place zeros in the spectrum. This approach may not directly yield good prototype filters for a multicarrier scheme

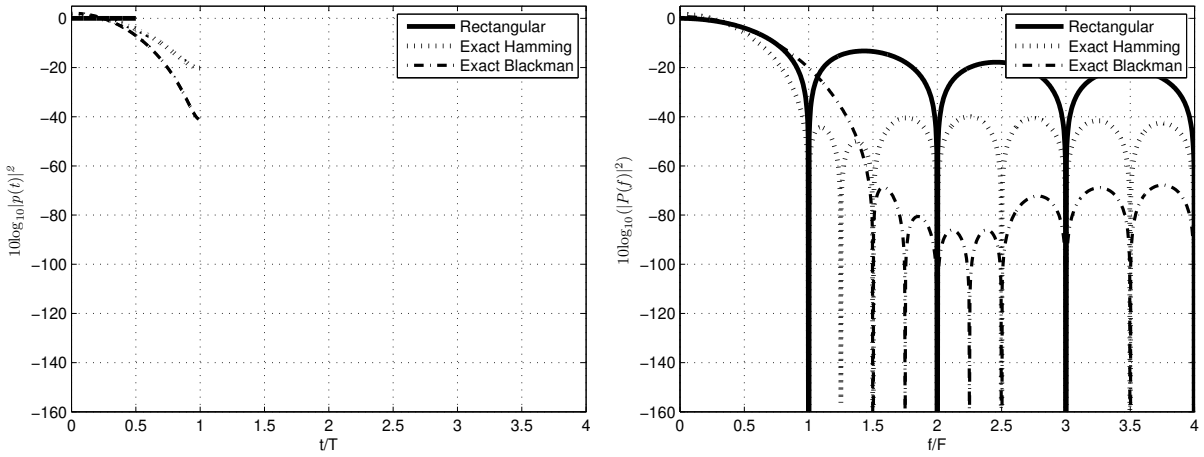

(a) Energy distribution in time.

(b) Energy distribution in frequency.

Figure 2.7 Time and frequency characteristics of the filters, designed based on spectrum-nulling approach and rectangular function.

because of the equal-ripple characteristics of the sidelobes. However, it is worth noting that the design criterion of these filters has some similarities with the existing sidelobe suppression techniques for the OFDM-based schemes, e.g. cancellation carriers [92]. The following filters are designed based on this approach:

2.4.3.1 Hamming Filter

Exact Hamming filter places a null at the position of the first sidelobe as shown in Figure 2.7.

2.4.3.2 Blackman Filter

Exact Blackman filter places nulls at the positions of the third and fourth sidelobes, as shown in Figure 2.7.

2.4.4 Design Criterion: Channel Characteristics and Hardware

Radio channel may hurt the orthogonality of the multicarrier schemes due to its dispersive characteristics in frequency and time, and causes inter-symbol interference (ISI) and inter-carrier interference (ICI). In order to combat with ISI and ICI, one may design pulse optimized to minimize interference among the points in the lattice.

2.4.4.1 Rectangular Function

Rectangular function distributes the symbol energy uniformly in time domain. It is the prototype filter for conventional cyclic-prefix OFDM (CP-OFDM) scheme. It provides an effective solution to combat with ICI and ISI

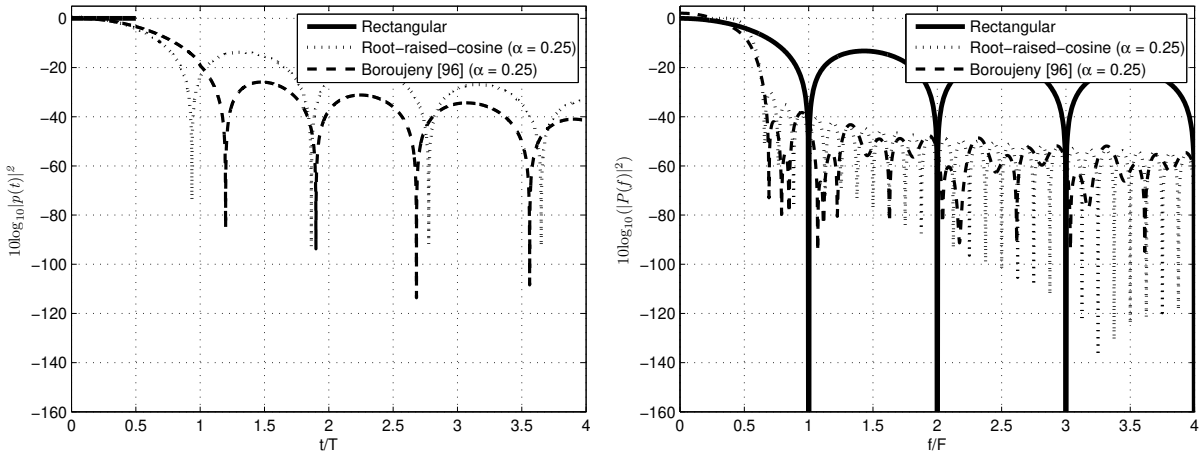

(a) Energy distribution in time.

(b) Energy distribution in frequency.

Figure 2.8 Time and frequency characteristics of the filters, designed based on channel constraints.

in time-invariant multipath channels via an extension on its duration at the transmitter. This approach exploits the uniformity of rectangular function.

2.4.4.2 Channel-based Pulses

Prototype filters can be designed to perform best for given channel characteristics. One of the methods is to use of optimally weighted combinations of the Hermite-Gaussian functions to construct new pulse shapes that are suitable for doubly dispersive channels. For example, in [93], the nulls in the ambiguity surface, which correspond to zero-interference regions, are widened using the Hermite-Gaussian functions to increase the robustness of the scheme in doubly dispersive channels. In [17], Hermite-Gaussian family is utilized as a basis to minimize ICI and ISI, while in [94], they are utilized to maximize the signal-to-interference ratio (SIR) considering biorthogonal schemes.

Based on different considerations, e.g. maximum signal-to-interference-plus-noise ratio (SINR) [22] and minimum ISI and ICI [23, 95], optimum pulses can be constructed using the Gaussian function itself an initial filter. As opposed to data communications, in [96], two prototype filter design procedures are proposed by relaxing the orthogonality constraint of the prototype filter for preamble transmission.

In addition to above considerations, one may design a prototype filter considering the hardware constraints. For example, a prototype filter which addresses the PAPR and timing jitter problems by minimizing the tails of the prototype filter is proposed in [97], which is shown in Figure 2.8.

2.5 Evaluation Metrics and Tools for Multicarrier Schemes

In this section, various tools and metrics are introduced in order to have a better understanding of the prototype filters and characterize their performance for multicarrier communications. These tools are instrumental for assessing the performances of different prototype filters along with multicarrier schemes. First, Heisenberg uncertainty parameter and direction parameter are given. Then, ambiguity surface is introduced and its usefulness on the evaluation of interference characteristics of multicarrier schemes is discussed. Further details about these tools and metrics may be found in [5, 7, 29, 82, 83].

2.5.1 Heisenberg Uncertainty Parameter

Time-frequency localization of a filter is measured by the Heisenberg uncertainty parameter ξ which is given by

$$\xi \equiv \frac{\|p(t)\|^2}{4\pi\sigma_{\mathrm{t}}\sigma_{\mathrm{f}}} \leq 1 \,, \tag{2.18}$$

where

$$\sigma_{\mathrm{t}} = \sqrt{\int_{\mathbb{R}} (t-\bar{t})^2 |p(t)|^2 \mathrm{d}t} \,, \tag{2.19}$$

$$\sigma_{\mathrm{f}} = \sqrt{\int_{\mathbb{R}} (f-\bar{f})^2 |P(f)|^2 \mathrm{d}f} \,, \tag{2.20}$$

σ_{t} is the time dispersion (or the standard deviation of the energy in time), and σ_{f} is the frequency dispersion (or the standard deviation of the energy in frequency), and $\bar{t}$ and $\bar{f}$ are the mean values of the supports of the pulse in time and frequency, respectively [5, 19, 26]. Filters with good localization characteristics have a Heisenberg parameter closer to 1. Heisenberg parameter is exactly equal to 1 with the Gaussian filter where $\rho = 1$.

2.5.2 Direction Parameter

The direction parameter $\kappa \in [0, \infty)$, which shows how a pulse shape lies in time-frequency plane, is given in [85] as

$$\kappa = \frac{\sigma_{\mathrm{t}}}{\sigma_{\mathrm{f}}} \,. \tag{2.21}$$

For example, while κ is equal to 0 for the rectangular filter, Gaussian filter where $\rho = 1$ yields $\kappa = 1$ because of its isotropic dispersion. A larger κ gives a pulse stretched more along the time axis compared to the frequency axis.

2.5.3 Ambiguity Function

In order to obtain the correlation between the points in the lattice, the projection of transmitter and receiver prototype filters should be calculated at every integer multiple of symbol spacing in both time and frequency as $\langle g_{mk}(t), \gamma_{nl}(t) \rangle$. By using fractional values instead of using n and l, ambiguity function is obtained as [5, 16, 26, 94]

$$A(\phi, \psi) \triangleq \int_{-\infty}^{\infty} p_{\text{tx}}\left(t + \frac{\phi}{2}\right) p_{\text{rx}}^{*}\left(t - \frac{\phi}{2}\right) e^{-j2\pi\psi t} \mathrm{d}t \,. \tag{2.22}$$

The properties of ambiguity function are given below:

- Ambiguity function is a two dimensional correlation function in the time-frequency plane. It gives an intuitive demonstration of the robustness against ICI/ISI due to different impairments, such as time and frequency selectivity of the propagation channel [5, 16, 26, 94].
- Ambiguity function yields real values in case of even-symmetric prototype filters.
- One may express Nyquist criterion in terms of the ambiguity function [5] as

$$A(n\tau_0, l\nu_0) = \begin{cases} 1\,, & n = l = 0 \\ 0\,, & \text{otherwise} \end{cases} . \tag{2.23}$$

- Similar to time-frequency localization of a filter, ambiguity function also cannot be concentrated arbitrarily. A similar expression to Heisenberg parameter is defined for ambiguity functions in [19].

Ambiguity surfaces for several filter pairs are provided in Figure 2.9. Without loss of generality, the filter length is set to $K \times T$, where $T = 1/F$ and K is an integer number. In Figure 2.9(a), both transmitter and receiver utilize a rectangular filter, which corresponds to plain OFDM. As it can be seen the nulls are located at the integer multiples of T and F. In Figure 2.9(b), rectangular filter at the transmitter is intentionally extended in time compared to the one at the receiver, which corresponds to the use of a CP. Hence, the nulls in the ambiguity surface are extended in time domain, around $t = 0$. The dual response of extension-in-time is given with sinc filters in Figure 2.9(d) and Figure 2.9(e) by extending the filter in frequency domain. Hence, same impact of cyclic prefix is obtained in frequency, instead of time. In Figure 2.9(c), ambiguity surface is obtained for the half-cosine function, i.e. RRC

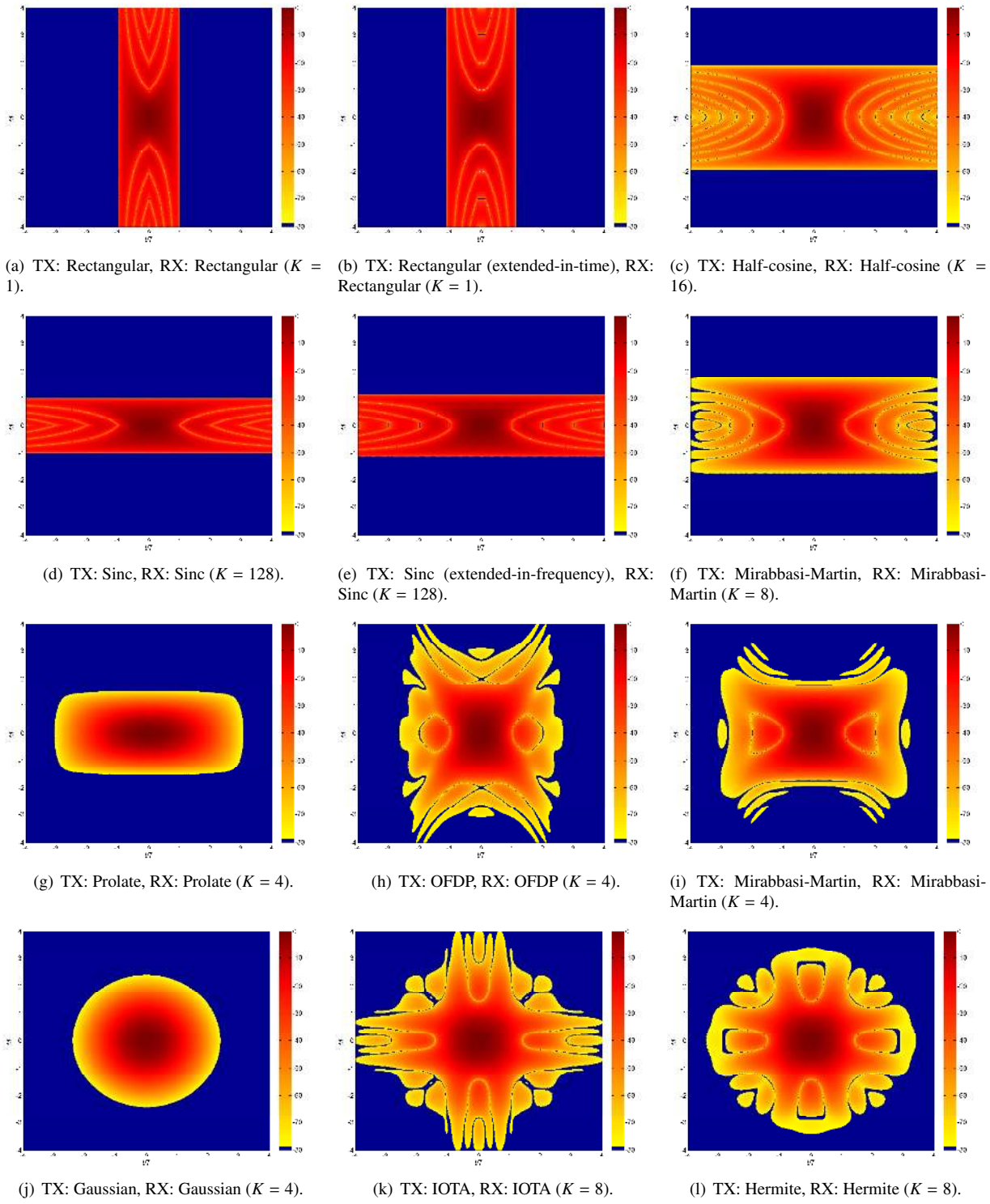

(a) TX: Rectangular, RX: Rectangular ($K = 1$).

(b) TX: Rectangular (extended-in-time), RX: Rectangular ($K = 1$).

(c) TX: Half-cosine, RX: Half-cosine ($K = 16$).

(d) TX: Sinc, RX: Sinc ($K = 128$).

(e) TX: Sinc (extended-in-frequency), RX: Sinc ($K = 128$).

(f) TX: Mirabbasi-Martin, RX: Mirabbasi-Martin ($K = 8$).

(g) TX: Prolate, RX: Prolate ($K = 4$).

(h) TX: OFDP, RX: OFDP ($K = 4$).

(i) TX: Mirabbasi-Martin, RX: Mirabbasi-Martin ($K = 4$).

(j) TX: Gaussian, RX: Gaussian ($K = 4$).

(k) TX: IOTA, RX: IOTA ($K = 8$).

(l) TX: Hermite, RX: Hermite ($K = 8$).

Figure 2.9 Ambiguity surfaces with known prototype filters in the literature ($10\log_{10}(|A(\phi,\psi)|^2)$).

where $\alpha = 1$. Since it has band-limited characteristic, it lies on the time domain. Also, it fulfills the Nyquist criterion as there are nulls located at the integer multiples of T and F. In Figure 2.9(f) and Figure 2.9(i), Mirabbasi-Martin functions are investigated for $K = 8$ and $K = 4$, respectively. It can be seen that Nyquist criterion does not always hold for Mirabbasi-Martin filter, especially in frequency. The ambiguity surface of prolate filter, given in Figure 2.9(g), is similar to the one obtained for the Gaussian pulse in Figure 2.9(j). Although the prolate window provides optimum concentration for a given filter length and bandwidth, it does not satisfy the Nyquist criterion. Since OFDPs in Figure 2.9(h) are derived from the proper combinations of prolate sequences, they are also concentrated while satisfying the Nyquist criterion. One may observe the nulls at the multiples of T and F in Figure 2.9(h). The ambiguity surfaces of Gaussian, IOTA, and Hermite-Gaussian combinations are given in Figure 2.9(j), Figure 2.9(k), and Figure 2.9(l), respectively. Gaussian filter provides a circular ambiguity surface without any nulls in the surface. However, the localization of Gaussian filter is the best compared to the other filters and decays fast in both time and frequency. Hermite-Gaussian combinations and IOTA filters provide localized ambiguity functions, while satisfying Nyquist criterion at the integer multiples of $\sqrt{2}T$ and $\sqrt{2}F$. The main reason of the selections of $\sqrt{2}T$ and $\sqrt{2}F$ is to obtain a prototype filter with identical responses in time and frequency, which is also suitable for the schemes with lattice staggering investigated in Section 2.2.5.

2.5.4 Signal-to-Interference Ratio in Dispersive Channels

It is possible to write the average SIR performance as

$$SIR = \frac{\sigma_{\mathrm{S}}^2}{\sigma_{\mathrm{I}}^2} , \tag{2.24}$$

where σ_{S}^2 and σ_{I}^2 are the power of the desired part and the interference leaking from other symbols, respectively. SIR, as defined here, should ideally be infinity for orthogonal and biorthogonal schemes, since no other interference sources are considered. However, orthogonality can be still spoiled by not only due to the lack of exact representation of the filter in digital domain, e.g. truncation, but also due to the dispersive channel. In the literature, statistical characteristics of the channel are generally described with wide-sense stationary uncorrelated scattering (WSSUS) assumption [98, 99] given by

$$\mathbb{E}\left[H(\tau,\nu)\right] = 0 , \tag{2.25}$$

$$\mathbb{E}\left[H(\tau,\nu)H^*(\tau_1,\nu_1)\right] = S_H(\tau,\nu)\,\delta(\tau\text{-}\tau_1)\delta(\nu\text{-}\nu_1) , \tag{2.26}$$

where $S_H(\tau, \nu)$ is the channel scattering function and $\mathbb{E}[\cdot]$ is the expected value operator. The term *wide sense stationary* means that the statical characteristics of the first two moments of the channel scattering function do not change with time, and are only related to the time difference as in (2.26). The term of *uncorrelated scattering* implies that one of the delay components of the received signal is uncorrelated to all the other delay components. However, note that the WSSUS assumption ignores the non-stationary characteristics due to the distance dependent path loss, shadowing, delay drift, and the correlation between the reflected rays from the same physical objects [100]. In addition, WSSUS assumption is not valid for short-term channel characteristics, especially, when the specular reflections dominate over diffuse scattering [101]. Yet, WSSUS assumption is widely used in the system models to characterize the wireless channels because of its simplicity. For example, exponential decaying multipath with Jakes Doppler spectrum [102] or ITU models [103] for different environments are commonly used for the channel scattering function for terrestrial communications.

Considering WSSUS assumption, analytical expressions of σ_{S}^2 and σ_{I}^2 can be obtained as follows. Assume that the impact of ICI and ISI on each subcarrier is statistically equal to each other, all subcarriers are utilized, X_{mk} are independent identically distributed with zero mean, and $\langle p_{\mathrm{tx}}(t), p_{\mathrm{rx}}(t) \rangle = 1$. Then, the power of desired part and the power of interference from other symbols in the lattice are obtained as

$$\sigma_{\mathrm{S}}^2 = \int_{\tau} \int_{\nu} S_H(\tau, \nu) |A(\tau, \nu)|^2 \mathrm{d}\nu \mathrm{d}\tau \,, \tag{2.27}$$

$$\sigma_{\mathrm{I}}^2 = \sum_{(m,k)\neq(0,0)} \int_{\tau} \int_{\nu} S_H(\tau, \nu) |A(m\tau_0 + \tau, k\nu_0 + \nu)|^2 \mathrm{d}\nu \mathrm{d}\tau \,, \tag{2.28}$$

respectively. The illustration of (2.28) is given in Figure 2.10, where the absolute value of the ambiguity function at the grid points (black circles) are equal to zero in time-invariant single-path channel, i.e., $\sigma_{\mathrm{I}}^2 = 0$. Due to time-variant multipath channel, the desired symbol (red circle at the middle) observes ISI/ICI from the neighboring points in the lattice, which is captured through (2.28).

2.6 Concluding Remarks

In this survey, multicarrier schemes are examined based on a generalized framework which relies on Gabor systems. The framework categorizes the multicarrier schemes based on their lattices, filters, and symbols. It explains the conventional CP-OFDM systems, while at the same time providing insights into multicarrier schemes different than CP-OFDM. Hence, the survey provides a useful framework to develop and analyze new types of waveforms, which may pave the way for further enhancements for the next generation radio access techniques.

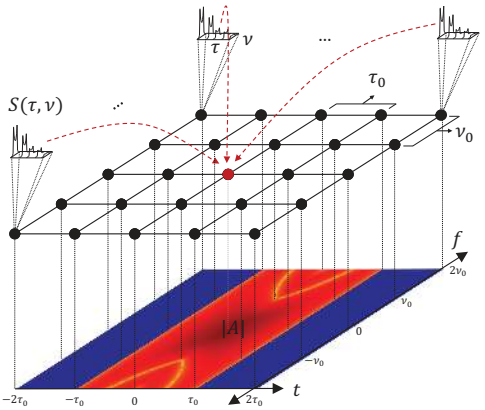

Figure 2.10 Interference analysis using the ambiguity function of rectangular filter in Figure 2.9(a).

The combined effect of filters, lattices, and symbols introduce different characteristics into the multicarrier schemes. Yet, for a given scenario, it is possible to addresses the system requirements via proper considerations within the provided framework. For example, CP-OFDM addresses low-complexity receiver implementation and multiple antenna functionalities, effectively. However, utilization of CP-OFDM may be an issue considering co-channel interference scenarios and operation under the frequency dispersive channels. One may provide solutions for these challenging issues via proper selections of lattices, filters, and symbols.

CHAPTER 3

A FILTER ADAPTATION: EDGE WINDOWING

3.1 Introduction

The structure of orthogonal frequency division multiplexing (OFDM) is based on rectangular pulse shape as discussed in Chapter 2, corresponding to combinations of sinc functions in frequency domain. Due to this specific structure, OFDM suffers from high sidelobes, which results in significant out-of-band (OOB) radiation[1]. In the literature, there are many methods proposed to suppress the sidelobes and prevent OOB radiation. Disabling a set of subcarriers, i.e., guard subcarriers, may be used for reducing the impact of the sidelobes. However, sacrificing these subcarriers decreases the spectral efficiency of OFDM. One of the well-known techniques for suppressing the sidelobes is to apply windowing to the OFDM symbol in time domain. In [106], raised cosine windowing is suggested. However, an extra time period (in addition to cyclic prefix) is necessary between two consecutive OFDM symbols, decreasing the spectrum efficiency. Another method for sidelobe suppression is to insert cancellation carriers instead of guard carriers [92]. Cancellation carriers are modulated subcarriers with complex coefficients which are calculated depending on the input data symbols. Drawbacks of this method are reduced bit error rate (BER) performance because of the extra power consumption for cancellation carriers and additional computational processing [107]. In [108], a sidelobe suppression method, which is based on smoothing the transition between consecutive OFDM symbols in an adaptive manner, is proposed. This approach is similar to cancellation carrier technique, but it is in time domain and it does not increase the peak-to-average-power ratio (PAPR). As it can be seen from the literature, all the successful techniques introduce some penalties on the scheme for the sake of sidelobe suppression.

The major goal of this chapter is to suppress OOB radiation of OFDM while minimizing the penalties introduced by the applied methodology, e.g., spectral efficiency degradation and high-complexity. To this end, in this chapter, we propose a spectrally efficient sidelobe suppression method, referred to as *edge windowing*. Unlike the aforementioned sidelobe suppression techniques, we use different pulse shapes on subcarriers by considering various windowing durations. Heavy windowing is applied on the subcarriers located at the edges of the band (edge subcarriers) and light windowing is applied on the subcarriers located at the middle of the band (inner subcarriers), since

[1]The content of this section is partially published in [104, 105]. Copyright for these publications can be found in Appendix A.

OOB radiation is mainly affected by the edge subcarriers. In addition, we reduce the cyclic prefix size of the edge subcarriers to maintain the spectral efficiency.

Edge windowing offers a trade-off in achieving spectral efficient multicarrier scheme and self-interference, essentially. As long as the self-interference problem is a manageable with some solutions, e.g., adaptive modulation or equalization, the introduced trade-off allows sidelobe suppression while maintaining spectral efficiency. In this investigation, in order to overcome the self-interference problem without complexity in physical layer, the advantage of multi-user environment is taken into account, which is also new degree-of-freedom to known sidelobe suppression methods. The dependency of the channel dispersion characteristics to the distance between the transmitter and the receiver is exploited with edge windowing. Considering a proper scheduling, e.g., distance-based scheduling or delay-spread based scheduling, in multiple accessing environments, inter-symbol interference (ISI) on the edge subcarriers is avoided and inter-carrier interference (ICI) on the inner subcarriers located at the middle of the band is mitigated.

3.2 Edge Windowing

Consider an OFDM symbol with N available subcarriers, C cyclic prefix size, T_s symbol duration, and N_G guard carriers. In the conventional windowing techniques, the transition between two consecutive OFDM symbols is smoothed in order to suppress the sidelobes. Therefore, an extra windowing time W is placed between two consecutive OFDM symbols to maintain the smooth transition. While the subcarriers of the previous OFDM symbol fade out in this interval, the subcarriers of the consecutive OFDM symbol fade in as in Figure 3.1(a). The smooth transition is provided with point-to-point multiplication of the windowing function and the OFDM symbol extended with postfix[2] and prefix[3]. Then, only W samples from the last part of the previous OFDM symbol and W samples from the beginning part of consecutive OFDM symbol are overlapped to maintain the orthogonality. Since the duration of the windowed OFDM symbol is $N + C + W$, conventional windowing decreases the spectrum efficiency of the OFDM symbol depending on W. In addition, there is no self-interference problem due to the multipath delay spread as the cyclic prefix part of the OFDM symbol remain same.

Edge windowing is based on the fact that the inner subcarriers have less impact on the sidelobes compared to the edge subcarriers, since the subcarriers spread as sinc function in frequency domain [106]. Thus, the smooth transition between consecutive OFDM symbols can be achieved by considering mostly the edge subcarriers for windowing operation. Therefore, windowing is heavily applied to N_{edge} edge subcarriers and the windowing size of the inner subcarriers is decreased to $W_{inner} < W$. In addition, while the sizes of the cyclic extensions of the inner subcarriers remain

[2] Adding W samples from the beginning of the OFDM symbol to the end of it.
[3] Adding $C + W$ samples from the last part of the OFDM symbol to the beginning of it.

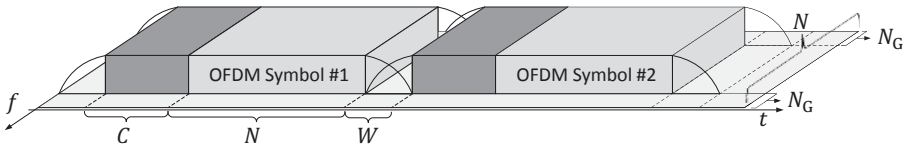

(a) Conventional windowing

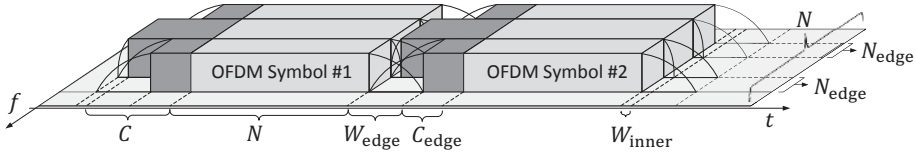

(b) Edge windowing

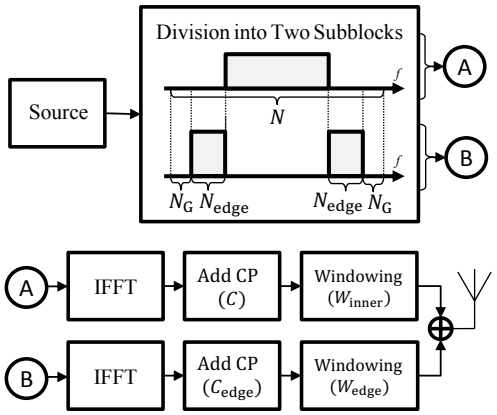

(c) Generating OFDM symbols with edge windowing.

Figure 3.1 Time-frequency representations of conventional windowing and edge windowing approaches.

as C, the sizes of the cyclic extensions of the edge subcarriers are reduced to $C_{\text{edge}} < C$. Subsequently, the remaining parts from the cyclic extensions are utilized for the windowing of edge subcarriers as $W_{\text{edge}} = C + W_{\text{inner}} - C_{\text{edge}}$. Thus, the windowing is combined with the cyclic prefix and the duration of the OFDM symbol is reduced to $N + C + W_{\text{inner}}$ as shown in Figure 3.1(b).

The important points for edge windowing are given as follows:

- Edge windowing maintains the spectrum efficiency of OFDM at the expense of self-interference while achieving sidelobe suppression.
- A better spectrum shaping is provided by increasing N_{edge}. However, increasing N_{edge} results in less number of inner subcarriers which have larger cyclic extensions and introduces more ISI and ICI, depending on the channel dispersiveness. Also, increasing W_{edge} for a given time period of two consecutive OFDM

symbols result in a better sidelobe suppression performance. However, it can cause more ICI and ISI, since it reduces the cyclic extensions for the edge subcarriers.

- It is possible to make $W_{\text{inner}} = 0$, which causes no windowing for inner subcarriers. In that case, sidelobe suppression only relies on the edge subcarriers. This approaches maintains the spectral efficiency of OFDM maximally.

- If the maximum excess delay spread is equal or less than C_{edge}, orthogonality is preserved on both edge and inner subcarriers. On the contrary, if the maximum excess delay spread is larger than C_{edge}, both ISI and ICI are observed in the edge subcarriers. In addition, since the orthogonality is lost between the edge and inner subcarriers, ICI is observed at inner subcarriers.

- The first W_{edge} samples of the edge subcarriers constitutes the combinations of two consecutive OFDM symbols as in Figure 3.1(b). Since the time distance between main parts of the two sequential OFDM symbols is still more than C and the edge subcarriers of previous OFDM symbol fade out in windowing period, the power of the observed ICI on the inner subcarriers will be mitigated by the characteristics of used windowing function.

- Since inverse fast Fourier transformation (IFFT) and windowing are linear operations, edge windowing method can be implemented by employing two branches for edge and inner subcarriers, i.e., an IFFT and windowing just for inner subcarriers and another IFFT and windowing just for edge subcarriers as in Figure 3.1(c). Edge windowing requires point-to-point multiplication of windowing function and IFFT results and point-to-point summation of the results of the two branches. Thus, edge windowing does not significantly increase the computation complexity of the transmitter which is $\mathrm{O}(N \log_2 N)$ due to the IFFT operation.

- Edge windowing can be applied not only to OFDM, but also to other OFDM-like systems, e.g., single carrier frequency division multiple accessing (SC-FDMA).

- In the literature, there are numerous windowing functions to suppress the sidelobes. Since edge windowing is a method to apply the windowing function to OFDM, different windowing functions can be utilized with edge windowing.

- For the sake of simplicity, edge windowing is exhibited via grouping the subcarriers as inner and edge subcarriers with two windowing operations. It is possible to extend the edge windowing by employing different windowing functions or different windowing sizes for more than two subcarrier groups.

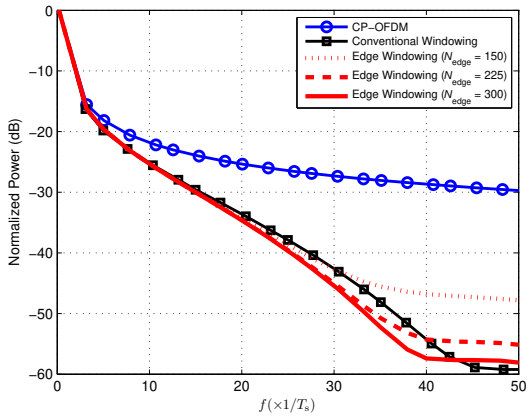

(a) Out-of-band radiation ($C_{\text{edge}} = 32, W_{\text{edge}} = 36$).

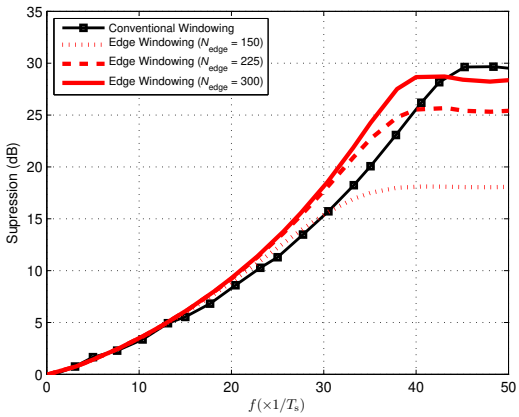

(b) Suppression performance relative to CP-OFDM ($C_{\text{edge}} = 32, W_{\text{edge}} = 36$).

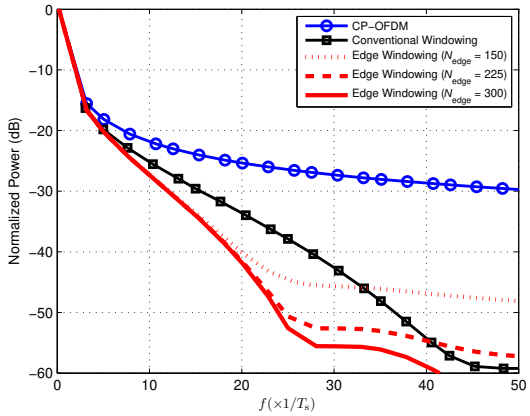

(c) Out-of-band radiation ($C_{\text{edge}} = 16, W_{\text{edge}} = 52$).

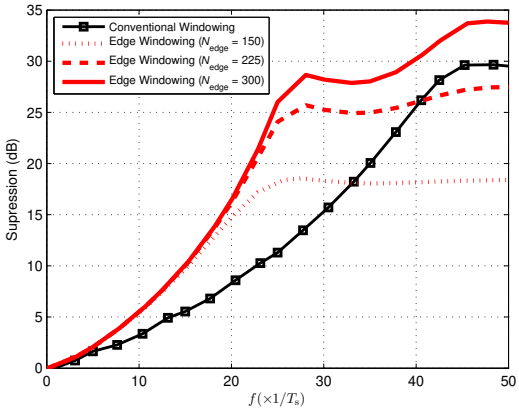

(d) Suppression performance relative to CP-OFDM ($C_{\text{edge}} = 16, W_{\text{edge}} = 52$).

Figure 3.2 Sidelobe suppression performance of edge windowing.

3.3 Performance of Edge Windowing: Suppression, Spectral Efficiency, Self-Interference

In order to evaluate the performance of edge windowing, we consider raised-cosine function [106], which corresponds to tapered-cosine function per subcarrier in time, given in Chapter 2.4.2.2. We set the parameters as $N = 1024$, $C = 64$, $T_s = 66.7\ \mu$s, $N_G = 100$, $W = 32$, $W_{\text{inner}} = 4$. We consider ITU Vehicular A given in [103] for multipath channel model. We use Rayleigh distribution in each channel realization and normalize the total power of the generated channel to 1. We perform the simulations over 5000 OFDM symbols and 20000 different channel realizations.

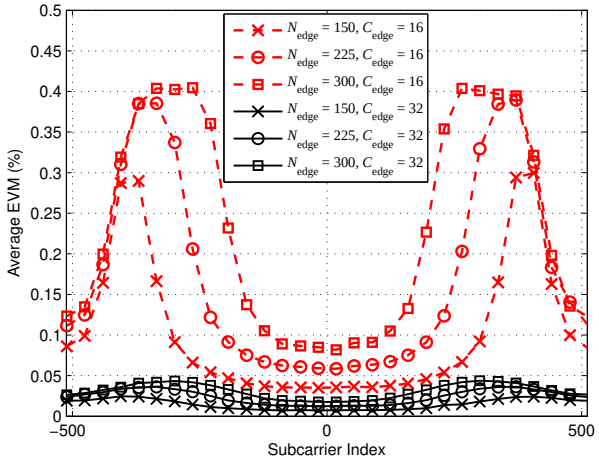

Figure 3.3 Average EVM on subcarriers for different N_{edge} and C_{edge} values.

In Figure 3.2, sidelobe suppression performance and OOB radiation of edge windowing and conventional windowing are compared relative to the plain OFDM. We consider that $C_{\text{edge}} = 32$ ($W_{\text{edge}} = 36$) and $C_{\text{edge}} = 16$ ($W_{\text{edge}} = 52$). If N_{edge} increases, the suppression performance of edge windowing increases as in both cases. The proposed method approaches to the suppression performance of conventional windowing when $N_{\text{edge}} = 300$. It is worth noting that edge windowing offers sharper sidelobe suppression than the conventional windowing due to the heavy windowing on edge subcarriers, which is important for cognitive radio applications.

In Figure 3.3, we analyze the impact of the edge windowing on the average error vector magnitude (EVM)[4] performances of each subcarrier due to the self-interference in multipath channel for different N_{edge} and C_{edge} values. The last tap of the ITU Vehicular A model is at 2510 ns (or nearly 39 samples for the simulation model). Thus, if C_{edge} is selected as greater than or equal 39, self-interference will be avoided totally. If C_{edge} becomes less than 39, self-interference is observed due to the insufficient cyclic prefix. Since ISI/ICI on edge subcarriers and only ICI on inner subcarriers are observed. Therefore, EVM performance on the edge subcarriers is worse than the inner subcarriers. Besides that, increasing N_{edge} results in more EVM for the cases of $C_{\text{edge}} < 39$, since the orthogonality between inner subcarriers and edge subcarriers is lost for more number of edge subcarriers.

The impact of the edge windowing parameters on spectral efficiency, sidelobe suppression and average EVM are summarized in Table 3.1 for a given cyclic prefix size. While increasing N_{edge} provides more sidelobe suppression, it causes more EVM on subcarriers. If W_{edge} increases, more suppression is achieved but more error is observed due to

[4]EVM is well-known metric to evaluate the performance of the recoverability of the symbols at the receiver. It essentially corresponds the ratio between the magnitude of error and the magnitude of ideal symbol.

the insufficient cyclic prefix for edge subcarriers. On the other hand, employing larger W_{inner} provides better sidelobe suppression and less error while decreasing the spectral efficiency.

Table 3.1 Trade-offs introduced by edge windowing

Item	Spectral Efficiency	Suppression	Error	C_{edge}
$\uparrow N_{\text{edge}}$	-	$\uparrow$	$\uparrow$	-
$\uparrow W_{\text{edge}}$	-	$\uparrow$	$\uparrow$	$\downarrow$
$\uparrow W_{\text{inner}}$	$\downarrow$	$\uparrow$	$\downarrow$	-

Edge windowing reduces the additional windowing time of the conventional windowing approach. Hence, edge windowing yields a more spectral efficient scheme than the system with the conventional windowing. The increment on the spectral efficiency (ΔR) is calculated in percent as

$$\Delta R = 100 \frac{W - W_{\text{inner}}}{N + C + W_{\text{inner}}}. \tag{3.1}$$

Considering the simulation parameters, edge windowing provides 5% increment on throughput relative to the system with conventional windowing.

3.4 Leveraging Edge Windowing in Multi-User Environment

In this section, the introduced trade-off between spectral efficiency and self-interference by edge windowing is discussed in multiple accessing environment. The dependency of the channel dispersive characteristics to the distance between transmitter and receiver is exploited to eliminate self-interference due to the edge windowing. Scheduling strategies which fits to the structure edge windowing in multiple accessing environment are investigated. Note that scheduling in a practical system may follow various strategies based on different considerations, e.g., channel conditions of the users, the demands of the applications, and fairness in the network. In this study, these strategies are not considered in order to reveal the limits on the elimination of self-interference introduced by edge windowing.

3.4.1 System Model

Consider the downlink of an orthogonal frequency division multiple accessing (OFDMA) based system with a coverage radius[5] of R. The base station is located at center of the cell and the locations of mobile stations are distributed uniformly. We assume the power delay profile of the multipath channel between the base station and the

[5] A circular shape is considered rather than hexagonal shape in order to simplify the analysis.

mobile stations decaying exponentially. The model of the exponential decaying is given in [109][6] as

$$P[n] = Be^{-n\frac{T_s}{N\tau_0}}\ , \tag{3.2}$$

where B and τ_0 are the constants to be obtained to adjust the desired average power and the desired root mean square (RMS) delay spread (T_{rms}) of the channel. The summation of $P[n]$ is set equal to 1. Hence, B is derived as

$$\sum_{n=0}^{\infty} P[n] = 1 \rightarrow B = 1 - e^{-\frac{T_s}{N\tau_0}}. \tag{3.3}$$

Since T_{rms} of the channel can be obtained from the second order central moment of (3.2), by calculating its inverse function, τ_0 is derived in [109] as

$$\tau_0 = \frac{T_{\text{rms}}\beta}{2\ln\left(\frac{\beta}{2} + 1\sqrt{1 + \left(\frac{\beta}{2}\right)^2}\right)},\ \ \beta \equiv \frac{T_s}{NT_{\text{rms}}}. \tag{3.4}$$

Also, we consider that T_{rms} depends on the distance between base station and mobile station. The mathematical expression which relates T_{rms} and d is given [110] as

$$T_{\text{rms}} = T_1 d^{\epsilon} y \tag{3.5}$$

where d is the distance between base station and mobile station in kilometers, ϵ is a distance coefficient lies between $0.5 \leq \epsilon \leq 1$, T_1 is the median value of T_{rms} at $d = 1\ km$, and y is a lognormal distributed random variable. The standard deviation of y lies as $2 \leq \sigma_y \leq 6$ in dB. Thus, the distribution of T_{rms} is also lognormal.

3.4.2 Scheduling Strategies

According to the equation given in (3.5), the nearby mobile stations to base station have less dispersive channels than the mobile stations located at farther distances. Therefore, the required cyclic prefix size for the nearby mobile station is less than the one for the far mobile station. It is possible to exploit this feature to avoid ISI for edge windowing. The proper scheduling approach for edge windowing is to group the mobile stations with similar dispersion characteristics and to assign them to the proper subcarriers which do not cause ISI. In this section, we

[6] In [109], spike-plus-exponential model is proposed for channel power delay profile. We consider only the exponential part of this model for a pessimistic scenario.

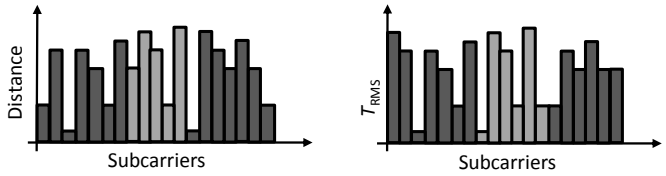

(a) Random scheduling.

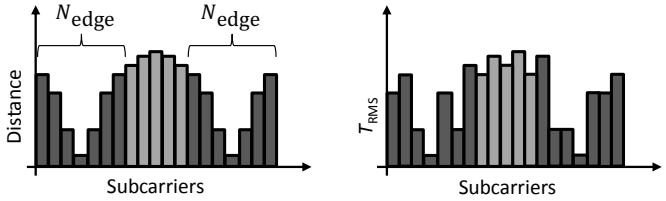

(b) Distance-based scheduling.

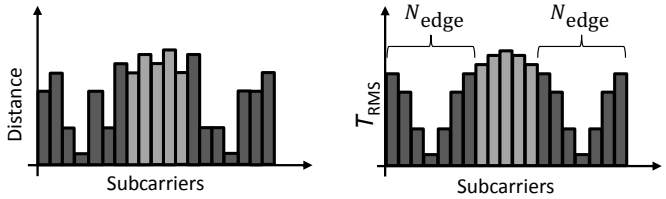

(c) Delay-spread based scheduling.

Figure 3.4 Scheduling strategies.

investigate three scheduling strategies for the edge windowing; random scheduling, distance-based scheduling and, delay-spread based scheduling.

3.4.2.1 Random Scheduling

Random scheduling strategy is considered to observe the impact of ignoring scheduling on the edge windowing. In this scheduling strategy, all the spectrum resources are distributed randomly to the mobile stations as in Figure 3.4(a). Thus, the channel dispersion characteristics and the distance between mobile stations and base station are ignored for scheduling decision.

3.4.2.2 Distance-Based Scheduling

Distance-based scheduling exploits the relation between the distance and dispersion given in (3.5). Thus, it is performed after estimating the distances of the mobile stations relative to the base stations with ranging operations. In this scheduling approach, the nearby mobile stations are assigned to the edge subcarriers, and the far mobile stations are assigned to inner subcarriers as shown in Figure 3.4(b). While the spectrum resources located at the center of

the edge subcarriers are employed for the nearest mobile station, the spectrum resources located at the center of inner subcarriers are used for the farthest mobile station.

It is worth noting that distance-based scheduling does not guarantee to group the mobile stations considering their T_{rms} values. Therefore, the mobile stations scheduled to subcarriers at the edges of the edge subcarriers (i.e. located at middle distances) can observe severe ISI because of the having probability of high T_{rms}. Also, the distribution of the distance between the mobile stations and base station for uniformly distributed mobile stations in the cell area is given by

$$f_d(d) = \frac{2d}{R^2} \ , \ 0 \leq d \leq R \, . \tag{3.6}$$

Hence, the expected number of the mobile stations at farther distances is higher than the number of the closer ones. Therefore, increasing N_{edge} also increases the probability of having ISI on these subcarriers.

3.4.3 Delay-Spread Based Scheduling

Delay-spread based scheduling is similar to the distance-based scheduling discussed in Section 3.4.2.2. However, it considers T_{rms} for each mobile stations, rather than the link distance. The mobile stations with low T_{rms} values and mobile stations with high T_{rms} values are scheduled to the edge subcarriers and inner subcarriers, respectively, as in Figure 3.4(c). While the spectrum resources located at the center of the edge subcarriers are utilized for the mobile station with lowest T_{rms}, the spectrum resources located at the center of inner subcarriers are assigned for the mobile station with highest T_{rms}.

In order to achieve delay-spread based scheduling, the base station requires the channel dispersion information of each mobile station. In most of the cases (i.e. Wi-Fi, LTE), the base station has ability to extract the downlink channels of the mobile stations. Thus, it is reasonable to have T_{rms} information of each mobile stations at the base station. Also, we should note that T_{rms} is a random variable depending on the distance between mobile station and the base station as in (3.5). Thus, T_{rms} scheduling approach does not guarantee that the mobile stations are ordered on the spectral resources considering their distances.

3.5 Numerical Results

In order to reveal the performance of edge windowing along with aforementioned scheduling strategies, we consider that $N = 1024$, $C = 128$, $T_{\text{s}} = 66.7$ μs, $N_{\text{G}} = 80$, $C_{\text{inner}} = 6$ for scheme parameters and $T_1 = 1$ μs, $\epsilon = 0.5$, and $\sigma_y = 2$ dB for the channel parameters for the urban environments. Therefore, edge windowing parameters become

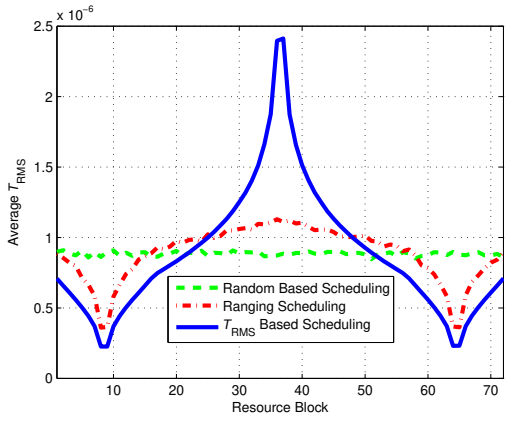

Figure 3.5 RMS delay spread on each resource block ($N_{\text{edge}} = 192$).

$0 \leq C_{\text{edge}} \leq 128$ and $0 \leq N_{\text{edge}} \leq 432$. Also, we consider 12 subcarriers (one resource block) per mobile station and 72 mobile stations which are distributed uniformly in $R = 1000$ m cell radius. All results shown are obtained over 50 OFDMA symbols per channel realization and 300 different channel realization per mobile stations.

3.5.1 Grouping Users with Same RMS Delay Spread

Average T_{rms} values of the channels on each resource block are provided in Figure 3.5 ($N_{\text{edge}} = 192$). Since random scheduling does not consider the channel dispersion characteristics and the distances, average T_{rms} does not vary over the resource blocks. For distance-based scheduling, average T_{rms} decreases on the resource blocks where the windowing is applied and it increases at the middle of the OFDMA band. Since delay-spread based scheduling exploits the knowledge of T_{rms} of each mobile station's channel, it provides a better grouping of the mobile station with the same T_{rms}. Thus, the average T_{rms} values with delay-spread based scheduling are less than the ones with distance-based scheduling at the center of the band of the edge subcarriers. Also, delay-spread based scheduling provides larger average T_{rms} values at the middle of the OFDM band.

3.5.2 Error Performance of Edge Windowing in Multi-User Environment

In order to investigate the impact of the scheduling, we simulate the average EVM on each subcarriers and average EVM at different distances for different N_{edge} values ($C_{\text{edge}} = 64$, $W_{\text{edge}} = 70$) in Figure 3.6. If the scheduling is performed randomly, the average EVM on the edge subcarriers become drastically high compared to the inner subcarriers as shown in Figure 3.6(a). Since the cyclic extension size of the edge subcarriers are insufficient for the mobile stations which have high dispersive channels, ISI reduces the EVM performances of these subcarriers significantly. Especially, it impacts the mobile stations located at farther distances. As shown in Figure 3.6(b), the

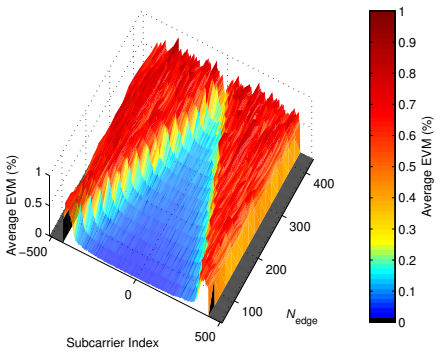

(a) Random scheduling.

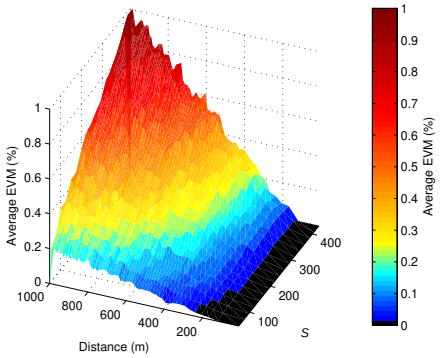

(b) Random scheduling.

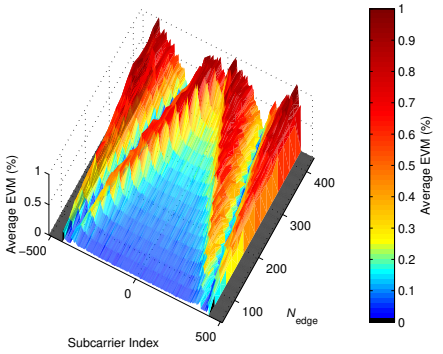

(c) Distance-based scheduling.

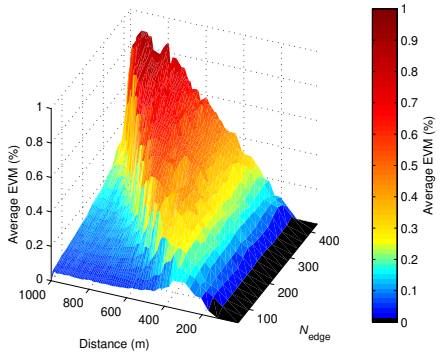

(d) Distance-based scheduling.

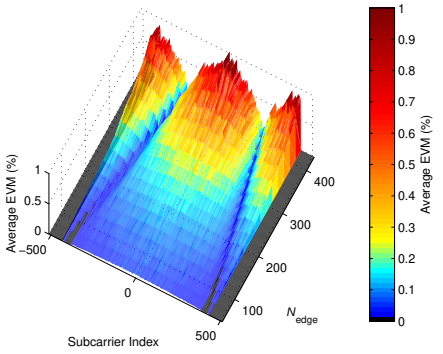

(e) Delay-spread based scheduling.

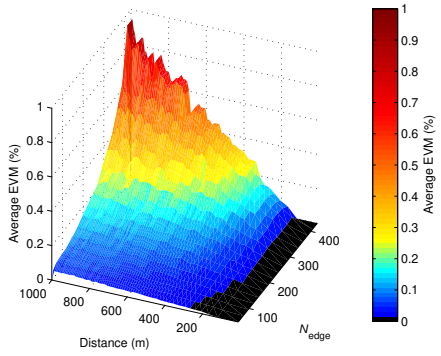

(f) Delay-spread based scheduling.

Figure 3.6 The impact of scheduling on average EVM of subcarriers ($C_{\text{edge}} = 64$, $W_{\text{edge}} = 70$, $W_{\text{inner}} = 6$).

mobile stations located at the edge of the cell observe higher average EVM. It indicates that the average EVM increases rapidly with the distance between the mobile station and base station. Also, it shows the dependency of average EVM to N_{edge}.

If the scheduling is performed considering the distance between the mobile stations and the base station, average EVM rises on the edges of the edge subcarriers as in Figure 3.6(c). It is clear that the nearby mobile stations which are assigned to the center of the edge subcarriers do not observe ISI since their channels are expected to be less dispersive. However, the mobile stations which are scheduled to the edges of the edge subcarriers can observe severe ISI due to their distances. The equation given in (3.6) shows that the average number of the mobile station increases linearly with the distance. Since more mobile stations are located at the large distances, more mobile station have the channels with high T_{rms} as shown in Figure 3.5. Therefore, the mobile stations scheduled to these subcarriers can observe high EVM with distance-based scheduling. This issue is also given in Figure 3.6(d). Since distance-based scheduling strategy assigns the edge subcarriers of the edge subcarriers to the mobile stations at middle distances, these mobile stations observe high EVM particularly. For instance, the mobile stations at 600 m away from the base station have higher average EVM than the other distances when $N_{\text{edge}} = 192$ according to the simulation results shown in Figure 3.6(d).

If the base station schedules the mobile stations considering the T_{rms} of the each mobile station's channels, EVM performances on subcarriers increase significantly as in Figure 3.6(e). Since delay-spread based scheduling provides better grouping of the mobile stations with the same T_{rms} than the distance-based scheduling, it offers better EVM performance. However, using higher N_{edge} values (i.e. $N_{\text{edge}} \geq 300$) impacts the EVM on the edges of the edge subcarriers. Also, increasing N_{edge} degrades the average EVM of the far mobile stations because they have highly dispersive channels. The relation between the distance of the mobile station and average EVM is given for different N_{edge} values in Figure 3.6(f). If we consider the $N_{\text{edge}} = 192$ for the system design, average EVM does not exceed the 0.16% in both Figure 3.6(e) and Figure 3.6(f).

3.6 Conclusion

In this study, a new windowing technique which introduces controllable trade-off between sidelobe suppression and self-interference while maintaining the spectral efficiency of OFDM is presented. Heavy windowing and light windowing are applied to edge and inner subcarriers, respectively, to improve the suppression performance of OFDM. In other words, different pulse shapes for various subcarrier groups are considered in a multicarrier scheme via edge windowing. Then, edge windowing is levitated by exploiting the multi-user environment. For the first time, the user diversity in the network is taken into account for the sake of sidelobe suppression. Self-interference due to the edge windowing is eliminated by using the discrepancy of delay-spread characteristics of the users. As a result of our analysis, a proper scheduling provides both sidelobe suppression and increments on the throughput with toler-

able error levels on subcarriers. Delay-spread based scheduling along with provides sufficient improvement on error performance of the edge windowing. In addition, it is important to emphasize that the introduced trade-off by edge windowing can be also exploited further with subcarrier-based approaches like adaptive modulation and power control to improve the performance of OFDM based wireless communication systems.

CHAPTER 4

A LATTICE ADAPTATION: CHANNEL-AWARE FRAME STRUCTURES

4.1 Introduction

Efficient usage of the electrospace with orthogonal frequency division multiplexing (OFDM) based multicarrier schemes has gained an extra importance with the recent wireless communication standards, e.g. Long Term Evolution (LTE)[1] [112]. One of the fundamental reasons of this attraction on OFDM-based multicarrier schemes is the fact that OFDM offers a simple and flexible structure to exploit the time-frequency plane efficiently, as discussed in Chapter 2. In this chapter, our focus is the further utilization of time-frequency plane for OFDM in multi-user environment. Essentially, we exploit having multiple users with different doubly dispersive channels by adapting the lattice structure of orthogonal frequency division multiple accessing (OFDMA) frame.

Subcarrier spacing and cyclic prefix (CP) duration are the two fundamental parameters that determine the lattice structure of an OFDMA frame. As a special case, larger subcarrier spacing in OFDM increase the distances between symbols in frequency while decreasing the distance between symbols in time (see the illustration provided in Figure 2.1(b)). Besides that CP corresponds to a guard period, which also increases the distance between the symbols in time. The proper choices of subcarrier spacing and CP duration are related to both frequency spread and delay spread characteristics of the channel. On one hand, a wider subcarrier spacing is desired to tolerate the inter-carrier interference (ICI) due to the frequency spreading in the channel, on the other hand, decreasing subcarrier spacing would be helpful to increase the spectral efficiency of the scheme due to less CP utilization. CP duration depends on the delay spread characteristics of the channel. While longer CP duration is desirable to avoid inter-symbol interference (ISI) between OFDMA symbols, employing shorter CP duration increases the spectral efficiency.

In the conventional lattice design for OFDM frame, subcarrier spacing and CP duration are set to certain values considering the worst case channel scenario supported by the system. Hence, fixed symbol spacings in time and frequency are used within the frame, as shown in Figure 4.1, as long as the orthogonality between subcarriers is provided sufficiently for the worst case channel scenario. However, this approach does not exploit having multiple users with different doubly dispersive channel characteristics. For example, it does not consider the nearby users

[1]The content of this section is partially published in [111]. Copyright for this publication can be found in Appendix B.

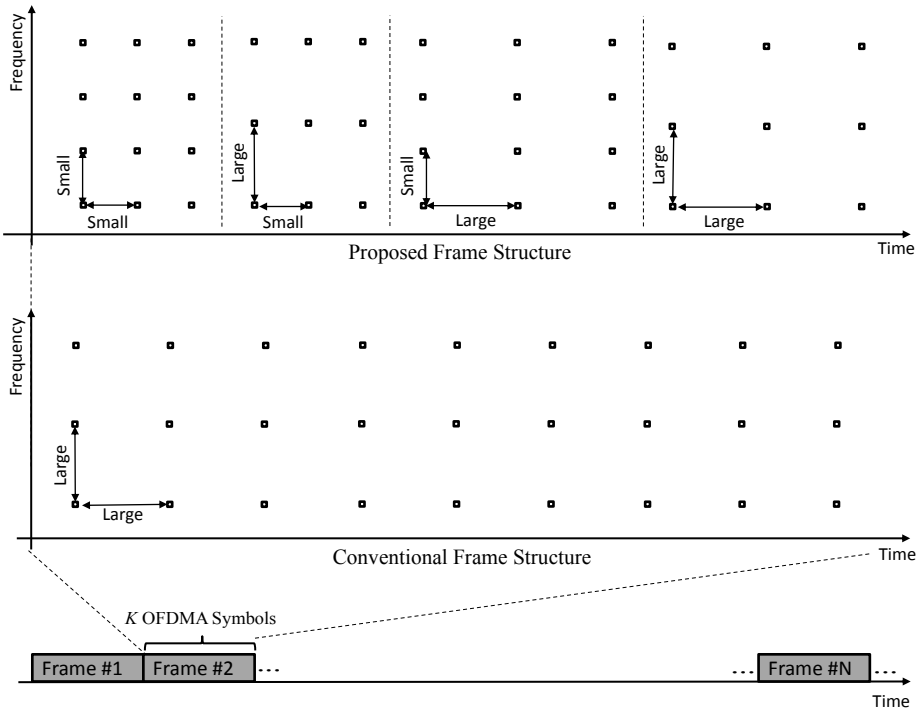

Figure 4.1 Conventional and proposed frame structures in time and frequency domains.

to the base station, which have less maximum excess delays than the worst-case scenario [110]. Also, it does not employ narrower subcarrier spacing to reduce the redundancy for stationary users. To address this issue, in this chapter, we propose doubly dispersive channel adaptive lattice structure for OFDMA frames. Multiple CP durations and multiple subcarrier spacings within the frame are employed to provide the adaptations to the doubly dispersive channels of the users, which corresponds to various spacing in time and frequency as shown in Figure 4.1. While multiple CP durations within a frame are utilized considering the distances between the users and the base station, multiple subcarrier spacings within the frame are used to increase to the frequency spread immunity of the users considering their mobility characteristics. The proposed channel-aware lattice adaptation is investigated with the statistical approaches.

The chapter is organized as follows: The studies related to the lattice adaptation for OFDM-based systems are discussed in Section 4.2. The proposed frame structure is introduced in Section 4.3. Determining the parameters of the proposed frame structure with statistical approaches is investigated in Section 4.4. An example design is presented is Section 4.5. Finally, the chapter is concluded in Section 4.6.

4.2 Related Work

In literature, it is possible to find adaptation methods on the lattice structure of OFDMA frame. In [113], adaptation on CP duration is investigated for OFDM-based systems. After the transmitter estimates the root mean square (RMS) delay spread of the channel, CP duration is adaptively selected as twice of the estimated RMS delay spread of the channel as a rule of thumb. Asserting the delay spread criterion is not sufficient to select CP duration, the system capacity is given as a function of CP duration and signal-to-noise ratio (SNR) in [114]. Based on the analysis of the distribution of the capacity, CP duration is investigated for the IEEE 802.11 channel models for the distances between 3 m and 60 m. In their following studies, the joint allocation of the power and CP duration is considered to maximize the system capacity [115] and the optimal criterion for the capacity is given to adapt CP duration considering the power line communication systems [116]. However, as indicated in [117], the approaches in [114–116] rely on given values of RMS delay spread. Therefore, being aware of the importance of the statistical knowledge of the RMS delay spread, an adaptation scheme based on a priori knowledge of the channel statistics is suggested to reduce feedback requirements in [117]. Employing the prior statistics of RMS delay spread, CP duration is optimized considering the system capacity. In [118], subcarrier spacing is dynamically changed for each OFDMA frame to increase the throughput. However, using different subcarrier spacing for each frame changes the frame duration and increases the complexity of initial accessing and synchronization algorithms. Also, if all users are mapped into the frame, performances of the users cannot be optimized with frame-to-frame adaptation. In LTE and WiMaX, adaptations on CP duration and subcarrier spacing are employed, even if these standards are based on fixed CP duration and subcarrier spacing within the frame. For example, CP duration is adaptive from one base station to another one in LTE and WiMAX systems. For example, short CP duration (4.69 μs) and long CP duration (16.6 μs) are used for small and large cells respectively, on the condition that fixed CP duration within the cell is utilized. Also, different subcarrier spacing options are allowed in fixed WiMAX by keeping the subcarrier spacing fixed for all users within a frame. In order to cope with signal-to-interference-plus-noise ratio (SINR) degradation due to the mobility, general approach is to change the coding rate and modulation order adaptively instead of subcarrier spacing. The number of subcarriers per unit bandwidth is doubled only for broadcasting scenarios in order to avoid the overhead arising from the CP in LTE [112, p. 330]. Also, the reader can find the required SINR and modulation order in [119, p. 221] for a given mobile speed (v) to obtain the desired spectral efficiency. As it can be seen from the literature, even if the studies are aware of the advantage of the variation of the user channel characteristics, to best of our knowledge, having multiple OFDMA symbols with various CP durations and subcarrier spacings within the frame is not investigated statistically in the literature.

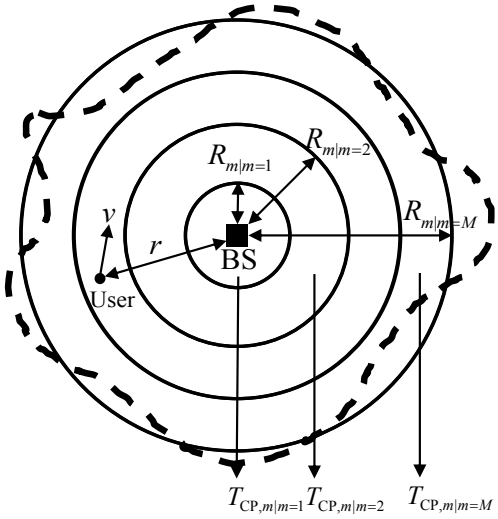

Figure 4.2 Cyclic prefix durations in the proposed frame structure are calculated by dividing the cell with circles.

4.3 Proposed Frame Structure

Proposed frame structure exploits the diversity of the users' channels in the cell. As the users have different delay spread and mobility characteristics in the cell, employing multiple CP durations and multiple subcarrier spacings yields provide spectral efficient lattice structure and immunity against frequency spreading due to the mobility. It is important to emphasize that RMS delay spread is related to the distance between the user and the base station statistically. The mathematical expression relating RMS delay spread with a certain distance is proposed in [110] as

$$T_{\mathrm{rms}} = T_1 r^{\epsilon} y \tag{4.1}$$

where r is the distance between the base station and the user in kilometers, ϵ is a distance coefficient lies between $0.5 \leq \epsilon \leq 1$, T_1[2] is the median value of RMS delay spread at $r = 1$ km, and y is a lognormal distributed random variable as

$$f_y(y) = \frac{\xi}{\sigma_y y \sqrt{2\pi}} \mathrm{e}^{-\frac{(10\log_{10} y)^2}{2\sigma_y^2}}. \tag{4.2}$$

In (4.2), ξ is $10/\ln(10)$ and σ_y is the standard deviation of y which lies as $2 \leq \sigma_y \leq 6$ in dB depending on the environment. If we assume the power delay profile of the channel decays exponentially, using the equations given

[2]Note that even if T_1 is given as a constant in [110], its value changes for a given cell type e.g. the urban microcells (0.4 μs) and urban macrocell (0.4 μs-1 μs). This change on T_1 is in favor of the proposed frame structure in terms spectral efficiency increment compared to fixed frame structure. For the sake of sticking to the proposed model in [110], T_1 is considered as a constant.

in [109], the relationship between maximum excess delay and RMS delay spread is obtained as $T_{\max} \cong \ln(X) T_{\text{rms}}$ where X shows the fall in linear scale relative to the maximum tap power. For example, if $X = 20$ dB, maximum excess delay is approximately expressed as $T_{\max} \cong 5T_{\text{rms}} = 5T_1 r^{\epsilon} y$. Thus, we can interpret that if the distance between the user and the base station increases, higher maximum excess delay values are expected. Hence, if the cell is divided into M inner circles with the radius of R_m where $m = 1, 2, ..., M$ as in Figure 4.2, the sufficient CP duration ($T_{\text{CP},m}$) for each area between consecutive inner circles is calculated statistically for a given confidence limit (γ_{CP}). The confidence limit basically gives a probability for selected CP duration which is longer than γ_{CP} of the maximum excess delay variation and it is between 0 and 1. For example, $T_{\text{CP},m}$ can be selected as high as to cover 90% of the maximum excess delay variation (which means $\gamma_{\text{CP}} = 0.9$) for given R_{m-1} and R_m. Note that since $T_{\text{CP},m} \leq T_{\text{CP},M}$, the spectral efficiency of the system will increase compared to the conventional frame structure. In addition to using different CP durations, L multiple subcarrier spacings (Δf_ℓ) are employed within the frame where $\ell = 1, 2, ..., L$. Considering the different mobility characteristics of the users, Δf_ℓ is determined for given confidence limit ($\gamma_{\Delta f}$), carrier frequency (f_c), and tolerable ICI power (P_{ICI}). Similar to γ_{CP}, $\gamma_{\Delta f}$ indicates Δf_ℓ which supports $\gamma_{\Delta f}$ portion of the users at different speeds in the cell and it lies between 0 and 1.

The number of OFDMA symbols with $T_{\text{CP},m}$ and Δf_ℓ are determined using the distributions of r and v of the users belonging to the base station, respectively. Consider that K OFDMA symbols are transmitted in the frame. The number of OFDMA symbols with same $T_{\text{CP},m}$ and the number of OFDMA symbols with same Δf_ℓ within the frame are calculated as $K_m = \rho_m K$ and $K_\ell = \rho_\ell K$, respectively. While ρ_m represents the ratio of the number of the users located in the area between the circles with R_m and R_{m-1} to the total number of users in the cell, ρ_ℓ is the probability of the covered speed variation in the cell where generated ICI is less than P_{ICI} between Δf_ℓ and $\Delta f_{\ell-1}$. Also, each group of OFDMA symbol with the same $T_{\text{CP},m}$ and Δf_ℓ is determined as $K_{m,\ell} = \rho_m \rho_\ell K$.

The duration of the proposed frame structure is less than the conventional frame structure since the proposed frame reduces the redundant CP usage. The increment on the spectral efficiency (ΔR) compared to the conventional frame structure with the same design criteria (i.e. bandwidth, P_{ICI}, γ_{CP} and $\gamma_{\Delta f}$) are calculated in percent as

$$\Delta R = \left[\sum_{\ell=1}^{L} \frac{100\rho_\ell \left(1 + \Delta f_L T_{\text{CP},M}\right)}{1 + \sum_{m=1}^{M} \rho_m \Delta f_\ell T_{\text{CP},m}} \right] - 100 \,. \tag{4.3}$$

4.4 Determining the Parameters of the Proposed Frame Structure

In this section, the selections of the parameters of the proposed frame structure are discussed. Firstly, the distributions of $T_{\max}$ and r are investigated to determine $T_{\mathrm{CP},m}$ and ρ_m, respectively. Then, the distributions of mobility in the cell is obtained to find Δf_ℓ and ρ_ℓ.

4.4.1 Determining $T_{\mathrm{CP},m}$ and ρ_m

In order to use multiple CP durations within the frame structure properly, cumulative distribution function (CDF) of maximum excess delay should be calculated for a given R_m and R_{m-1}. In order to calculate the distribution of r for a given area between consecutive circles, we rewrite (4.1) as

$$T_{\max} \cong \ln(X) T_1 r^{\epsilon} y = k r^{\epsilon} y \tag{4.4}$$

for the sake of generalization for $T_{\max}$. If we assume that the user density is uniform in the area between the consecutive inner circles, probability density function (PDF) of r is obtained as

$$f_r(r) = \frac{2r}{R_m^2 - R_{m-1}^2}. \tag{4.5}$$

We should indicate that the user density might be different in the cell. If the difference between R_m and R_{m-1} is relatively small to R, the user density in the area of the consecutive inner circles can be assumed as uniform. Therefore, considering PDF given in (4.5) would be approximately correct for other practical user densities i.e. Gaussian and exponential.

Applying the rule of function of a random variable and derivations for PDF of RMS delay spread in [110], PDF of maximum excess delay is found as

$$f_{T_{\max}}(T_{\max}) = \frac{e^{\frac{2\sigma_y^2}{\xi^2\epsilon^2}} T_{\max}^{\frac{2}{\epsilon}-1} \left[\operatorname{erf}\right|_{\frac{10}{\sqrt{2}\sigma_y}\log_{10}\left(\frac{T_{\max}}{kR_{m-1}^{\epsilon}}\right)+\frac{\sqrt{2}\sigma_y}{\xi\epsilon}}^{\frac{10}{\sqrt{2}\sigma_y}\log_{10}\left(\frac{T_{\max}}{kR_m^{\epsilon}}\right)+\frac{\sqrt{2}\sigma_y}{\xi\epsilon}}}{\epsilon k^{\frac{2}{\epsilon}}\left(R_m^2 - R_{m-1}^2\right)} \tag{4.6}$$

where $\text{erf}|_{\text{b}}^{\text{a}} = \text{erf}\,(\text{a}) - \text{erf}\,(\text{b})$ and $\text{erf}\,(\cdot)$ is Gaussian error function. Integrating (4.6), closed-form CDF of maximum excess delay is obtained as

$$\text{F}_{T_{\max}}\left(T_{\max}\right) = \frac{1}{2} - \frac{\text{e}^{\frac{2\sigma_y^2}{\xi^2\epsilon^2}} T_{\max}^{\frac{2}{\epsilon}} \left[\Lambda(T_{\max}, R_m) - \Lambda(T_{\max}, R_{m-1})\right]}{2k^{\frac{2}{\epsilon}} \left(R_m^2 - R_{m-1}^2\right)} \tag{4.7}$$

where

$$\Lambda(T_{\max}, Z) = \text{erf}\left(\frac{10}{\sqrt{2}\sigma_y} \log_{10}\left(\frac{T_{\max}}{kZ^{\epsilon}}\right) + \frac{\sqrt{2}\sigma_y}{\xi\epsilon}\right) - e^{-\frac{2\sigma_y^2}{\xi^2\epsilon^2}} \left(\frac{T_{\max}}{kZ^{\epsilon}}\right)^{-\frac{2}{\epsilon}} \text{erf}\left(\frac{10}{\sqrt{2}\sigma_y} \log_{10}\left(\frac{T_{\max}}{kZ^{\epsilon}}\right)\right). \tag{4.8}$$

Therefore, $T_{\text{CP},m}$ is calculated as

$$\text{F}_{T_{\max}}\left(T_{\text{CP},m}\right) \geq \gamma_{\text{CP}} \tag{4.9}$$

using (4.7) for given T_1, R_m, R_{m-1} and γ_{CP}. In order to calculate the number of OFDMA symbols with the same CP duration within the frame, the probability of having of a user being in the area between consecutive circles should be calculated. Once it is obtained via CDF of r for given R_m and R_{m-1}, ρ_m is obtained by calculating

$$\rho_m = \text{F}_r\left(R_m\right) - \text{F}_r\left(R_{m-1}\right) \tag{4.10}$$

for every m.

Heuristically, we assume that geographical user distribution is uniform in the area. However, note that even if the geographical user density is uniform, the users linked to the corresponding base station might not be uniform depending on the overlapping cell scenarios and shadowing characteristics of the environment [120]. In order to obtain a realistic user distance distribution, the methodology introduced in [120] is followed. In the geographical environment, average path loss and shadowing are modeled as $\overline{L}(\cdot) = A + B\log_{10}(\cdot)$ and lognormal distribution with σ standard variation, respectively. K base stations with equal transmission power (P_{tx}) are deployed at (r_k, θ_k) coordinates with equal distance (L_{d}). Additionally, the users are shared between base stations according to the received signal strength indicator (RSSI) measurements. Therefore, by defining the link probability between a user located at (r, θ) and kth base station as

$$\mathcal{P}_k\left(r, \theta\right) = \frac{1}{2} - \frac{1}{2}\text{erf}\left(\frac{P_{\min} + \Delta - P_{\text{tx}} + \overline{L}(d_k(r, \theta))}{\sqrt{2}\sigma}\right)$$

where $P_{\min}$ is the receiver sensitivity, Δ is the handover margin [121, Ch. 2], the distance between user and kth base station is given by

$$d_k(r,\theta) = \sqrt{r^2 + r_k^2 - 2rr_k\cos(\theta - \theta_k)}\,, \tag{4.11}$$

and the distribution of r is given by

$$f_r(r) = \frac{\int_0^{2\pi} \mathbf{P}(r,\theta) r d\theta}{\int_0^{\infty}\int_0^{2\pi} \mathbf{P}(r,\theta) r d\theta dr} \tag{4.12}$$

where

$$\mathbf{P}(r,\theta) = \sum_{i=1}^{K} \gamma(r,\theta)\mathcal{P}_1(r,\theta)\mathbf{C}_{i-1}(r,\theta)\,, \tag{4.13}$$

$$\mathbf{C}_x(r,\theta) = \sum_{\forall \mathcal{L}\in\mathcal{K}_x} \prod_{\substack{l\in\mathcal{L} \\ m\in\mathcal{L}^c}} \mathcal{P}_l(r,\theta)(1-\mathcal{P}_m(r,\theta))\,. \tag{4.14}$$

In (4.13) and (4.14), $\mathbf{P}(r,\theta)$ is the probability of establishing a link between a user located at (r,θ) to the $(k=1)$th base station considering all other deployed base stations, i is the sharing index, $\gamma(r,\theta)$ is the user sharing function which is suggested as the ratio of the received signal power from $(k=1)$th base station to the summation of the received signal powers from all base stations for RSSI based sharing, $\mathbf{C}_x(r,\theta)$ is the probability of observing x base stations (excluding $(k=1)$th base station) which can provide power more than $P_{\min}+\Delta$ at the receiver, $\mathcal{K}_x$ is the set of index subset generated with x-combinations of $\{2,...,K\}$, $\mathcal{L}$ and $\mathcal{L}^c$ are index set and complementary index set, respectively. By evaluating the integration of (4.12), it is possible to solve (4.10) for the sake obtain realistic ρ_m values.

4.4.2 Determining Δf_ℓ and ρ_ℓ

In the literature, the mobility of the user is modeled with several PDFs, e.g., beta distribution [122] and Rice-plus-normal distribution [123] including both urban streets and major roads. It is possible to find mobility models which also take the car stops at crossroads [124] and different the street patterns [125] into account. Since the suggested mobility model in [123] includes the validation with measurements, we consider the mobility model as

$$f_v(v) = (1-p_{\text{road}})\frac{v}{\sigma_v^2}\mathrm{e}^{-\frac{v^2+\bar{v}_{\text{city}}^2}{2\sigma_v^2}} I_0\left(\frac{v\bar{v}_{\text{city}}}{\sigma_v^2}\right) + p_{\text{road}}\frac{1}{\sigma_v\sqrt{2\pi}}\mathrm{e}^{-\frac{(v-\bar{v}_{\text{road}})^2}{2\sigma_v^2}} \tag{4.15}$$

where p_{road} is the probability of cars on the major roads, $\bar{v}_{\text{city}}$ is the mean speed in the city, $\bar{v}_{\text{road}}$ is the mean speed of the major-road traffic, σ_v is the deviation of the speed, and $I_0(.)$ is the modified Bessel function of the first kind with order zero. Integrating (4.15), CDF of v is obtained as

$$\mathrm{F}_v(v) = (1 - p_{\text{road}})\left[1 - Q_1\left(\frac{\bar{v}_{\text{city}}}{\sigma_v}, \frac{v}{\sigma_v}\right)\right] + p_{\text{road}}\left[1 - Q\left(\frac{v - \bar{v}_{\text{road}}}{\sigma_v}\right)\right] \tag{4.16}$$

where $Q_1(\cdot,\cdot)$ is the Marcum Q-function [126] and $Q(\cdot)$ is the Q-function.

Universal upper bound of the relative ICI power leaking from the normalized signal power due to the mobility is given by [127]

$$P_{\text{ICI}} \leq \frac{1}{12}\left(2\pi\frac{f_{\text{d}}}{\Delta f}\right)^2 = \frac{1}{12}\left(2\pi\frac{v f_{\text{c}}}{c\Delta f}\right)^2 \tag{4.17}$$

where f_{d} is the maximum Doppler shift and c is the speed of the light. Therefore, combining (4.16) and (4.17), CDF of Δf is derived as

$$\mathrm{F}_{\Delta f}(\Delta f) = \mathrm{F}_v\left(v = \frac{\sqrt{3P_{\text{ICI}}}}{\pi\frac{f_{\text{c}}}{c\Delta f}}\right). \tag{4.18}$$

Using (4.18), Δf_L is obtained as

$$\mathrm{F}_{\Delta f}(\Delta f_L) \leq \gamma_{\Delta f}. \tag{4.19}$$

Since each selected Δf_ℓ indicates a speed limit on the curve of $\mathrm{F}_{\Delta f}(\Delta f_L)$ for a given P_{ICI}, ρ_ℓ is found as

$$\rho_\ell = \mathrm{F}_{\Delta f}(\Delta f_\ell) - \mathrm{F}_{\Delta f}(\Delta f_{\ell-1}). \tag{4.20}$$

4.5 A Design Example

A design example is given in order to compare analytical findings with simulations and to investigate the performance of proposed frame structure. An urban environment where the path loss characteristics is modelled as *Urban Macro (UMa)* with the parameters given in [128] is taken into account. Operating frequency is set to 2 GHz. Thus, the path loss parameters are obtained as $A = 19.6$ and $B = 39$, and $\sigma = 4$ dB. The channel scattering in time is modeled with exponential decaying power delay profile where $X = 20$ dB. In addition, ϵ, σ_y, and T_1 are selected as 0.5, 2 dB, and 0.41μs, respectively [110]. In the area, 7 base stations are deployed considering hexagonal tessellation

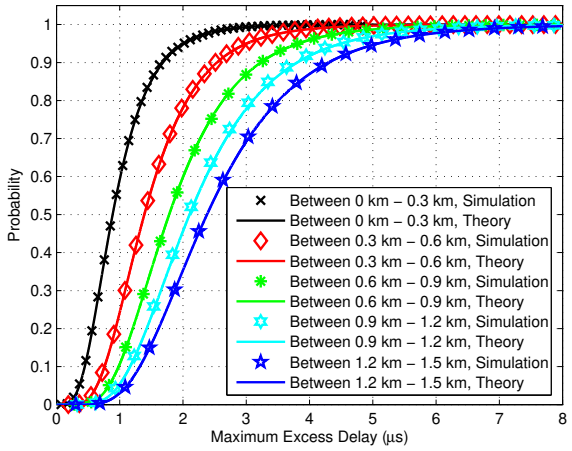

Figure 4.3 CDF of maximum excess delay spread for the area between consecutive inner circles.

where $L_{\mathrm{d}} = 2400$ m. Also, Δ and P_{tx} is set to 4 dB and 36 dBm, respectively. The frame structure is generated with $K = 140$ OFDMA symbols. In order to construct the frame structure of the center base station, we divide the cell into $M = 5$ circles where $R_{m|m=1,2,\ldots,5} = [0.3,\ 0.6,\ 0.9,\ 1.2,\ 1.5]$ in kilometers.

In Figure 4.3, theoretical and simulation results for CDF of maximum excess delay are given for the area between the circles with radius of R_m and R_{m-1}. Monte Carlo simulations match with the closed-form CDF in (4.6). If γ_{CP} is selected 0.95, sufficient $T_{\mathrm{CP},m|m=1,2,\ldots,5}$ are obtained as $[2,\ 3,\ 3.8,\ 4.5,\ 5.1]$ in μs. Therefore, if the conventional approach is employed for the same range, all OFDMA symbols should have at least $5.1\mu s$ for the CP duration for the same γ_{CP}. In the proposed frame structure, 5 different CP durations which are between 2-5.1 μs are used in one frame. In Figure 4.4, CDF of r is given using (4.12) in order to obtain the number of OFDMA symbol with $T_{\mathrm{CP},m}$ within the frame. The values of $\rho_{m|m=1,2,\ldots,5}$ are obtained approximately as $9\%,\ 26\%,\ 37\%,\ 23\%,\ 5\%]$.

Table 4.1 The number of OFDMA symbols with different cyclic prefix durations and subcarrier spacings within the frame.

$T_{\mathrm{CP},m\|m=1,2,\ldots,5}$	=	$2\mu s$	$3\mu s$	$3.8\mu s$	$4.5\mu s$	$5.1\mu s$
$\Delta f_{\ell\|\ell=1} = 7.5$ kHz	$\Rightarrow$	7	19	27	17	3
$\Delta f_{\ell\|\ell=2} = 15$ kHz	$\Rightarrow$	5	13	19	12	3
$\Delta f_{\ell\|\ell=3} = 20$ kHz	$\Rightarrow$	1	4	5	4	1
$K_{m,\ell\|m=1,2,\ldots,5}$	=	13	36	51	33	7

For the mobility model, we consider $p_{\mathrm{road}} = 0.4$, $\bar{v}_{\mathrm{city}} = 20$ km/h, $\bar{v}_{\mathrm{road}} = 70$ km/h, and $\sigma_v = 15$ km/h. Considering $\gamma_{\Delta f} \cong 1$ for $P_{\mathrm{ICI}} = -35$ dB, three different Δf_ℓ where $\Delta f_{\ell|\ell=1,2} = [7.5,\ 15,\ 20]$ kHz are determined to employ in the frame. CDF of Δf which satisfies $P_{\mathrm{ICI}} = -35$ dB upper bound is given in Figure 4.5. Y-axis of CDF curve shows the supported portion of the speed variation in the cell. When the subcarrier spacing is selected as 7.5

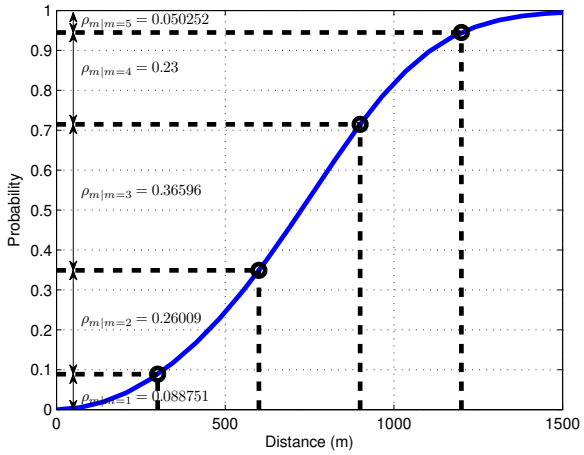

Figure 4.4 The probability of having a user between circle with radius of R_m and R_{m-1} also represents ρ_m.

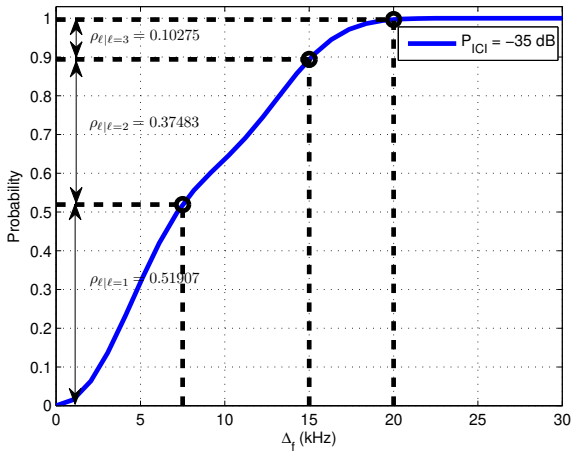

Figure 4.5 CDF of subcarrier spacing which satisfies $P_{\text{ICI}} = -35$ dB upper bound where y-axis represents the portion of the covered speed variation in the cell.

kHz, ICI will be less than -35 dB for $v \leq 40$ km/h according to (4.17). On the other hand, ICI will be less than -35 dB for $v \leq 80$ for $\Delta f = 15$ kHz and $v \leq 105$ km/h for $\Delta f = 20$ kHz. Therefore, $\rho_{\ell|\ell=1,2,3}$ are obtained over calculating the probability of less than 40 km/h, the probability of having between 40 km/h and 80 km/h and the probability of having between 80 km/h and 105 km/h using Figure 4.5 as [52%, %38, 10%], respectively. As a result, 52%, 38% and 10% of 140 OFDMA symbols have the same subcarrier spacings of 7.5 kHz, 15 kHz and 20 kHz, respectively. The number of OFDMA symbols with same CP size and subcarrier spacing in the frame structure are obtained as in Table 4.1. The increment on the spectral efficiency becomes nearly 5.5% according to (4.3). In order to compare the increment on the spectral efficiency, the redundancy caused by CP duration is around 7% in LTE [119, p. 217].

4.6 Conclusion

In this chapter, a channel-aware OFDMA frame structure is proposed to exploit the doubly dispersive channels of the users. Multiple CP durations and multiple subcarrier spacings are employed in the proposed frame structure. The values of CP sizes and subcarrier spacings which will be utilized in one frame are obtained based on a priori knowledge of the statistical characteristics of $T_{\max}$ and the user velocity in the cell. By employing proposed frame structure, nearly %5.5 increment on the spectral efficiency compared to frame structure designed for the worst case scenario is achieved by reducing redundant CP usage. At the same time, more frequency spread immune frame structure is obtained.

Note that having multiple CP durations and subcarrier spacings within the frame impacts the media access control (MAC) layer. While the users are assigned anywhere within the frame in the conventional scheduling, the resource blocks which are suitable for the users are limited in the proposed frame structure. This might impact the flexibility of the MAC protocols. Besides that, the time and frequency spread statistics are required for the proposed structure. The static adaptation with the proposed frame structure might be problematic considering several issues which requires dynamic adaptations. As an extension of this investigation, requiring feedback information, dynamic adaptations methods and scheduling which consider the channel quality information can be investigated in order to yield better frame structures.

CHAPTER 5

PARTIAL OVERLAPPING TONES FOR UNCOORDINATED NETWORKS

5.1 Introduction

Traditional broadband wireless networks have been strained with emerging demands such as being always-connected to the network and very high throughput to satisfy data-hungry applications such as real-time video. Satisfaction of these demands constitutes the main driving force for heterogeneous networks (HetNets) in which multiple tiers with varying coverage co-exist over the same network. In HetNets, interference among the tiers or the devices might dominate the noise and create interference-limited networks. The interference issues become prominent especially when dense and unplanned deployments such as device-to-device (D2D) communications are taken into account. Considering this issue, a new technique in which certain features of the waveform itself are used to mitigate the interference is proposed.

A waveform, which is one of the core elements determining the characteristics of a communication system, describes the formation of associated resources in signal space [30, 129]. Robustness of the transmitted signal to dispersion in the transmission medium, channel access, and hardware complexity are just few features affected by the selected waveform. Hence, waveform design should be able to address the requirements specified by the system. When the performance of the network is limited by noise, main consideration for the waveform design can naturally be on individual link properties such as reducing the interference created by the time and frequency dispersion of the channel [130]. However, interference created by other users is many times a major factor limiting the performance of a network and as such the impact of the other-user interference might be more significant compared to the interference due to the channel dispersion. *Conventionally*, the interference between the devices are elaborated with the approaches which question the amount of the interference power at the receiver location without including the impact of the waveform itself. Most of the solutions devised to address the interference problem rely either on media access control (MAC) based coordination or interference cancellation. For example, interference coordination mechanisms with proper scheduling and resource allocation aim to minimize the interference power [131]. In physical layer, methods like interference cancellation [132], multiuser detection [133], and interference alignment [134] mitigate the other-

user interference by exploiting the difference between desired and interfering signal strengths, codes, and multipath channel.

As opposed to the conventional solutions, in this chapter, a new concept based on utilizing the time-frequency characteristics of waveforms to reduce the other-user interference is proposed. The main contributions of this study are:

- We introduce the concept of partially overlapping tones (POT) in which it is allowed for subcarriers allocated to interfering links to partially overlap. The overlap is achieved by introducing an intentional CFO between the links and its amount is controlled by appropriately designing the time-frequency utilization of the waveforms.
- It is shown that with orthogonal waveforms, there is a tradeoff between other-user interference and spectral efficiency. Mitigation of the other-user interference can be achieved at the expense of a loss in spectral efficiency.
- It is further shown that with non-orthogonal waveforms, there is a tradeoff between other-user interference and self-interference. Mitigation of the other-user interference can be achieved at the expense of increased self-interference while spectral efficiency remains unchanged.
- A tractable bit error rate (BER) analysis for an uncoordinated network deployment is provided. The analysis allows to understand the system performance for various network densities and waveform designs.

The rest of chapter is organized as follows: Related work is discussed in Section 5.2. The system model including the physical layer parameters is provided in Section 5.3 while the concept of POT for orthogonal and non-orthogonal waveform structures is introduced in Section 5.4. Then, bit error rate (BER) analysis is provided in Section 5.5 and numerical results evaluating the performance of the proposed approach are provided in Section 5.6. Finally, the chapter is concluded in Section 5.7.

5.2 Related Work

The concept of overlapping wireless channels exists within the several 802.11 families (e.g. Wi-Fi systems). However, the simultaneous access to the channels is usually avoided due to interference. The utilization of overlapping channels to improve throughput has been investigated in several papers [135–140]. In [135], it is emphasized that the channel separation between the two pairs of Wi-Fi nodes can be interpreted as the physical separation between the nodes. Therefore, if partially overlapping channels are used carefully, it can provide greater spatial re-use. These

papers consider the total spectrum utilization of the transmission, and do not show the impact of the partial overlapping on *individual subcarriers*. To the best of our knowledge, detailed time-frequency analysis on the interference due to the partially overlapping pulse shapes is not available in the literature.

Some of the challenging aspects of the other-user interference are its asynchronous nature and its statistical characterization, which depend on the deployment model and waveform structure utilized in the network. orthogonal frequency division multiplexing (OFDM) is a well-investigated multicarrier scheme in case of asynchronous interference, e.g., femtocell-macrocell coexistence [141–143]. By providing some timing offset between the tiers intentionally, the different types of the interference, i.e. inter-carrier interference (ICI) and inter-symbol interference (ISI), is converted into each other in [143]. Yet, the total other-user interference is kept constant. A theoretical BER analysis investigating ISI versus ICI trade-offs in OFDM downlink is provided in [144]. In [145], BER degradation due to the adjacent channel interference is investigated by emphasizing superiority of filter bank multicarrier (FBMC) based cellular systems over an OFDM based approach. Although these investigations provide useful intuitions on the performance degradation, the analyses are performed for idealistic assumptions, such as grid-based cell deployment and uniform user density. In [146], it is emphasized that even if the geographical user density is uniform, the distance of the users linked to the corresponding serving points might not be uniform due to the irregular base station deployment and shadowing characteristics. In [147, 148], homogeneous Poisson point processes (PPP) are considered to model the deployment of the base stations. This approach, which is pessimistic compared to highly idealized grid-based models and real deployment scenarios, yields a tractable tool which exploits the stochastic geometry. In the following studies, e.g., [149] and [150], analytical models for uplink and K-tier heterogeneous networks are provided using PPPs.

Investigation on the impact of PPPs on physical layer is limited, but available. For example, coexistence between ultra wide band (UWB) and narrow band systems is investigated using PPPs and impact of pulse shape is emphasized for aggregate network emission [147]. In [151], error rate analyses are provided for quadrature amplitude modulation (QAM) and phase shift keying (PSK) modulations using PPPs, excluding the impact of waveforms.

5.3 System Model

Consider an uncoordinated network where transmission points (TP) and their corresponding reception points (RP) are distributed in an area as a realization of homogeneous 2-D PPP of Φ with the intensity λ as in Figure 5.1. Interfering TPs and the RP investigated are called as *aggressors* and *victim*, respectively. Without any loss of generality, victim is located at the origin of the polar coordinates (0,0). The distance between the ith aggressor and the victim is given as r_i. Minimum distance between the aggressors and the victim is set to $r_{\min}$. While the distance between RP and

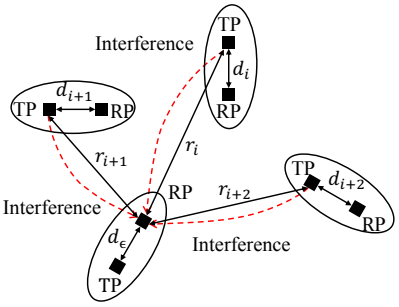

Figure 5.1 Illustration of interference in an uncoordinated network.

its associated TP for *i*th aggressor link is denoted by d_i, the same distance is expressed by d_ϵ for the desired link for the victim. Also, it is assumed that aggressors are farther away than d_ϵ, i.e., $r_i > r_{\min} \geq d_\epsilon$, which is widely considered for the interference analyses based on PPPs [152]. In the following subsections, signal model for transmission and reception based on multicarrier schemes and channel model that includes large and small scale effects are given for further discussions on partially overlapping tones (POT).

5.3.1 Signal Model for Transmission

The transmitted signal from the desired TP and the transmitted signal from the *i*th aggressor are given by

$$s^{\epsilon}(t) = \sum_{n=-\infty}^{\infty} \sum_{l=0}^{N-1} X_{nl}^{\epsilon} g_{nl}^{\epsilon}(t) \,, \tag{5.1}$$

and

$$s^{i}(t) = \sum_{n=-\infty}^{\infty} \sum_{l=0}^{N-1} X_{nl}^{i} g_{nl}^{i}(t) \,, \tag{5.2}$$

respectively, where X_{nl}^{ϵ} and X_{nl}^{i} are the information symbols which are independent and identically distributed (i.i.d) with zero mean on the *l*th subcarrier and *n*th symbol, N is the number of subcarriers, and $g_{nl}^{\epsilon}(t)$ and $g_{nl}^{i}(t)$ are the *synthesis functions* which map information symbols into time-frequency plane based on a rectangular lattice as

$$g_{nl}^{\epsilon}(t) = g^{\epsilon}\left(t - n\tau_0\right) e^{j2\pi l \nu_0 t} \tag{5.3}$$

and

$$g_{nl}^{i}(t) = g^{i}\left(t - n\tau_0\right) e^{j2\pi l \nu_0 t} \,. \tag{5.4}$$

The family of functions in (5.3) and (5.4) are often referred to as *Gabor frame* or *Weyl-Heisenberg frame*, where $g^{\epsilon}(t)$ and $g^{i}(t)$ are the prototype filters employed at the transmitters, ν_0 is the subcarrier spacing and τ_0 is the symbol spacing [2, 27]. For the sake of notation simplicity, ν_0 and τ_0 are given in units of F and T, respectively (e.g., $\nu_0 = 1.2 \times F$ and $\tau_0 = 1.3 \times T$), where $F = 1/T$ and F is a number based on the design. Without loss of generality, the energy of $g^{\epsilon}(t)$ and the energy of $g^{i}(t)$ are normalized as

$$\|g^{\epsilon}(t)\|^2_{\mathcal{L}^2(\mathbb{R})} = \|g^{i}(t)\|^2_{\mathcal{L}^2(\mathbb{R})} = \int_{-\infty}^{\infty} |g^{\epsilon}(t)|^2 \, \mathrm{d}t = 1 \, , \tag{5.5}$$

where $\mathcal{L}^2(\mathbb{R})$ denotes the square-integrable function space over $\mathbb{R}$ and $\|\cdot\|$ is the $\mathcal{L}^2$-norm of function.

5.3.2 Large Scale Impacts

Considering various path loss models depending on the environment, the path loss is characterized by $L_{\mathrm{m}}(\cdot) = a + b \log_{10}(\cdot)$ where the path loss parameters a and b are scalars and the argument is the distance in meters. The received interference power from the ith aggressor and the desired signal power at victim location per subcarrier are denoted by P_i and P_{ϵ}, respectively. Impact of shadowing is not considered in this study. Main reason for this issue is to give insights on the POT rather than introducing extra complexity for the system model. However, using the methodologies proposed for the moment generation function of the summations of lognormal distributed lognormal variables [153] and [154], it is possible to include the impact of shadowing on the investigation.

For the link transmission, open loop fractional power control is applied and some amount of the path loss, i.e., $\beta(a + b \log_{10}(\cdot))$, is compensated, where $\beta \in [0, 1]$ is the path loss compensation parameter. Note that TP might transmit with the maximum transmit power in some cases. However, since link distances considered are small, the possibility of transmission at maximum power is excluded.

5.3.3 Small Scale Impacts

Time-varying multipath channel is taken into account between all RPs and TPs. Channel impulse response is characterized by $h(\tau, t) = \sum_{\ell=0}^{L-1} \varrho_{\ell}(t) \delta(\tau - \tau_{\ell})$ where L denotes the total number of multipaths, ℓ is the path index, and τ_{ℓ} is the delay of the ℓth path. It is assumed that the path gains, $\varrho_{\ell}(t)$, are independent and identically distributed variables and the signals experience Rayleigh fading, which is a common model for interference analysis. Also, the expected channel power is considered as $\sum_{\ell=0}^{L-1} \mathbb{E}\left[|\varrho_{\ell}(t)|^2\right] = 1$. For the sake of notation, the channel between ith interfering TP and the victim RP and the channel between desired TPs and the victim RP are expressed as $h_i(\tau, t)$ and $h_{\epsilon}(\tau, t)$, respectively.

5.3.4 Synchronization

As discussed in [155] and [156], synchronization to the received signal in the presence of interference might be challenging, especially at low signal-to-interference-plus-noise ratio (SINR)s. However, the impairments like timing offset and carrier frequency offset (CFO) are often related to the preamble structure rather than the data portion of the frame. Therefore, perfect synchronization at the pair of interest is assumed. Besides, timing misalignment between the aggressor's signals and synchronization point of the victim is taken into account. The timing misalignment of ith aggressor signal with respect to the synchronization point of the victim RP is denoted by Δt_i and its distribution $f_{\Delta t_i}(\Delta t_i)$ is assumed as uniform between 0 and τ_0. Besides, intentional CFO between ith aggressor and the victim RP is given by Δf_i in order to generate POT which is discussed in Section 5.4. The impact of CFO due to the hardware mismatches between the aggressor's signals and desired signal is ignored. This is because of the fact that the impact of CFO due to the hardware mismatches is relatively smaller than Δf_i for POT. For example, when carrier spacing is set to 15 kHz and CFO is 500 Hz, normalized CFO becomes 0.033 (500 Hz / 15 kHz). However, the amount of normalized Δf_i for POT, throughout the study, is at least 0.5, which is significantly larger than CFO due to the hardware error.

5.3.5 Signal Model for Reception

Considering all interfering TPs, and assuming a wide-sense stationary uncorrelated scattering (WSSUS) channel model [98], the received signal at the victim is obtained as

$$r(t) = \underbrace{\sqrt{P_\epsilon}\int_\tau\int_\nu H_\epsilon(\tau,\nu)s^\epsilon(t-\tau)e^{j2\pi\nu t}\mathrm{d}\nu\mathrm{d}\tau}_{\text{Desired signal}} + \underbrace{\sum_{i\in\Phi}\sqrt{P_i}\int_\tau\int_\nu H_i(\tau,\nu)s^i(t+\Delta t_i-\tau)e^{j2\pi\nu t}\mathrm{d}\nu\mathrm{d}\tau}_{\text{Interfering signals}} + \underbrace{w(t)}_{\text{Noise}} \tag{5.6}$$

where $H_\epsilon(\tau,\nu)$ and $H_i(\tau,\nu)$ are the Fourier transformations of $h_\epsilon(\tau,t)$ and $h_i(\tau,t)$, respectively, and $w(t)$ is the additive white Gaussian noise (AWGN) with zero mean and variance σ^2_{noise}. In order to get the information symbol on the kth subcarrier and mth symbol, the received signal is correlated by the *analysis function* where $\gamma^\epsilon_{mk}(t) = \gamma^\epsilon(t-m\tau_0)e^{j2\pi k\nu_0 t}$. Then, the output of the correlator is sampled with the sampling period to obtain the received symbol as

$$\begin{aligned}\tilde{X}^\epsilon_{mk} &= \langle r(t),\gamma^\epsilon_{mk}(t)\rangle \triangleq \int_t r(t)\gamma^{\epsilon*}_{mk}(t)dt \\ &= \underbrace{\sqrt{P_\epsilon}X^\epsilon_{mk}A^\epsilon_{mkmk}}_{\text{desired part}} + \underbrace{\sqrt{P_\epsilon}\sum_{\substack{n=-K+1\\ n\neq m}}^{K-1}\sum_{\substack{l=0\\ l\neq k}}^{N-1}X^\epsilon_{nl}A^\epsilon_{nlmk}}_{\text{self-interference part}} + \underbrace{\sum_{i\in\Phi}\sqrt{P_i}\sum_{n=0}^{K-1}\sum_{l=0}^{N-1}X^i_{nl}A^i_{nlmk}}_{\text{other-user interference}} + \underbrace{W_k}_{\text{noise}},\end{aligned} \tag{5.7}$$

$$A^{\epsilon}_{nlmk} = \int_{\tau}\int_{\nu} H_{\epsilon}(\tau,\nu)\int_{t} g^{\epsilon}_{nl}(t-\tau)\gamma^{\epsilon *}_{mk}(t)e^{j2\pi\nu t}\mathrm{d}t\mathrm{d}\nu\mathrm{d}\tau\ , \tag{5.8}$$

$$A^{i}_{nlmk} = \int_{\tau}\int_{\nu} H_{i}(\tau,\nu)\int_{t} g^{i}_{nl}(t-\Delta t_i-\tau)e^{j2\pi\Delta f_i(t-\Delta t_i-\tau)}\gamma^{\epsilon *}_{mk}(t)e^{j2\pi\nu t}\mathrm{d}t\mathrm{d}\nu\mathrm{d}\tau\ , \tag{5.9}$$

and A^{i}_{nlmk} and A^{ϵ}_{nlmk} show the correlation between the symbols (n,l) and (m,k) including the dispersion due the channel. As it is seen in (5.7), while other-user interference is caused by aggressor links, self-interference can occur due to the time-varying multipath channel, hardware impairments, or non-Nyquist filter utilization. Considering (5.7), SINR can be expressed as

$$\mathrm{SINR} = \frac{\overbrace{\left|A^{\epsilon}_{mkmk}\right|^2}^{G_{\epsilon}}}{\underbrace{\underbrace{\sum_{\substack{n=-K+1\\ n\neq m}}^{K-1}\sum_{\substack{l=0\\ l\neq k}}^{N-1}\left|A^{\epsilon}_{nlmk}\right|^2}_{I_{\mathrm{self}}} + \underbrace{\sum_{i\in\Phi}\frac{P_i}{P_{\epsilon}}\underbrace{\sum_{n=-K+1}^{K-1}\sum_{l=0}^{N-1}\left|A^{i}_{nlmk}\right|^2}_{G_i}}_{I_i}}_{I_{\mathrm{other}}} + \frac{\sigma^2_{\mathrm{noise}}}{P_{\epsilon}}}_{I_{\mathrm{total}}}}\ , \tag{5.10}$$

where K is the filter length in terms of symbol spacing, I_{total} is the total interference, I_{self} and I_{other} are the self-interference and other-user interference, respectively, I_i is the interference due to ith aggressor, G_{ϵ} and G_i are the interference gains including fading and filter characteristics, and

$$\frac{P_i}{P_{\epsilon}} = d_{\epsilon}^{\frac{b-\beta b}{10}} d_i^{\frac{\beta b}{10}} r_i^{\frac{-b}{10}}\ . \tag{5.11}$$

Note that K is related to the representation of the filter in time domain. As long as K is selected properly, the filter truncation has a minor impact on self-interference compared to the interference due to the time-varying multi-path channel or hardware impairments at the RP and/or TP. While G_{ϵ} is a random variable with unit mean exponential distribution because of the Rayleigh fading [144, 145], G_i can be characterized for a given Δt_i and Δf_i by exponential distribution where its mean is given by

$$\sigma^2_i(\Delta t_i,\Delta f_i) = \sum_{n=0}^{K-1}\sum_{l=0}^{N-1}\left|\langle g^{i}_{nl}(t-\Delta t_i)e^{j2\pi\Delta f_i t},\gamma^{\epsilon}(t)\rangle\right|^2\ , \tag{5.12}$$

Conventionally, $\sigma^2_i(\Delta t_i,\Delta f_i)$ is considered as 1 for link-level analyses [148], similar to the mean of G_{ϵ}. However, expressing it as in (5.12) gives flexibility to include the impact of transmit and receive filters and calculate interference

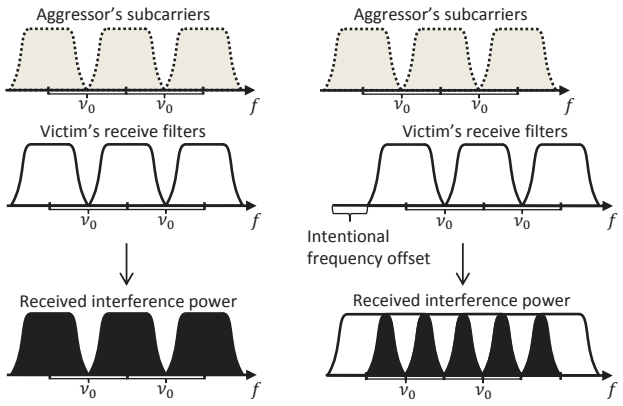

(a) Fully overlapping tones. (b) Partially overlapping tones.

Figure 5.2 Illustrations for full overlapping and partial overlapping.

when an additional processing is performed to reduce other-user interference. Finally, I_{self} is also a random variable with exponential distribution where, considering the Rayleigh fading assumption [145], its mean is given by

$$\sigma^2_{\text{self}} = \sum_{\substack{n=-K+1 \\ n\neq m}}^{K-1} \sum_{\substack{l=0 \\ l\neq k}}^{N-1} \left| \langle g^{\epsilon}_{nl}(t), \gamma^{\epsilon}(t) \rangle \right|^2 . \tag{5.13}$$

Essentially, calculations of both σ^2_{self} and $\sigma^2_i(\Delta t_i, \Delta f_i)$ are based on the projection operation onto receive filters, which can be derived via corresponding ambiguity functions [129].

5.4 Partially Overlapping Tones

The main goal of the POT is to mitigate other-user interference given in (5.12) by using the waveform structure. It relies on intentional CFO between aggressor's Gabor system and victim's Gabor system. For example, while one of the links operates at carrier frequency f_c, the other link operates at $f_c + \nu_0/2$. By allowing this operation, instead of full-overlapping between the subcarriers of the links, POT is obtained. This approach also fits the asynchronous nature of other-user interference as it does not introduce any timing constraint between interfering signals. One can interpret the intentional CFO as an interference alignment strategy in frequency domain.

In Figure 5.2, a motivating example based on filtered multitone (FMT) is illustrated for POT. In FMT, each subcarrier is generated via a band-limited filter [40]. As opposed to the conventional understanding of OFDM, the subcarriers are not overlapped in frequency domain. By providing additional guard bands, orthogonality between subcarriers is maintained. Note that these guard bands are also useful to provide immunity against self-interference due to the time-frequency impairments. In the provided example in Figure 5.2, these guard bands are exploited further

and they are used to mitigate the other-user interference. By applying an intentional CFO between two different links, other-user interference mitigation is provided in an uncoordinated network.

POT is fundamentally related to the utilization of the time-frequency plane by the waveform structure. Transmit filter, receiver filter, and density of symbols in time-frequency plane determine the available resource opportunities jointly for the other-user interference mitigation by using POT, as exemplified in Figure 5.2. Besides, further utilization of the waveform structure via non-orthogonal schemes along with POT lead to a trade-off for uncoordinated networks: *other-user interference versus self-interference*. This trade-off is desirable in an uncoordinated network as long as self-interference is handled via self-interference cancellation methods, e.g., equalization. In the following subsections, orthogonality of schemes is stressed in conjunction with POT. POT with orthogonal schemes and non-orthogonal schemes are investigated theoretically along with numerical results and their potential drawbacks.

5.4.1 Partially Overlapping Tones with Orthogonal Schemes

For orthogonal schemes, transmitter and receiver utilize the same prototype filter, i.e., $g^{\epsilon}_{mk}(t) = \gamma^{\epsilon}_{mk}(t)$. In addition, inner products of the different basis functions derived from the prototype filter yield zero correlations, i.e., $\langle g^{\epsilon}_{nl}(t), \gamma^{\epsilon}_{mk}(t)\rangle = \delta_{nlmk}$. Many fundamental schemes, e.g., OFDM, FMT, and FBMC, rely on orthogonality. In digital communication, orthogonality in a multicarrier scheme is generally perceived as a necessary condition. It simplifies the receiver algorithms significantly and provides optimum signal-to-noise ratio (SNR) performance in AWGN channels. Besides these features, orthogonal schemes have another fundamental property due to orthogonal basis functions at the receiver: the energy of a signal before the projection onto receive filters is equal to the energy after the projection onto receiver filters. This is typically expressed through the Plancherel formula given by

$$\|s(t)\|^2 = \sum_{m,k} |\langle s(t), u_{mk}(t)\rangle|^2 \,, \tag{5.14}$$

where $s(t)$ is an arbitrary signal, and $\{u_{mk}(t)\}$ is a set of orthogonal basis functions. Assume that $s(t)$ is the interfering signal. When an orthogonal transformation, e.g., discrete Fourier transformation (DFT), is applied to $s(t)$ at the receiver, the total amount of the interference does not change after the transformation. This issue leads to an undesirable result: only way to *mitigate* the other-user interference is to discard some of subcarriers or to construct an *incomplete* Gabor system, i.e., $\tau_0\nu_0 > 1$ [129, 130], which causes less spectrally efficient schemes. In other words, POT with orthogonal schemes would be beneficial only when some of subcarriers are not utilized or $\tau_0\nu_0 > 1$. Indeed, norm-preserving feature of orthogonal transformations at the receivers explain *why orthogonal schemes do not directly provide immunity against the other-user interference*.

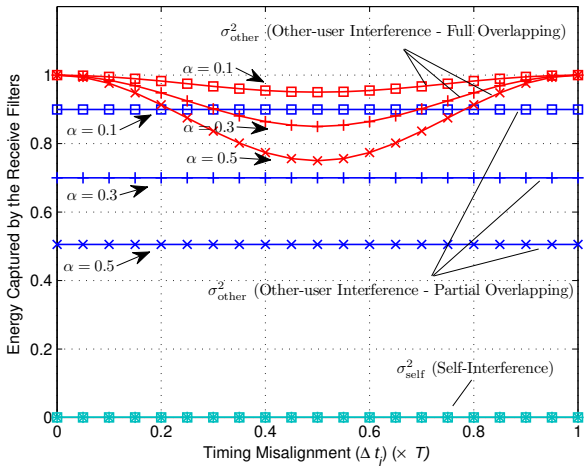

(a) Impact of timing misalignment when root raised cosine filter is employed along with FMT.

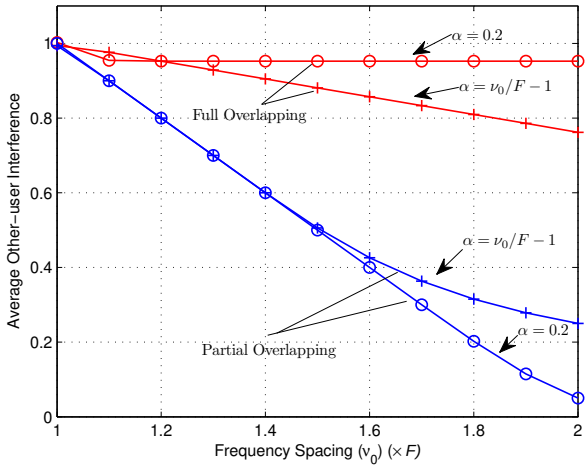

(b) Trade-off between spectral efficiency and other-user interference.

Figure 5.3 Other-user interference mitigation without introducing self-interference, but loss in spectral efficiency.

POT offers intentional CFO between the different links based on the fact that timing synchronization between TPs in an uncoordinated network is a challenging issue. However, the intentional CFO approach also introduces some constraints on the waveform structure. For example, orthogonal multicarrier schemes which provide non-overlapping subcarriers in frequency domain, e.g., FMT, complies with the intentional CFO approach introduced by POT. However, POT might not be as beneficial as in the case of FMT to the schemes where the orthogonality is maintained strictly on certain localizations in the time-frequency plane, as in OFDM. Considering this issue, analyses throughout the study are performed based on FMT.

In Figure 5.3, considering timing misalignment between one aggressor and the victim, Δt_i is swept for one symbol period when $\Delta f_i = \nu_0/2$. FMT is generated based on root-raised-cosine (RRC) filter. Note that RRC filter is a band-limited filter and the excess bandwidth of the RRC filter is controlled via a roll-off factor of α, where $0 \leq \alpha \leq 1$. In Figure 5.3(a), $\sigma_i^2(\Delta t_i, \Delta f_i)$ is calculated numerically, based on (5.12). In case of full overlapping, $\sigma_i^2(\Delta t_i, \Delta f_i)$ is mitigated maximally when $\Delta t_i = 0.5 \times T$, $\tau_0 = T$, and $\nu_0 = (1 + \alpha) \times F$. This is because of the reduction of the ICI components maximally due to the additional guard bands, when timing misalignment occurs. In case of partial overlapping, impact of Δt_i is removed totally, and $\sigma_i^2(\Delta t_i, \Delta f_i)$ is significantly reduced since the receive filters reject the main portion of the interference, depending on the utilized α. Assuming the aggressor interference has a uniform timing misalignment characteristics, trade-off between spectral efficiency and other-user interference is given for two different FMT cases in Figure 5.3(b). When ν_0 is set to $(1 + \alpha) \times F$, $\sigma_i^2(\Delta t_i, \Delta f_i)$ decreases for both full overlapping and partial overlapping due to the less ICI components with the timing misalignment, as given in Figure 5.3(a). When α is fixed to 0.2, other-user interference is mitigated more via partial overlapping, since this approach provides more gap in frequency for other-user interference mitigation.

Major concern of using POT with orthogonal schemes might be having less spectral efficient transmission for the sake of other-user interference mitigation. However, as indicated before, it allows the devices interrupted by the interference to achieve a better BER performance with a simple approach.

5.4.2 Partially Overlapping Tones with Non-orthogonal Schemes

Similar to the orthogonal schemes, transmitter and receiver utilize the same prototype filters for non-orthogonal structures, i.e., $g_{mk}^{\epsilon}(t) = \gamma_{mk}^{\epsilon}(t)$. However, inner products of the different basis functions do not yield zero correlations, i.e., $\langle g_{nl}^{\epsilon}(t), \gamma_{mk}^{\epsilon}(t) \rangle \neq \delta_{nlmk}$. For example, non-orthogonal frequency division multiplexing (NOFDM) can be constructed by using the rectangular lattice of OFDM with non-Nyquist transmit filters and receive filters, e.g., Gaussian functions. For non-orthogonal schemes, the utilized basis functions at the receiver also corresponds to a nonorthogonal transformations, i.e., $\langle \gamma_{nl}^{\epsilon}(t), \gamma_{mk}^{\epsilon}(t) \rangle \neq \delta_{nlmk}$. In that case, the condition given in (5.14) is relaxed as

$$A\|s(t)\|^2 \leq \sum_{m,k} |\langle s(t), u_{mk}(t) \rangle|^2 \leq B\|s(t)\|^2 \,, \tag{5.15}$$

where $\{u_{mk}(t)\}$ is a set of non-orthogonal elements, A and B are the lower bound and upper bound, respectively, and $0 < A \leq B < \infty$. Based on (5.15), when a non-orthogonal transformation is applied at the receiver, the energy of $s(t)$ does not have to be preserved after the transformation. In other words, the non-orthogonal transformations at the

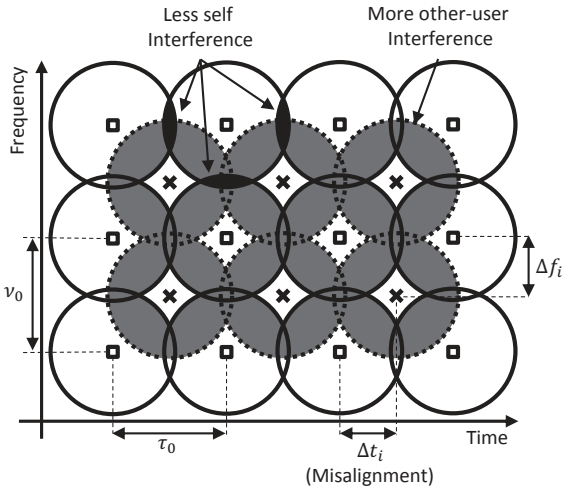

(a) Less self-interference, but more other-user-interference.

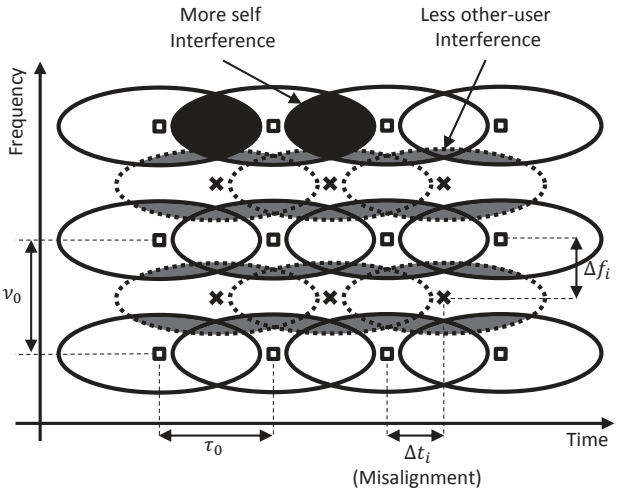

(b) More self-interference, but less other-user-interference.

Figure 5.4 Illustration for the trade-off between self-interference and other-user interference with the concept of POT (Solid Line: Desired signal, Dashed line: Interfering signal).

receivers are able to alter the amount of the observed interference energy. Hence, when POT is taken into account with non-orthogonal schemes, it is possible to mitigate other-user interference even when $\tau_0\nu_0 = 1$.

In order to understand the utilization of POT with non-orthogonal schemes, assume that $\tau_0\nu_0 = 1$ and the transmit pulse shape and the receive filter are Gaussian filters. Gaussian filter is the optimally-concentrated pulse in time-frequency domain and it is expressed as

$$p(t) = (2\rho)^{1/4} e^{-\pi\rho t^2}, \tag{5.16}$$

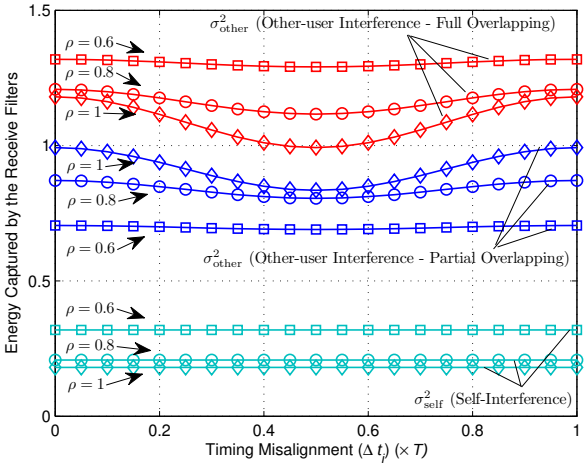

(a) Impact of timing misalignment when Gaussian filter is employed.

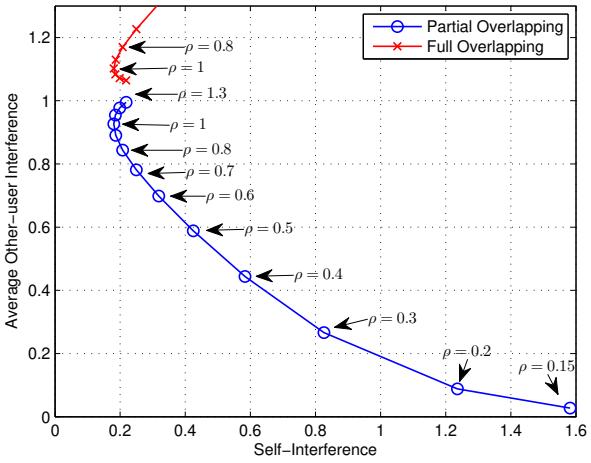

(b) Trade-off between self-interference and other-user interference.

Figure 5.5 Other-user interference mitigation without loss in spectral efficiency and power, but at the expense of self-interference.

where ρ is the control parameters for the dispersion of the pulse in time and frequency and $\rho > 0$. While the selection of $\rho = 1$ yields a Gaussian filter that has isotropic dispersion in time and frequency, smaller ρ causes more dispersion in time domain and less dispersion in frequency domain. Since Gaussian filter is not a Nyquist filter, consecutive symbols overlap more with smaller ρ, yielding more self-interference in time, i.e., ISI. However, introducing more ISI is also beneficial to mitigate the other-user interference, when POT is considered, as illustrated in Figure 5.4(a) and Figure 5.4(b) for $\Delta f_i = \nu_0/2$. In other words, non-orthogonal schemes yield a trade-off between the other-user interference and self-interference by exploiting the POT.

Considering the density of the symbols on time-frequency plane of the victim RP, it is important to emphasize the differences between faster-than Nyquist (FTN) signaling [157] and POT with non-orthogonal schemes. In FTN signaling, the density of the symbols in time-frequency plane is increased more than Nyquist rate, i.e., $\tau_0\nu_0 < 1$, intentionally. However, each individual link operates at the Nyquist rate, i.e., $\tau_0\nu_0 = 1$, for POT. The time-frequency plane of the victim RP is packed due to the aggressors' signals, which is common in co-channel interference problems. In addition, POT does not suggest a structured symbol packing into the time-frequency plane, as in FTN signaling. It allows timing misalignment among the individual links.

Similar to the investigations given in Section 5.4.1, Δf_i is set to $\nu_0/2$ and Δt_i is swept for one symbol period. Impact of timing misalignment is given in Figure 5.5(a). In case of full overlapping, when $\Delta t_i = 0$, the receive filter has full correlation with the concentric symbol of the aggressor and partial correlations with the neighboring symbols. Hence, the total energy after the correlation becomes more than 1. In case of partial overlapping, receive filters only capture energy from only the neighboring symbols of aggressors, which yields that $\sigma^2_{\text{self}} < 1$ as in Figure 5.5(a). In Figure 5.5(b), the trade-off between self-interference and average other-user interference is given, assuming uniform timing misalignment. As in Figure 5.5(b), Gaussian filter provides flexible trade-off between self-interference and other-user interference.

There are two potential drawbacks of this approach: 1) necessity for a self-interference cancellation method, e.g., equalization, since the filters do not satisfy Nyquist criterion and 2) colored noise due to the non-orthogonal receiver filters. For the first issue, the introduced complexity due to self-interference cancellation method might be preferable in comparison with the complexities of the methods for handling *asynchronous* other-user interference. For the second point, note that non-orthogonal transformations always introduce correlation between samples [130]. If a sequence-based equalizer, e.g., maximum likelihood sequence estimator (MLSE), is employed, a whitening filter should also be utilized to improve the performance of the receiver. Note that assuming the small link distances for the pairs, noise might become a secondary problem when interference is a dominant issue.

5.5 Average BER Analysis

In this section, average BER analysis is provided for POT for orthogonal schemes that do not introduce self-interference as discussed in Section 5.4.1. To obtain theoretical (but tractable) BER analysis, a useful method for BER calculations introduced in [158] is combined with spatial PPP approaches [147, 148, 151]. First, BER is expressed along SINR given in (5.10). Then, its expected value is obtained considering other-user interference. Its computation complexity is significantly reduced by using spatial PPP and ambiguity function. For the trade-off introduced in

Section 5.4.2, investigation on BER performance is performed through the numerical analysis in Section 5.6, since achievable BER performance depends highly on the employed self-interference cancellation method at the receiver.

Closed-form expression for BER of a square M-QAM in AWGN channel is readily available in the literature and it is given by

$$\mathrm{BER}\left(SNR\right) = \sum_{q}^{\sqrt{M}-2} c_q \mathrm{erfc}\left(\left(2q+1\right)\sqrt{\frac{SNR}{2}}\right) \tag{5.17}$$

where M is the constellation size, c_q are the constants depending on the modulation order and $\sum_{q=0}^{\sqrt{M}-2} c_q = 1/2$ [159]. For instance, $c_q = \{1/2\}$ and $q = \{0\}$ for 4-QAM and $c_q = \{3/8, 2/8, -1/8\}$ and $q = \{0, 1, 2\}$ for 16-QAM, respectively.

By substituting (5.10) into (5.17), BER is obtained for given I_{total}, G_ϵ, and d_ϵ as

$$\mathrm{BER}\left(E_\mathrm{b}/N_0|G_\epsilon, I_{\mathrm{total}}, d_\epsilon\right) = \sum_{q=0}^{\sqrt{M}-2} c_q \mathrm{erfc}\left(\frac{2q-1}{\sqrt{2}}\sqrt{\frac{G_\epsilon}{I_{\mathrm{total}} + \frac{M-1}{3\log_2 M}\frac{1}{E_\mathrm{b}/N_0}}}\right). \tag{5.18}$$

Since the target is to calculate average BER under interference, the terms, I_{total}, and G_ϵ, have to be averaged out. In order to obtain average BER, we refer to following lemma introduced in [158]:

Lemma-I: Let x and y be unit-mean exponential and arbitrary non-negative random variables, respectively. Then

$$\mathbb{E}_{x,y}\left[\mathrm{erfc}\left(\sqrt{\frac{x}{ay+b}}\right)\right] = 1 - \frac{1}{\sqrt{\pi}}\int_0^\infty \frac{e^{-z(1+b)}}{\sqrt{z}}\mathcal{L}_y\left(az\right)\mathrm{d}z$$

where $\mathcal{L}_y\left(z\right) = \mathbb{E}_y\left[e^{-yz}\right]$ is the moment generation function (MGF) with negative argument (or Laplace transformation) of random variable y.

If *Lemma-I* is applied to (5.18) (see e.g., [144, 145, 158, 160]), average BER is obtained as

$$\mathrm{BER}\left(E_\mathrm{b}/N_0|, d_\epsilon\right) = \sum_{q=0}^{\sqrt{M}-2} c_q\left(1 - \frac{1}{\sqrt{\pi}}\int_0^\infty \frac{e^{-z(1+\frac{2}{(2q-1)^2}\frac{M-1}{3\log_2 M}\frac{1}{E_\mathrm{b}/N_0})}}{\sqrt{z}}\mathcal{L}_{I_{\mathrm{total}}}\left(\frac{2z}{(2q-1)^2}\right)\mathrm{d}z\right), \tag{5.19}$$

$$= \frac{1}{2} - \frac{1}{\sqrt{\pi}}\sum_{q=0}^{\sqrt{M}-2} c_q \int_0^\infty \frac{e^{-z(1+\frac{2}{(2q+1)^2}\frac{M-1}{3\log_2 M}\frac{1}{E_\mathrm{b}/N_0})}}{\sqrt{z}}\mathcal{L}_{I_{\mathrm{total}}}\left(\frac{2z}{(2q+1)^2}\right)\mathrm{d}z\,. \tag{5.20}$$

Therefore, the complexity introduced by (5.18) reduces to calculate Laplace transformation of I_{total}. In the following subsections, Laplace transformation of I_{total} is calculated in cases of single aggressor and multiple aggressors.

5.5.1 Single Aggressor

If only ith aggressor is considered, the Laplace transformation of the total interference is obtained as

$$\begin{aligned}\mathcal{L}_{I_{\text{total}}}(z) &= \mathbb{E}_{I_{\text{total}}}\left[e^{-zI_{\text{total}}}\right] \\ &\overset{(a)}{=} \mathbb{E}_{I_{\text{self}}}\left[e^{-zI_{\text{self}}}\right] \times \mathbb{E}_{I_i}\left[e^{-zI_i}\right] = \mathbb{E}_{I_i}\left[e^{-zI_i}\right] \\ &\overset{(b)}{=} \int_0^{\tau_0} \frac{f_{\Delta t_i}(\Delta t_i)}{1 + z d_\epsilon^{\frac{b-\beta b}{10}} d_i^{\frac{\beta b}{10}} r_i^{\frac{-b}{10}} \sigma_i^2(\Delta t_i, \Delta f_i)} \mathrm{d}\Delta t_i \end{aligned} \tag{5.21}$$

where (a) follows from the independent assumption of random variables I_i and I_{self} and the assumptions of zero self-interference via orthogonal schemes, (b) is because of the exponential distribution of I_{other} and the randomness of timing misalignment. Considering the uniform timing misalignment assumption and being a constant function of $\sigma_i^2(\Delta t_i, \Delta f_i)$ respect to Δt_i, as in Figure 5.3(a), (5.21) is simplified as

$$\mathcal{L}_{I_{\text{total}}}(z) = \frac{1}{1 + z d_\epsilon^{\frac{b-\beta b}{10}} d_i^{\frac{\beta b}{10}} r_i^{\frac{-b}{10}} \sigma_i^2(\Delta f_i)} \tag{5.22}$$

5.5.2 Multiple Aggressors

When multiple aggressors exist in the network, the choice of Δf_i within the link affects the performance of POT. In order to avoid the coordination, it is assumed that Δf_i is selected randomly from the set Ω given by $[\psi_0, \psi_1, \ldots, \psi_r, \ldots]$. The selection is performed based on a probability mass function (PMF) where p_r corresponds to the probability of rth intentional CFO. Based on this assumption, the Laplace transformation of the total interference is obtained as

$$\begin{aligned}\mathcal{L}_{I_{\text{total}}}(z) &= \mathbb{E}_{I_{\text{total}}}\left[e^{-zI_{\text{total}}}\right] \\ &\overset{(a)}{=} \mathbb{E}_{I_{\text{self}}}\left[e^{-zI_{\text{self}}}\right] \times \mathbb{E}_{\Phi, I_i}\left[e^{-z\sum_{i\in\Phi} I_i}\right] \\ &\overset{(b)}{=} \mathbb{E}_{\Phi, I_i}\left[e^{-z\sum_{i\in\Phi} I_i}\right] = \mathbb{E}_{\Phi}\left[\prod_{i\in\Phi} \mathbb{E}_{I_i}\left[e^{-zI_i}\right]\right] \qquad (5.23) \\ &\overset{(c)}{=} \exp\left[-2\pi\lambda \int_{r_{\min}}^{\infty} \left(1 - \mathbb{E}_{I_i}\left[e^{-zI_i}\right]\right) v \mathrm{d}v\right] \qquad (5.24)\end{aligned}$$

where (a) follows from the independent assumption of random variables I_{other} and I_{self}, (b) is because of zero self-interference via orthogonal schemes, and (c) is caused by the probability generating functional of PPP, which states $\mathbb{E}_\Phi\left[\prod_{i\in\Phi} f(x)\right] = \exp\int_{\mathbb{R}^2}(1 - f(x))\mathrm{d}x$ for an arbitrary function $f(x)$ and the assumption of i.i.d interference from each aggressor I_i and independent Φ from other random variables in the interference function I_{other} [148]. Considering

randomness of aggressors' distances d_i, $\mathbb{E}_{I_i}\left[e^{-zI_i}\right]$ is obtained as

$$\mathbb{E}_{I_i}\left[e^{-zI_i}\right] = \mathbb{E}_{d_i,G_i}\left[e^{-z\frac{P_i}{P_\epsilon}G_i}\right] = \sum_r p_r \int_0^\infty \frac{f_u(u)}{1 + z d_\epsilon^{\frac{b-\beta b}{10}} u^{\frac{\beta b}{10}} \nu^{\frac{-b}{10}} \sigma_i^2(\psi_r)} \mathrm{d}u \tag{5.25}$$

which is based on the Laplace transformation of an exponentially disturbed random variable, uniform timing misalignment assumption, and being a constant function of $\sigma_i^2(\Delta t_i, \Delta f_i)$ respect to Δt_i. In (5.25), the probability density function (PDF) of d_i is given by $f_u(u) = 2\pi\lambda u e^{-\lambda\pi u^2}$ [149]. Then, $\mathcal{L}_{I_{\text{total}}}(z)$ is obtained as

$$\mathcal{L}_{I_{\text{total}}}(z) = \exp\left[-2\pi\lambda \int_{r_{\min}}^\infty \left(1 - \sum_r p_r \int_0^\infty \frac{2\pi\lambda u e^{-\lambda\pi u^2}}{1 + z d_\epsilon^{\frac{b-\beta b}{10}} u^{\frac{\beta b}{10}} \nu^{\frac{-b}{10}} \sigma_i^2(\psi_r)} \mathrm{d}u\right) \nu \mathrm{d}\nu\right] \tag{5.26}$$

by substituting (5.25) into (5.24). Note that (5.26) does not always yield a closed-form solution since $\int_0^\infty \frac{x e^{-ax^2}}{1+bx^c} \mathrm{d}x$ produces an expression in terms of standard mathematical functions depending on a, b, and c. Nonetheless, (5.26) does not require Monte Carlo simulations.

5.6 Numerical Results

Numerical results are given in order to validate analytical findings with simulations and to investigate the performance of uncoordinated networks along with POT. In the simulations, POT with orthogonal schemes and POT with non-orthogonal schemes are exhibited by utilizing FMT with RRC filter and zero forcing equalization and by using NOFDM with Gaussian filter and symbol-spaced MLSE equalization, respectively. For MLSE, 7 taps are utilized for each subcarrier and trace-back depth for MLSE is set to 20. Unless otherwise stated, numerical result are obtained for Rayleigh channels.

In Figure 5.6, impact of partial overlapping is presented in Rayleigh channel for the aforementioned trade-offs when a dominant aggressor interrupts the transmission with the equal received signal power (i.e., signal-to-interference ratio (SIR) is set to 0 dB). In Figure 5.6(a), α is set to 0.2 and the subcarrier spacing is swept from $1.2 \times F$ to $2 \times F$, referring to the POT with orthogonal schemes. Also, simulation results are verified with the theoretical results based on (5.20) and (5.22). As it can be seen in Figure 5.6(a), efficacy of POT in the BER performance increases with the subcarrier spacing, which also causes less spectrally efficient schemes. In Figure 5.6(b), the same analysis is performed for NOFDM to address the POT with non-orthogonal schemes. When other-user interference do not exist, orthogonal schemes reach the Rayleigh bound and introduce superior BER performance compared to non-orthogonal schemes. This is mainly because of the fact that MLSE loses its optimality under the colored noise caused by the non-orthogonal transformation at the receiver. However, when the other-user interference exists, orthogonal schemes

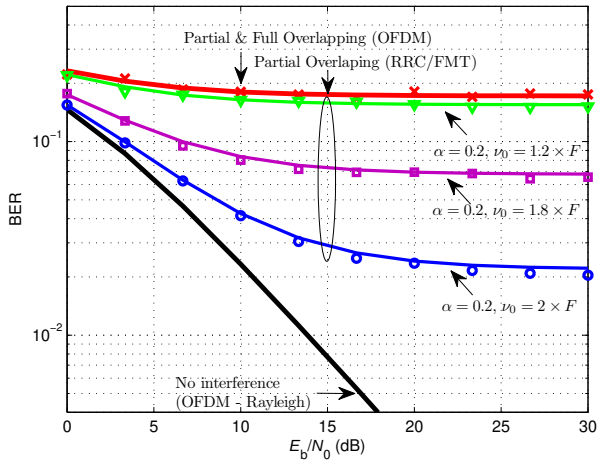

(a) RRC/FMT/4QAM (Solid lines: Analytical results based on (5.20) and (5.22)).

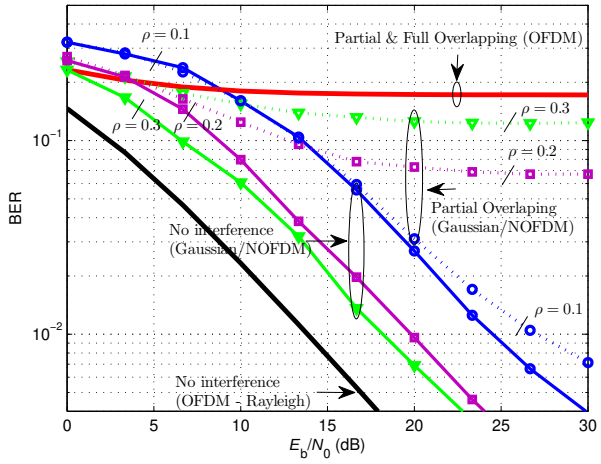

(b) Gaussian/NOFDM/4QAM.

Figure 5.6 BER performance with partial overlapping when there is a single aggressor.

capture the total amount of the other-user interference and BER performance deteriorates significantly. In contrast to orthogonal waveforms, non-orthogonal schemes become notable with the concept of POT under the other-user interference. By providing sufficient non-orthogonality, e.g., $\rho = 0.1$, BER performance remains the same of the case without other-user interference for NOFDM for low to medium SNR, as it can be seen in Figure 5.6(b). Essentially, the results show that BER performance is enhanced without sacrificing the spectral efficiency at the expense of complexity at the receiver.

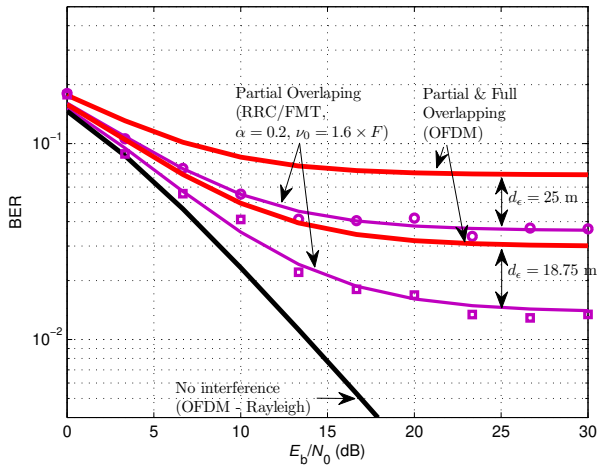

(a) RRC/FMT/4QAM (Solid lines: Analytical results based on (5.20) and (5.26)).

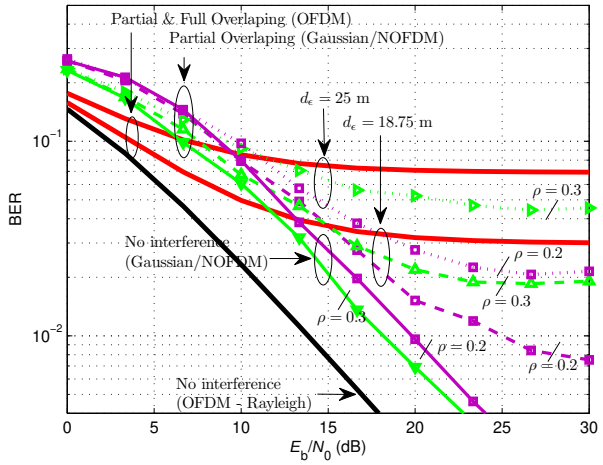

(b) Gaussian/NOFDM/4QAM.

Figure 5.7 BER performance with partial overlapping when there are multiple aggressors modeled with PPP.

In Figure 5.7, impact of POT on BER performance is shown when there are multiple aggressors. In the simulation, the path loss is modeled with the parameters given in [161] as

$$L(d) = 11.8 + 45\log_{10}(f_c) + 40\log_{10}(d/1000) \tag{5.27}$$

where f_c is the carrier frequency in MHz (3500 MHz) and d is the distance in meters. Using given parameters, the path loss formula is calculated as $L(\cdot) = 51.3 + 40\log(\cdot)$ where the argument is in terms of meters. Accordingly, a and b are set to 51.3 and 40, respectively. The intensity of TP and $r_{\min}$ are set to $1/(\pi 50^2)$ and 25 m, respectively.

In order to see the best possible BER performance, all aggressors' signals are partially overlapped with the desired signal. Then, BER curves are obtained for different victim link distance d_ϵ. As expected, BER is directly related to the user distance. Especially, the degradation becomes severe for the users located at far distances. In Figure 5.7(a), it is shown that orthogonal schemes allow better BER performance with the concept of POT by losing their spectral efficiencies. Also, simulation results match with the theoretical results based on (5.20) and (5.26). In Figure 5.7(b), the impact of non-orthogonal schemes on BER performance are shown for the same scenario and better BER performance is obtained for high E_b/N_0 without any spectral efficiency loss, but complexity at the receiver. Considering Figure 5.6(b) and Figure 5.7(b), it is important to emphasize that one may obtain the optimum ρ, considering the amount of the attainable self-interference and the amount of mitigated other-user interference. Although the selection of $\rho = 0.1$ significantly improve the BER performance when the amount of the other-user interference is equal to signal power, the same scheme might not yield optimum BER performance when other-user interference becomes weaker due to the path loss. Essentially, this issue indicates that there is a point where non-orthogonality starts to be harmful. Therefore, the best selection of ρ depends on the equalizer performance and the amount of the other-user interference.

5.7 Concluding Remarks

In this study, by allowing intentional CFO between the interfering links, other-user interference is mitigated in an uncoordinated network without any timing constraints via orthogonal or non-orthogonal schemes. For a well-coordinated network, transmission over orthogonal schemes might lead to better performance compared to non-orthogonal schemes due to the absence of self-interference. However, when other-user interference is inevitable and significant in an uncoordinated network, spectral efficiency has to be sacrificed for orthogonal schemes in order to allow other-user interference mitigation. Specifically, schemes which allow non-overlapping subcarriers in frequency, e.g., FMT, complies with the intentional CFO approach to avoid timing misalignment problems with POT. As opposed to orthogonal waveforms, non-orthogonal schemes come into the prominence along with POT for an interesting reason; self-interference problem is easier than other-user interference problem in an uncoordinated networks. By utilizing non-orthogonal waveforms, POT is able to change the type of interference from other-user interference to self-interference. This is beneficial when the receiver has proper self-interference cancellation mechanisms. Especially, it is promising when two pairs sharing the same spectrum are close to each other.

Throughout the study, POT is presented for two intentional CFO levels, i.e., f_c and $f_\mathrm{c} + \nu_0/2$. Although the POT with two intentional CFO levels heuristically matches to two-users scenarios, it might be a suboptimum solution for the multiple-user scenarios. However, it is possible to utilize multiple CFO levels to extend POT to multiple-

user scenarios. In addition, when the difference between the power levels of interfering signal and desired signal are significantly large, well-known interference cancellation methods, e.g. successive interference cancellation (SIC), might provide better results than POT. However, the combination of POT and interference cancellation techniques can increase the performance substantially. Since POT is able to increase the difference between the norm of interference and the norm of desired signal power, POT is also able to increase the separability of the signals.

CHAPTER 6

NUMBER OF REQUIRED EQUALIZER TAPS FOR MULTICARRIER SCHEMES

6.1 Introduction

In a wireless communication medium, the transmitted signal travels along multiple paths and arrives at the receiver at different time instants, which causes dispersion in time. Additionally, the signal strength might vary due to mobility, which leads to dispersion in frequency. Hence, one symbol might be interfered by its neighboring symbols in time and frequency, known as self-interference. In addition to the dispersive communication medium, the amount of self-interference is related to the transmit filter and the receiver filter since their responses jointly determine the occupancy of symbol in time and frequency [129]. Therefore, one can interpret that transmit filter, communication medium, and receive filter result in a *composite effect* that determines the characteristics of the interference among the symbols in time and frequency [162–164].

In order to handle the self-interference, one option is to employ an equalizer at the receiver, which requires information about the self-interference characteristics, e.g., number of symbols that interfere the desired symbol, the locations of the interfering symbols in time and frequency, and their strengths. However, due to the random dispersion of the signal and the operation under the noise, the number of interfering symbols and their locations in time and frequency are uncertain at the receiver. While taking a smaller number of interfering symbols than the required ones into account does not remove the self-interference at the equalization stage completely, using a larger number of taps folds noise into the channel estimation. This brings up a question that we investigate in this study: *Considering the uncertainty of the noise and the random characteristics of the dispersion in time and frequency, how many equalizer taps are needed to be taken into account in the channel estimation for a multicarrier scheme to yield a precise receiver design?* Based on this question, the main contributions of this study are:

- It is explicitly shown that employing more equalizer taps than the required ones in the channel estimation not only increases the complexity of the equalizer, but also degrades the bit error rate (BER) performance of the receiver.

- The number of required equalizer taps, which improves BER performance, is theoretically obtained. Furthermore, under practical scenarios, the number of required equalizer taps is also extracted via Akaike information criterion (AIC).

- The locations of interfering symbols in time and frequency are obtained for given multicarrier structure, channel characteristics, and signal-to-noise ratio (SNR). Therefore, an additional information for self-interference, which can be used in the equalization, is obtained.

The rest of paper is organized as follows: Related work is discussed in Section 6.2. System model based on multicarrier schemes is provided in Section 6.3. The trade-off between folding noise into the channel estimation and lack of description of the channel is investigated in Section 6.4, theoretically. Numerical results are provided in Section 6.5. Finally, the paper is concluded in Section 6.6.

6.2 Related Work

In the literature, various methods are proposed to obtain the number of equalizer taps. One of the well-known methods is to use the eigenvalues of the autocorrelation matrix of received signal with an information criterion, e.g., minimum description length (MDL) or Akaike information criterion (AIC) [165,166]. In [167], the method introduced in [165] is applied to find the number of paths in communication channel. In [168], the complexity arising from the calculation of the autocorrelation matrix and their eigenvalues is reduced by utilizing the power delay profile of the channel. In [169], a method for the estimation of the channel length is suggested for single carrier communications, based on the minimization of the mean square error (MSE) of channel estimation. In [170], length of channel impulse response is analyzed considering the difference between the statistical characteristics of multipath channel response and the noise. It is emphasized that while channel coefficients are effective for the window of channel length, additive noise per tap is uniformly distributed over the length of estimated channel. By utilizing an auxiliary function, the number of equalizer taps and estimation of noise variance are estimated. Although these studies provide promising results for the estimation of channel length, they do not address that the required number of equalizer taps at the receiver. In addition, to the best of our knowledge, the detailed investigation on the number of required equalizers taps for multicarrier schemes in both time and frequency, which captures the composite effect of transmit filter, multipath, and receiver filter, is not available in the literature.

This study is the extension of [171] which discusses the relation between the number of required equalizer taps and the composite effects of the transmit filter, communication medium, and the receiver filter for multicarrier schemes, heuristically.

6.3 System Model

In this section, we introduce the system model that is considered throughout the paper. The system model is based on a generalized framework for multicarrier schemes, which captures both orthogonal and non-orthogonal schemes [129].

6.3.1 Signal Model for Transmission

In a multicarrier scheme, the symbols are transmitted as

$$x(t) = \sum_{m=-\infty}^{\infty} \sum_{k=0}^{N-1} X_{mk} g_{mk}(t) \,, \tag{6.1}$$

where $g_{mk}(t) = p_{\text{tx}}(t - m\tau_0)\, e^{j2\pi k \nu_0 t}$, $p_{\text{tx}}(t)$ is the transmit filter, m is the symbol index, k is the subcarrier index, N is the number of subcarriers, τ_0 and ν_0 are the symbol spacing in time and frequency, respectively, and X_{mk} is the independent and identically distributed symbol of zero mean. Throughout the study, ν_0 and τ_0 are given in units of F and T, respectively (e.g., $\nu_0 = 1.1 \times F$ and $\tau_0 = 1.2 \times T$), where $F = 1/T$ and F is a number based on the design.

6.3.2 Multipath Channel

A linear time-varying channel is assumed for communication medium and it is denoted as $h(\tau, t)$. After the transmitted signal passes through the communication medium, the received signal is obtained as

$$\begin{aligned} y(t) &= \int_{\tau} h(\tau, t) x(t - \tau) d\tau + \omega(t) \\ &= \int_{\tau} \int_{\nu} H(\tau, \nu) x(t - \tau) e^{j2\pi\nu t} \mathrm{d}\nu \mathrm{d}\tau + \omega(t) \,, \end{aligned} \tag{6.2}$$

where $H(\tau, \nu)$ is the Fourier transform of $h(\tau, t)$ and $\omega(t)$ is the additive white Gaussian noise (AWGN). The statistical characteristics of the communication medium are described with wide-sense stationary uncorrelated scattering (WSSUS) assumption [98] given by

$$\mathrm{E}\left[H(\tau, \nu)\right] = 0 \,, \tag{6.3}$$

$$\mathrm{E}\left[H(\tau, \nu) H^*(\tau_1, \nu_1)\right] = S(\tau, \nu)\, \delta(\tau - \tau_1) \delta(\nu - \nu_1) \,, \tag{6.4}$$

where $\mathrm{E}[\cdot]$ is the expected value operator and $S(\tau, \nu)$ is the scattering function. Note that WSSUS assumption is widely utilized to characterize the wireless channels. For example, exponential decaying multipath with Jakes Doppler spectrum [102] or ITU models [103] for different environments are commonly used models for terrestrial communications.

6.3.3 Signal Model for Reception

At the receiver, the received signal is correlated by analysis function $\gamma_{nl}(t) = p_{\mathrm{rx}}(t - n\tau_0)\, e^{j2\pi l\nu_0 t}$ where $p_{\mathrm{rx}}(t)$ is the receive filter. Then, the output of the correlator is sampled with the symbol period to obtain the received symbol as

$$\begin{aligned}\tilde{X}_{nl} &= \langle y(t), \gamma_{nl}(t)\rangle \triangleq \int_t y(t)\gamma^*_{nl}(t)dt \\ &= \underbrace{X_{nl}H_{nlnl}}_{\text{desired part}} + \underbrace{\sum_{\substack{m=n-L_{\mathrm{t}}^- \\ m\neq n}}^{n+L_{\mathrm{t}}^+} \sum_{\substack{k=l-L_{\mathrm{f}}^- \\ k\neq l}}^{l+L_{\mathrm{f}}^+} X_{mk}H_{nlmk}}_{\text{interference part}} + \underbrace{\omega_p}_{\text{noise}} .\end{aligned} \tag{6.5}$$

In (6.5), $\{L_{\mathrm{t}}^-, L_{\mathrm{t}}^+\}$ and $\{L_{\mathrm{f}}^-, L_{\mathrm{f}}^+\}$ define the boundaries of all possible region of supports (RoS) in time and frequency, respectively, as illustrated in Figure 6.1. A RoS is denoted as $R^{(L)}$, where L is the number of symbols in RoS, which also corresponds to the number of taps for a symbol-spaced equalizer. It is assumed that the amount of the interference between the desired symbol and the symbols beyond these boundaries is 0. In (6.5), H_{nlmk} corresponds to the projection of the transmit filter located at (m, k) to the receive filter located at (n, l) including the dispersion due the communication medium as

$$H_{nlmk} = \int_\tau \int_\nu H(\tau, \nu) \int_t g_{mk}(t - \tau)\gamma^*_{nl}(t)e^{j2\pi\nu t}\mathrm{d}t\mathrm{d}\nu\mathrm{d}\tau\ . \tag{6.6}$$

In other words, H_{nlmk} shows the composite effects of the transmit filter, communication medium, and receiver filter. It is assumed that H_{nlmk} is a symmetric complex Gaussian random variable of zero mean, considering Rayleigh fading channel. The analytical expression of the expected interference contribution from a symbol at the point (m, k) to the desired symbol at the point (n, l) is given as

$$\begin{aligned}\sigma^2_{nlmk} &= \mathrm{E}\left[|H_{nlmk}|^2\right] = \\ &= \int_\tau \int_\nu S(\tau, \nu)\, |A((m - n)\tau_0 + \tau, (k - l)\nu_0 + \nu)|^2 \mathrm{d}\nu\mathrm{d}\tau\ ,\end{aligned} \tag{6.7}$$

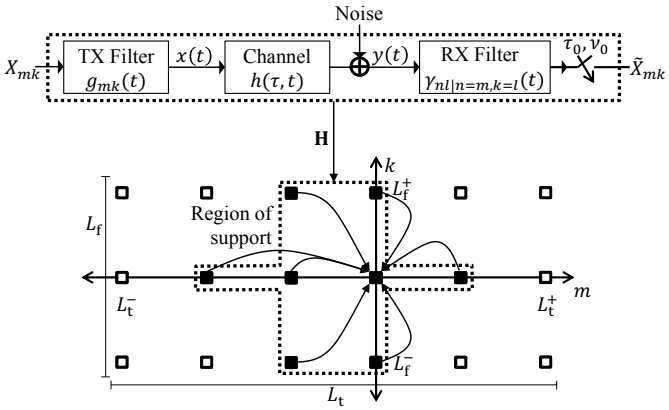

Figure 6.1 Self-interference due to the transmit filter, dispersion in communication medium, and receive filter.

where $A(\phi, \psi)$ is the ambiguity function [129], given by

$$A(\phi,\psi) \triangleq \int_{-\infty}^{\infty} p_{\mathrm{tx}}\left(t+\frac{\phi}{2}\right) p_{\mathrm{rx}}^{*}\left(t-\frac{\phi}{2}\right) e^{-j2\pi\psi t}\mathrm{d}t\,. \tag{6.8}$$

In the following subsections, we focus on a single subcarrier without loss of generality. For sake of increasing readability, H_{nlmk} and σ^2_{nlmk} are denoted as H_{mk} and σ^2_{mk}.

6.3.4 Composite Channel Response

Let $\mathbf{\Sigma}$ be a matrix that shows the expected scattering in time and frequency for given transmit filter, receiver filter, and channel scattering function as

$$\mathbf{\Sigma} = \begin{bmatrix} \sigma^2_{L_{\mathrm{f}}^{+}L_{\mathrm{t}}^{-}} & \cdots & \sigma^2_{L_{\mathrm{f}}^{+}L_{\mathrm{t}}^{+}} \\ \vdots & \sigma^2_{00} & \vdots \\ \sigma^2_{L_{\mathrm{f}}^{-}L_{\mathrm{t}}^{-}} & \cdots & \sigma^2_{L_{\mathrm{f}}^{-}L_{\mathrm{t}}^{+}} \end{bmatrix}, \tag{6.9}$$

which is based on (6.7). Providing that channel scattering function is presumable for the system design, $\mathbf{\Sigma}$ is also known at the receiver. For example, orthogonal frequency division multiplexing (OFDM) with a cyclic prefix (CP) does not introduce any correlation between the symbols in time-invariant channels. Hence, only σ^2_{00} is 1 while others are 0. However, an non-orthogonal scheme would cause interference among the symbols and $\sigma^2_{mk} \neq 0$ for some

$(m, k) \neq (0, 0)$. Using (6.9), the instantaneous response of the composite channel is given by

$$\mathbf{H} = \begin{bmatrix} \mathbf{h}_{L_{\mathrm{f}}^+} \\ \vdots \\ \mathbf{h}_0 \\ \vdots \\ \mathbf{h}_{L_{\mathrm{t}}^-} \end{bmatrix} = \begin{bmatrix} H_{L_{\mathrm{f}}^+ L_{\mathrm{t}}^-} & \cdots & H_{L_{\mathrm{f}}^+ L_{\mathrm{t}}^+} \\ \vdots & \vdots & \vdots \\ \vdots & H_{00} & \vdots \\ \vdots & \vdots & \vdots \\ H_{L_{\mathrm{f}}^- L_{\mathrm{t}}^-} & \cdots & H_{L_{\mathrm{f}}^- L_{\mathrm{t}}^+} \end{bmatrix}, \tag{6.10}$$

where $\mathbf{h}_k$ is $1 \times L_{\mathrm{t}}$ vector which shows the interference of the symbols on kth subcarrier to the desired symbol at $(0, 0)$. One also can interpret that $\mathbf{H}$ is a map that indicates the amount of the interfere due to the neighboring symbols in time and frequency. Based on (6.10), one may express the symbols in time on 0th subcarrier at the receiver as

$$\mathbf{y}_{\mathbf{X}} = \mathbf{\Phi}_{\mathbf{X}} \mathbf{h} + \boldsymbol{\omega} \tag{6.11}$$

and

$$\mathbf{X} = \begin{bmatrix} \mathbf{x}_{L_{\mathrm{f}}^-} & \cdots & \mathbf{x}_0 & \cdots & \mathbf{x}_{L_{\mathrm{f}}^+} \end{bmatrix}, \tag{6.12}$$

where $\mathbf{\Phi}_{\mathbf{X}}$ is a block Toeplitz matrix, $\mathbf{X}$ is the symbol matrix, $\tilde{\mathbf{x}}_k$ is the symbol vector on kth subcarrier, $\boldsymbol{\omega}$ is the noise vector, $\mathbf{y}$ is the received symbol vector, $\mathbf{h}$ is the $L_{\mathrm{t}} L_{\mathrm{f}} \times 1$ channel vector as

$$\mathbf{h} = \begin{bmatrix} \mathbf{h}_{L_{\mathrm{f}}^+} & \cdots & \mathbf{h}_0 & \cdots & \mathbf{h}_{L_{\mathrm{f}}^-} \end{bmatrix}^{\mathrm{T}}. \tag{6.13}$$

6.3.5 Channel Estimation

Without loss of generality, channel estimation is expressed as

$$\tilde{\mathbf{h}}^{(L)} = C_L\{\mathbf{y}_{\mathbf{T}}, \mathbf{T}\} \tag{6.14}$$

where $C_L\{\cdot, \cdot\}$ is the channel estimation operation, L is the hypothesized number of equalizer taps, $\tilde{\mathbf{h}}^{(L)}$ is the estimated channel, $\mathbf{y}_{\mathbf{T}}$ is the received signal, and $\mathbf{T}$ is $N_o \times L_{\mathrm{f}}$ matrix which includes the training symbols as

$$\mathbf{T} = \begin{bmatrix} \mathbf{t}_{L_{\mathrm{f}}^-} & \cdots & \mathbf{t}_0 & \cdots & \mathbf{t}_{L_{\mathrm{f}}^+} \end{bmatrix}, \tag{6.15}$$

where $\mathbf{t}_k$ is the $N_o \times 1$ training vector on kth subcarrier and N_o is the length of training sequence. Using (6.15), $\mathbf{\Phi}$, defined in (6.1), becomes $N_o \times L_\mathrm{t} L_\mathrm{f}$ matrix where its columns have the cyclically shifted versions of $\{\mathbf{t}_{L_\mathrm{f}^-}, \cdots, \mathbf{t}_0, \cdots, \mathbf{t}_{L_\mathrm{f}^+}\}$ as

$$\mathbf{\Phi_T} = \begin{bmatrix} \mathbf{C}_{\mathbf{t}_{L_\mathrm{f}^-}} & \cdots & \mathbf{C}_{\mathbf{t}_0} & \cdots & \mathbf{C}_{\mathbf{t}_{L_\mathrm{f}^+}} \end{bmatrix}, \tag{6.16}$$

where $\mathbf{C_x}$ is a $N_o \times L_\mathrm{t}$ circulant matrix where the first column of $\mathbf{C_x}$ is $\mathbf{x}$. Note that expressing each $\mathbf{t}_k$ circularly as in (6.16) also corresponds to extend $\mathbf{T}$ cyclically at the transmitter, which allows the receiver to exploit all samples of training sequence.

In order to estimate the channel properly, $\mathbf{T}$ should have good auto-correlation and cross-correlation properties, i.e., ensuring orthogonality between $\mathbf{t}_k$ and their cyclically shifted versions in time and frequency. One way of obtaining attainable correlation properties is to use random numbers, where longer sequence leads better correlation results. Another method is to utilize Zadoff-Chu sequences [172]. While Zadoff-Chu sequences exhibits orthogonality between its cyclically shifted shift versions and other sequences in the set, it gives constant cross-correlation between two prime length Zadoff-Chu sequences, i.e., $1/\sqrt{N_o}$. Similar to the pseudo number, longer sequence gives better correlation properties in the case of using Zadoff-Chu sequences. Yet, one still may obtain a training sequence with perfect auto-correlation and cross-correlation properties by losing the dimensionality of training sequence. For example, a Zadoff-Chu sequence is taken into account as a seed. Then, the set is constructed from the cyclically shifted version of the seed. As long as the amount of each shift is larger than L_t, it yields perfect auto-correlation and cross-correlation properties. Throughout the study, although we do not apply any restriction on training sequence, we generate $\mathbf{T}$ based on this approach to ensure that $\mathbf{T}$ has perfect auto-correlation and cross-correlation properties.

6.4 Determining Number of Equalizer Taps

Number of required equalizer taps that yields a good bit error rate (BER) performance is related to both signal-to-noise ratio (SNR) and the amount of the self-interference. In this section, this issue is investigated to obtain the number of equalizer taps that yields minimum error at the receiver, theoretically. In addition, the number of required equalizer taps is discussed considering the practical systems.

6.4.1 Theoretical Approach

Intuitively, as the performance of the channel estimation gets worse due to the such reasons, e.g., low SNR or undesired correlation properties of training sequence, the number of taps used in the equalization should be decreased

not to allow the additional error due to the insufficient channel estimation. In order to understand this fact, consider a training sequence with ideal correlation properties. Then, one can express the optimum channel estimation as least square (LS) estimator for AWGN, given by

$$C_L\{\mathbf{y_T}, \mathbf{T}\} = \left(\mathbf{\Phi}_{\mathbf{T}}^{(L)^*}\mathbf{\Phi}_{\mathbf{T}}^{(L)}\right)^{-1}\mathbf{\Phi}_{\mathbf{T}}^{(L)^*}\mathbf{y_T} = \Psi^{(L)}\mathbf{y_T}\,, \tag{6.17}$$

where $\mathbf{\Phi}_{\mathbf{T}}^{(L)}$ is the matrix that includes the L columns of $\mathbf{\Phi_T}$ and $\Psi^{(L)}$ is the pseudo inverse of $\mathbf{\Phi}_{\mathbf{T}}^{(L)}$. The operation in (6.17) corresponds to find a vector that includes the weights associated with the columns of $\mathbf{\Phi}_{\mathbf{T}}^{(L)}$ to yield the closest vector to $\mathbf{y_T}$, using $\mathbf{\Phi}_{\mathbf{T}}^{(L)}$. Based on (6.17), expected LS error and MSE of the channel estimation are obtained as (see Appendix C for the proofs)

$$\mathrm{E}\left[(\mathbf{y_T} - \tilde{\mathbf{y}}_{\mathbf{T}})^*(\mathbf{y_T} - \tilde{\mathbf{y}}_{\mathbf{T}})\right] = N_o\sigma^2_{\overline{\mathrm{R}}^{(\mathrm{L})}} + (N_o - L)\sigma^2_{\mathrm{n}}\,, \tag{6.18}$$

and

$$\mathrm{E}\left[(\mathbf{h} - \tilde{\mathbf{h}}^{(L)})^*(\mathbf{h} - \tilde{\mathbf{h}}^{(L)})\right] = \sigma^2_{\overline{\mathrm{R}}^{(\mathrm{L})}} + \frac{L}{N_o}\sigma^2_{\mathrm{n}}\,, \tag{6.19}$$

respectively, where $\sigma^2_{\overline{\mathrm{R}}^{(\mathrm{L})}}$ is the total power at the outside of the RoS. The first terms in (6.18) and (6.19) indicate the errors due to the lack of description of the channel, which are decreasing functions of L. The second terms shows the impact of the noise in the channel estimation. Although it is a decreasing function of L for (6.18), it is a monotonically increasing function of L for (6.19), which exhibits the trade-off between the lack of description of the channel and folding noise into channel estimation.

It is worth noting that one can find L based on the minimization of (6.19). However, the selection that minimizes the MSE of channel estimation does not consider the uncertainty of the noise component. Even though the noise is assumed as a stationary process, actual values of the noise is different during the channel estimation and equalization stages. In order to include this effect for the determination of L, we calculate the expected residual sum squares (RSS) using the two hypothetical training signals as

$$\mathbf{y}_{\mathbf{T},1} = \mathbf{\Phi_T h} + \boldsymbol{\omega}_1\,, \tag{6.20}$$

$$\mathbf{y}_{\mathbf{T},2} = \mathbf{\Phi_T h} + \boldsymbol{\omega}_2 \tag{6.21}$$

where $\mathbf{y}_{\mathbf{T},1}$ and $\mathbf{y}_{\mathbf{T},2}$ are the received signals exposed to the same channel but different noise components. First, channel estimation is perfomed based on $\mathbf{y}_{\mathbf{T},1}$. Then, expected RSS is calculated based on the estimated channel over $\mathbf{y}_{\mathbf{T},1}$ and $\mathbf{y}_{\mathbf{T},2}$ as (see Appendix C for the proof)

$$\mathrm{E}\left[(\mathbf{y}_{\mathbf{T},2}-\tilde{\mathbf{y}}_{\mathbf{T},1})^{*}(\mathbf{y}_{\mathbf{T},2}-\tilde{\mathbf{y}}_{\mathbf{T},1})\right]=N_o\sigma^2_{\bar{\mathrm{R}}^{(\mathrm{L})}}+(N_o+L)\sigma^2_{\mathrm{n}}\,, \tag{6.22}$$

Hence, (6.22) yields a *cross-validation* using two hypothetical training signal to obtain for the best L. Compared to (6.19), (6.22) introduces an additional σ^2_{n}, which is an additional penalty term for each symbol in training sequence considering the uncertainty of the noise. In order to achieve a good performance, best number of equalizer taps is obtained by

$$L_{\mathrm{best}}=\arg\min_{L}\{N_o\sigma^2_{\bar{\mathrm{R}}^{(\mathrm{L})}}+(N_o+L)\sigma^2_{\mathrm{n}}\}\,. \tag{6.23}$$

In addition, providing that $\mathbf{\Phi}^{(L)}_{\mathbf{T}}$ is a matrix that has the first L strongest column of $\mathbf{\Phi}$ (depending on σ^2_{mk}), it is also possible to obtain the locations of the interfering symbols in time and frequency.

6.4.2 Practical Approach

In practice, it might be challenging to generate $\mathbf{y}_{\mathbf{T},1}$ and $\mathbf{y}_{\mathbf{T},2}$ and estimate σ^2_{n}. To solve this issue and obtain L_{best} at the receiver dynamically, utilization of an information criterion is suggested. An information criterion indicates a balance between bias and variance of the estimated parameter. It is well-studied subject and various information criteria are available in the literature [166, 173], e.g., AIC [174], corrected Akaike information criterion (AICc) [175], and MDL [176].

Essentially, AIC is the estimation of the expected Kullback-Leibler discrepancy between the true model and the fitted model [174]. Similar to the cross-validation in (6.22), it also utilizes two hypothetical independent signals for estimation and cross-validation [166]. If the number of observations is large and the dimension of the fitted model is small, it behaves as unbiased estimator. In other case, it yields a large negative bias and limits its effectiveness. To obtain better estimation of the expected Kullback-Leibler discrepancy for small-sample applications, an additional bias-correction term is introduced to AIC [175], which yields AICc as

$$AIC_{\mathrm{c}}(K_o)=-2\mathcal{L}(\theta)+2K_o+\underbrace{\frac{2K_o(K_o+1)}{N_o-K_o-1}}_{\text{additional term}}\,, \tag{6.24}$$

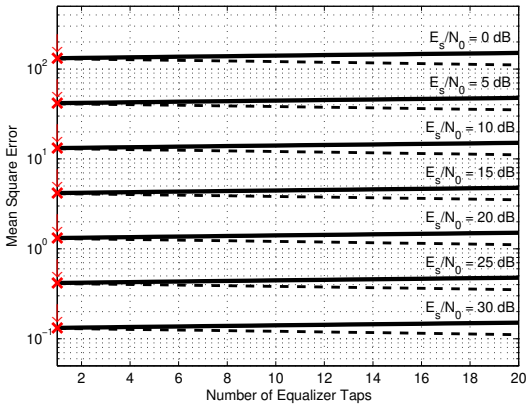

(a) Rectangular (OFDM, $T_{\text{CP}} = 0.07 \times T$, $F = 1/T = 15$ kHz).

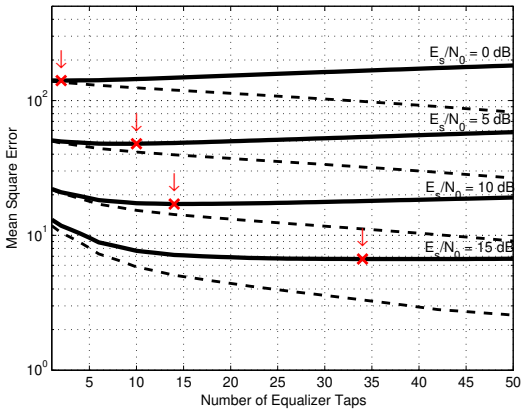

(b) Rectangular (OFDM, $T_{\text{CP}} = 0.07 \times T$, $F = 1/T = 300$ kHz).

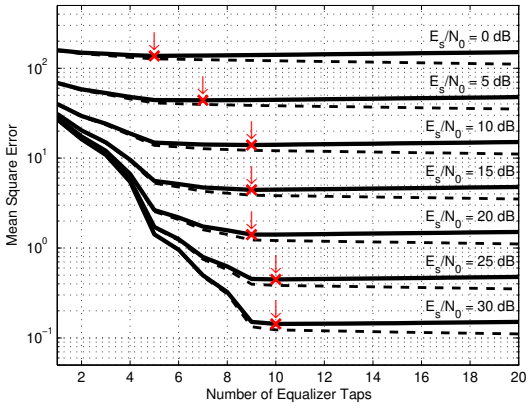

(c) Gaussian (NOFDM, $\rho = 1$, $F = 1/T = 300$ kHz).

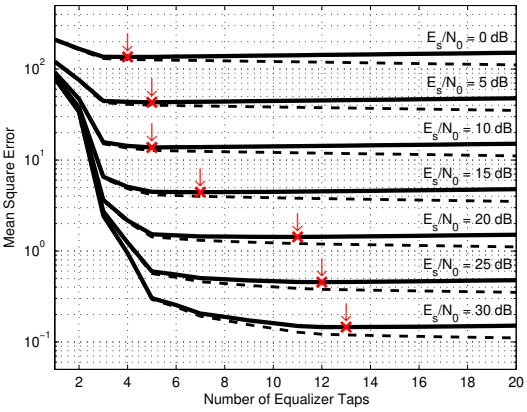

(d) Gaussian (NOFDM, $\rho = 0.4$, $F = 1/T = 300$ kHz).

Figure 6.2 Mean square errors based on (6.18) (dashed line) and (6.22) (solid line) (Channel: ITU Vehicular A).

where $\mathcal{L}(\theta)$ is the log-likelihood function, θ is the estimate of the parameter set, and K_o is the model order [174]. Throughout the study, L is investigated via AICc for the dynamic approach, considering the small length of the training sequence. However, one may follow the other information criteria in the literature.

If the statistical model of the random variable, i.e., noise, is characterized with AWGN, one may derive $\mathcal{L}(\theta)$ from the LS estimation and express (6.24) as

$$AIC_{\text{c}}(L) = N_o \log \frac{RSS^{(L)}}{N_o} + 2K_o + \frac{2K_o(K_o+1)}{N_o - K_o - 1}, \tag{6.25}$$

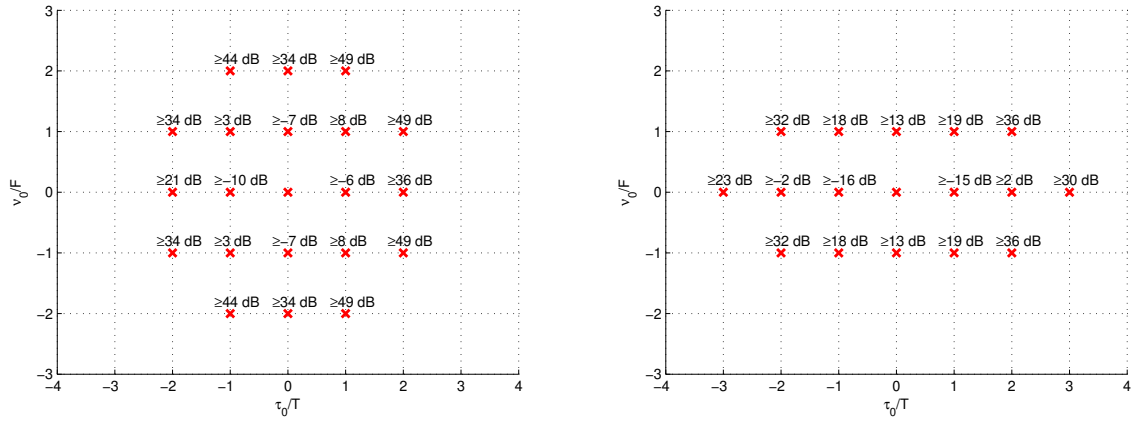

(a) Gaussian (NOFDM, $\rho = 1$). (b) Gaussian (NOFDM, $\rho = 0.4$).

Figure 6.3 Region of support for different SNR (Channel: ITU Vehicular A, $F = 1/T = 300$ kHz).

where $RSS^{(L)}$ is the instantaneous RSS for a hypothesized L and K_o is $L + 1$. Since Kullback-Leibler discrepancy indicates the information loss, the best model order among the set is obtained by minimizing AICc as

$$L_{\text{best}} = \arg\min_{L} \{AIC_{\text{c}}(L)\} \,. \tag{6.26}$$

6.5 Numerical Results

In this section, theoretical results given in the previous sections are investigated numerically considering the practical receivers. For the numerical investigations, ITU Vehicular A channel model is taken into account. Channel estimation is performed based on (6.17). Zadoff-Chu sequence is used for the channel estimation and N_o is set to 131. Two multicarrier schemes are taken into account: OFDM and non-orthogonal frequency division multiplexing (NOFDM) ($\nu_0 = F$ and $\tau_0 = T$). Rectangular and Gaussian filters are taken into account for OFDM and NOFDM, respectively. Note that Gaussian filter is the optimally-localized pulse in time-frequency and it is given by

$$p\,(t) = (2\rho)^{1/4} e^{-\pi\rho t^2} \,, \tag{6.27}$$

where ρ is the control parameters for the dispersion of the pulse in time and frequency and $\rho > 0$. For the equalization, maximum likelihood sequence detector (MLSD), which is optimum in AWGN, is considered.

In Figure 6.2, expected LS error in (6.18) and expected RSS in (6.22) are given for different L and E_{s}/N_0. As it can be seen in Figure 6.2, while dashed lines based on (6.18) monotonically decrease with L due to the better

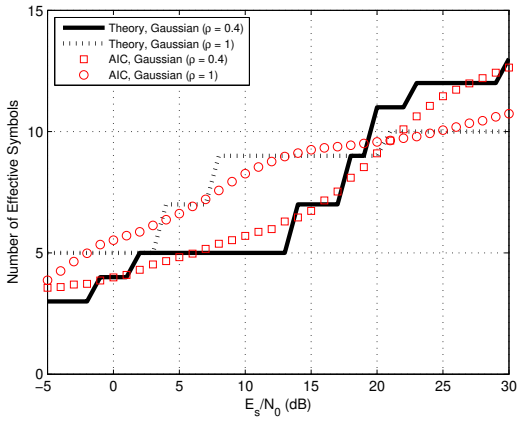

Figure 6.4 Practical performance using Akaike information criterion (Channel: ITU Vehicular A, $F = 1/T = 300$ kHz).

description of received signal, solid lines corresponding to (6.22) increase after certain value of L which indicates that the impact of the noise. Based on (6.23), single-tap equalizer is sufficient for a rectangular filter when F is set to 15 kHz, which also corresponds to OFDM in Long Term Evolution (LTE) where CP duration is set to $0.07 \times T_s$. However, if F is set to 300 kHz for the sake of demonstration, the same multicarrier structure requires significant amount of equalizer taps. For the same channel, required number of taps in the case of utilization of Gaussian pulse shape is less than the that of rectangular filter, which is reasonable for a practical receiver. Since higher E_s/N_0 yields a better channel estimation performance, it allows to use a larger number of equalizer taps.

In Figure 6.3, locations of interfering symbols and the minimum E_s/N_0 levels that interfering symbol starts to be effective on desired symbol, i.e., best RoS to improve the error performance at the receiver, are provided. For NOFDM, the neighboring symbols in both time and frequency cause significant amount of interference due to the Gaussian filter. The choice of $\rho = 1$ yields an isotropic ambiguity surface in time and frequency for an ideal channel. However, the symmetrical shape is distorted due to the dispersion in the multipath channel, and more interference is caused by the previous symbols. When ρ is set to 0.4, more overlapping is introduced in time, which also yields a larger number of equalizer taps in time domain.

In Figure 6.4, the average number of required equalizer taps is provided for NOFDM, based on AICc. It is shown that AICc, which is suggested for practical receiver structures, follows the theoretical results based on (6.23).

In Figure 6.5, BER performance of the receiver is investigated for various number of equalizer taps and E_s/N_0 for binary phase shift keying (BPSK). As it can be seen from Figure 6.5, using fewer or more taps than required ones degrades the BER performance. Theoretical result for L_{best} based on (6.23) approaches the minimum achievable BER for a given E_s/N_0 in both Figure 6.5(a) and Figure 6.5(b). It is worth noting that the strategy for L_{best} in (6.23) targets

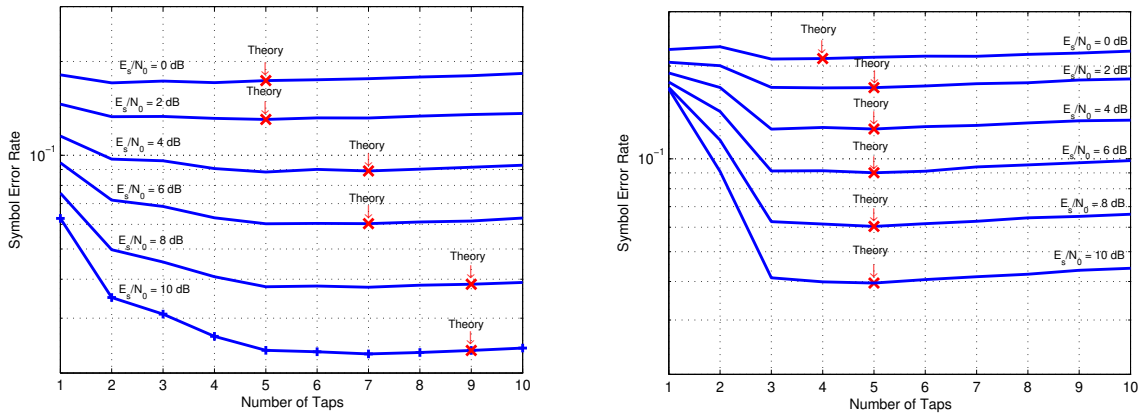

(a) Gaussian (NOFDM, $\rho = 1$). (b) Gaussian (NOFDM, $\rho = 0.4$).

Figure 6.5 BER versus number of equalizer taps (Channel: ITU Vehicular A, $F = 1/T = 300$ kHz).

to minimize expected RSS for the channel estimation by applying hypothetical cross-validation with another received signal as discussed in Section 6.4. Considering the performance in Figure 6.5, it is possible to choose a smaller number of equalizer taps at the expense of negligible BER degradation in practical conditions, which corresponds to apply more penalty term for the noise component in (6.23).

6.6 Concluding Remarks

In this study, we investigate the number of required equalizer taps for multicarrier schemes, based on the composite effects of the transmit filter, communication medium, and the receiver filter response. We explicitly show that employing more equalizer taps increases the complexity of the equalizer and degrades error rate performance of the receiver. Considering this issue, number of required equalizer taps and their locations in the time-frequency lattice are given theoretically as a function of communication medium characteristics, transmit filter, receive filter, and SNR. By exploiting the introduced concept for the determination of the number of required taps in multicarrier scheme, it is possible to develop adaptive multicarrier scheme based on the processing abilities at the receivers, or adaptive receiver architectures for a given multicarrier scheme. In other words, this approach promises a flexibility on both multicarrier schemes and receiver structures to adapt to the different conditions, e.g., dispersions in communication mediums.

REFERENCES

[1] D. Tse and P. Viswanath, *Fundamentals of wireless communication*. New York, NY, USA: Cambridge University Press, 2005.

[2] D. Gabor, "Theory of communication. part 1: The analysis of information," *Journal of the Institution of Electrical Engineers - Part III: Radio and Communication Engineering,*, vol. 93, no. 26, pp. 429–441, 1946.

[3] I. Daubechies, "The wavelet transform, time-frequency localization and signal analysis," *IEEE Trans. Inf. Theory*, vol. 36, no. 5, pp. 961–1005, Sep. 1990.

[4] T. Hwang, C. Yang, G. Wu, S. Li, and G. Li, "OFDM and its wireless applications: A survey," *IEEE Trans. Vehicular Technol.*, vol. 58, no. 4, pp. 1673–1694, 2009.

[5] B. Farhang-Boroujeny, "OFDM versus filter bank multicarrier," *IEEE Sig. Proc. Mag.*, vol. 28, no. 3, pp. 92–112, 2011.

[6] G. Matz, H. Bölcskei, and F. Hlawatsch, "Time-frequency foundations of communications," *IEEE Sig. Proc. Mag.*, Nov. (to appear) 2013.

[7] I. Daubechies, *Ten lectures on wavelets*. Philadelphia, PA, USA: Society for Industrial and Applied Mathematics, 1992.

[8] H. Feichtinger and T. Strohmer, *Gabor Analysis and Algorithms: Theory and Applications*, ser. Applied and Numerical Harmonic Analysis. Birkhäuser, 1998.

[9] O. Christensen, *An Introduction to Frames and Riesz Bases*, ser. Applied and Numerical Harmonic Analysis. Birkhäuser, 2003.

[10] J. J. Benedetto, C. Heil, and D. F. Walnut, "Differentiation and the Balian-Low theorem," *Journal of Fourier Analysis and Applications*, vol. 1, no. 4, pp. 355–402, 1994.

[11] A. Janssen, "Representations of Gabor frame operators," in *Twentieth Century Harmonic Analysis A Celebration*, ser. NATO Science Series, J. Byrnes, Ed. Springer Netherlands, 2001, vol. 33, pp. 73–101.

[12] O. Christensen, "Frames, Riesz bases, and discrete Gabor/wavelet expansions," *Bull. Amer. Math. Soc*, pp. 273–291, 2001.

[13] C. Heil, "History and evolution of the density theorem for Gabor frames," *Journal of Fourier Analysis and Applications*, vol. 13, no. 2, pp. 113–166, 2007.

[14] I. Daubechies, S. Jaffard, and J. Journ, "A simple Wilson orthonormal basis with exponential decay," *SIAM Journal on Mathematical Analysis*, vol. 22, no. 2, pp. 554–573, 1991.

[15] A. Janssen, "Duality and biorthogonality for Weyl-Heisenberg frames," *Journal of Fourier Analysis and Applications*, vol. 1, no. 4, pp. 403–436, 1994.

[16] B. Le Floch, M. Alard, and C. Berrou, "Coded orthogonal frequency division multiplex," *Proceedings of the IEEE*, vol. 83, no. 6, pp. 982–996, 1995.

[17] W. Kozek and A. Molisch, "Nonorthogonal pulseshapes for multicarrier communications in doubly dispersive channels," *IEEE J. Select. Areas Commun. (JSAC)*, vol. 16, no. 8, pp. 1579–1589, Oct. 1998.

[18] T. Strohmer, "Approximation of dual Gabor frames, window decay, and wireless communications," *Applied and Computational Harmonic Analysis*, vol. 11, no. 2, pp. 243–262, Sep. 2001.

[19] T. Strohmer and S. Beaver, "Optimal OFDM design for time-frequency dispersive channels," *IEEE Trans. Commun.*, vol. 51, no. 7, pp. 1111–1122, Jul. 2003.

[20] T. Werther, Y. Eldar, and N. Subbanna, "Dual Gabor frames: theory and computational aspects," *IEEE Trans. Sig. Proc.*, vol. 53, no. 11, pp. 4147–4158, 2005.

[21] G. Kutyniok and T. Strohmer, "Wilson bases for general time-frequency lattices," *SIAM Journal on Mathematical Analysis*, vol. 37, no. 3, pp. 685–711, 2005.

[22] P. Jung and G. Wunder, "The WSSUS pulse design problem in multicarrier transmission," *IEEE Trans. Commun.*, vol. 55, no. 10, pp. 1918–1928, Sep. 2007.

[23] G. Matz, D. Schafhuber, K. Grochenig, M. Hartmann, and F. Hlawatsch, "Analysis, optimization, and implementation of low-interference wireless multicarrier systems," *IEEE Trans. Wireless Commun.*, vol. 6, no. 5, pp. 1921–1931, May 2007.

[24] F.-M. Han and X.-D. Zhang, "Hexagonal multicarrier modulation: A robust transmission scheme for time-frequency dispersive channels," *IEEE Trans. Sig. Proc.*, vol. 55, no. 5, pp. 1955–1961, May 2007.

[25] F. M. Han and X. Zhang, "Wireless multicarrier digital transmission via Weyl-Heisenberg frames over time-frequency dispersive channels," *IEEE Trans. Commun.*, vol. 57, no. 6, pp. 1721–1733, June 2009.

[26] J. Du and S. Signell, "Classic OFDM systems and pulse-shaping OFDM/OQAM systems," *Technical Report (KTH - Royal Institute of Technology)*, pp. 1–32, Feb. 2007.

[27] P. L. Sondergaard, "Finite discrete Gabor analysis," Ph.D. dissertation, Danmarks Tekniske Universitet, 2007.

[28] P. Jung, "Weyl–Heisenberg representations in communication theory," Ph.D. dissertation, Technische Universität Berlin, 2007.

[29] J. Du, "Pulse shape adaptation and channel estimation in generalised frequency division multiplexing," Ph.D. dissertation, KTH Royal Institute of Technology, Stockholm, Sweden, Dec. 2008.

[30] C. Shannon, "Communication in the presence of noise," *Proceedings of the IEEE*, vol. 86, no. 2, pp. 447–457, 1998.

[31] P. Kabal and S. Pasupathy, "Partial-response signaling," *IEEE Trans. Commun.*, vol. 23, no. 9, pp. 921–934, Sep. 1975.

[32] J. E. Mazo, "Faster-Than-Nyquist Signaling," *Bell Syst. Techn. J.*, vol. 54, pp. 1451–1462, Oct. 1975.

[33] H. Bolcskei, P. Duhamel, and R. Hleiss, "Design of pulse shaping OFDM/OQAM systems for high data-rate transmission over wireless channels," in *IEEE Int. Conf. Commun. (ICC)*, vol. 1, Vancouver, Canada, June 1999, pp. 559–564.

[34] R. J. Duffin and A. C. Schaeffer, "A class of nonharmonic fourier series," *Transactions of the American Mathematical Society*, vol. 72, no. 2, pp. 341–366, Mar. 1952.

[35] G. Strang and T. Nguyen, *Wavelets and Filter Banks*. Wellesley-Cambridge Press, 1996.

[36] H. Bölcskei, *Orthogonal frequency division multiplexing based on offset QAM*, 2003, pp. 321–352.

[37] B. Farhang-Boroujeny and C. Yuen, "Cosine modulated and offset QAM filter bank multicarrier techniques: a continuous-time prospect," *EURASIP J. Advances in Sig. Proc.*, vol. Dec., pp. 1–6, 2010.

[38] B. Muquet, Z. Wang, G. Giannakis, M. De Courville, and P. Duhamel, "Cyclic prefixing or zero padding for wireless multicarrier transmissions?" *IEEE Trans. Commun.*, vol. 50, no. 12, pp. 2136–2148, 2002.

[39] G. Cherubini, E. Eleftheriou, and S. Olcer, "Filtered multitone modulation for VDSL," in *Proc. IEEE Global Telecommun. Conf. (GLOBECOM)*, vol. 2, Rio de Janeiro, Brazil, Dec. 1999, pp. 1139–1144.

[40] ——, "Filtered multitone modulation for very high-speed digital subscriber lines," *IEEE J. Select. Areas Commun.*, vol. 20, no. 5, pp. 1016–1028, June 2002.

[41] N. Benvenuto, S. Tomasin, and L. Tomba, "Equalization methods in OFDM and FMT systems for broadband wireless communications," *IEEE Trans. Commun.*, vol. 50, no. 9, pp. 1413–1418, 2002.

[42] A. Tonello, "Performance limits for filtered multitone modulation in fading channels," *IEEE Trans. Wireless Commun.*, vol. 4, no. 5, pp. 2121–2135, Sep. 2005.

[43] B. Farhang-Boroujeny, *Signal processing techniques for software radios*, 2nd ed. Lulu, 2010.

[44] F. Hlawatsch and G. Matz, *Wireless Communications Over Rapidly Time-Varying Channels*, ser. Academic Press. Elsevier Science, 2011.

[45] C. Siclet and P. Siohan, "Design of BFDM/OQAM systems based on biorthogonal modulated filter banks," in *Proc. IEEE Global Telecommunications Conference (GLOBECOM)*, vol. 2, 2000, pp. 701–705.

[46] G. Fettweis, M. Krondorf, and S. Bittner, "GFDM - generalized frequency division multiplexing," in *Proc. IEEE Vehicular Technology Conference (VTC)*, 2009, pp. 1–4.

[47] R. Datta, G. Fettweis, Z. Kollar, and P. Horvath, "FBMC and GFDM interference cancellation schemes for flexible digital radio PHY design," in *Proc. Euromicro Conf. Digital System Design (DSD)*, Oulu, Finland, Sept. 2011, pp. 335–339.

[48] S. Aldirmaz, A. Serbes, and L. Durak-Ata, "Spectrally efficient OFDMA lattice structure via toroidal waveforms on the time-frequency plane," *EURASIP J. Advances in Sig. Proc.*, pp. 1–13, June 2010.

[49] A. Liveris and C. Georghiades, "Exploiting faster-than-Nyquist signaling," *IEEE Trans. Commun.,*, vol. 51, no. 9, pp. 1502–1511, Sep. 2003.

[50] F. Rusek and J. Anderson, "The two dimensional Mazo limit," in *Proc. IEEE Int. Symp. on Information Theory (ISIT)*, Sep. 2005, pp. 970–974.

[51] F. Rusek and J. B. Anderson, "Successive interference cancellation in multistream faster-than-Nyquist signaling," in *Proc. Intl. Wireless Comm.and Mobile Computing Conf.* New York, NY, USA: ACM, 2006, pp. 1021–1026.

[52] ——, "Multistream faster than Nyquist signaling," *IEEE Trans. Commun.*, vol. 57, no. 5, pp. 1329–1340, May 2009.

[53] H. Sari, G. Karam, and I. Jeanclaude, "Transmission techniques for digital terrestrial TV broadcasting," *Communications Magazine, IEEE*, vol. 33, no. 2, pp. 100 –109, Feb. 1995.

[54] T. Ihalainen, A. Viholainen, T. Stitz, M. Renfors, and M. Bellanger, "Filter bank based multi-mode multiple access scheme for wireless uplink," in *Proc. European Signal Processing Conf. (EUSIPCO)*, vol. 9, Glascow, Scotland, Aug. 2009, pp. 1354–1358.

[55] H. Sari, G. Karam, and I. Jeanclaud, "Frequency-domain equalization of mobile radio and terrestrial broadcast channels," in *Proc. IEEE Global Telecommun. Conf. (GLOBECOM)*, vol. 1, Dec. 1994, pp. 1–5.

[56] D. Falconer, S. Ariyavisitakul, A. Benyamin-Seeyar, and B. Eidson, "Frequency domain equalization for single-carrier broadband wireless systems," *Communications Magazine, IEEE*, vol. 40, no. 4, pp. 58 –66, Apr. 2002.

[57] H. G. Myung, J. Lim, and D. J. Goodman, "Single carrier FDMA for uplink wireless transmission," *Vehicular Technology Magazine, IEEE*, vol. 1, no. 3, pp. 30–38, Sep. 2006.

[58] G. Berardinelli, L. Ruiz de Temino, S. Frattasi, M. Rahman, and P. Mogensen, "OFDMA vs. SC-FDMA: performance comparison in local area IMT-A scenarios," *Wireless Communications, IEEE*, vol. 15, no. 5, pp. 64 –72, october 2008.

[59] R. W. Chang, "Synthesis of band-limited orthogonal signals for multichannel data transmission," *The Bell System Technical J.*, pp. 1775–1796, Dec. 1966.

[60] B. Saltzberg, "Performance of an efficient parallel data transmission system," *IEEE Trans. Commun. Technol.*, vol. 15, no. 6, pp. 805–811, Dec. 1967.

[61] S. Weinstein and P. Ebert, "Data transmission by frequency-division multiplexing using the discrete Fourier transform," *IEEE Trans. Commun. Technol.*, vol. 19, no. 5, pp. 628–634, Oct. 1971.

[62] A. Peled and A. Ruiz, "Frequency domain data transmission using reduced computational complexity algorithms," in *Proc. IEEE Int. Conf. Acoustics, Speech, Sig. Proc. (ICASSP)*, vol. 5, Apr. 1980, pp. 964–967.

[63] B. Hirosaki, "An orthogonally multiplexed QAM system using the discrete Fourier transform," *IEEE Trans. Commun.*, vol. 29, no. 7, pp. 982–989, 1981.

[64] M. Bellanger, G. Bonnerot, and M. Coudreuse, "Digital filtering by polyphase network: Application to sample-rate alteration and filter banks," *IEEE Trans. Acoustics, Speech and Sig. Proc.*, vol. 24, no. 2, pp. 109–114, Apr. 1976.

[65] P. Vaidyanathan, "Multirate digital filters, filter banks, polyphase networks, and applications: A tutorial," *Proc. of the IEEE*, vol. 78, no. 1, pp. 56–93, Jan. 1990.

[66] P. Siohan, C. Siclet, and N. Lacaille, "Analysis and design of OFDM/OQAM systems based on filterbank theory," *IEEE Trans. Sig. Proc.*, vol. 50, no. 5, pp. 1170–1183, May 2002.

[67] H. Landau and H. Pollack, "Prolate spheroidal wave functions, Fourier analysis and uncertaintyii," *Bell Syst. Techn. J.*, vol. 40, p. 6594, 1961.

[68] D. Slepian and H. Pollack, "Prolate spheroidal wave functions, Fourier analysis and uncertaintyi," *Bell Syst. Techn. J.*, vol. 40, p. 4363, 1961.

[69] H. Landau and H. Pollack, "Prolate spheroidal wave functions, Fourier analysis and uncertaintyiii: the dimension of the space of essentially time and bandlimited signals," *Bell Syst. Techn. J.*, vol. 41, pp. 1295–1336, 1962.

[70] D. Slepian, "Prolate spheroidal wave functions, Fourier analysis and uncertaintyiv: extensions to many dimensions; generalized prolate spheroidal functions," *Bell Syst. Techn. J.*, vol. 43, pp. 3009–3057, 1964.

[71] ——, "Prolate spheroidal wave functions, Fourier analysis and uncertaintyv: The discrete case," *Bell Syst. Techn. J.*, vol. 57, pp. 1371–1430, 1978.

[72] ——, "Some comments on Fourier analysis, uncertainty and modeling," *SIAM Review*, vol. 25, no. 3, pp. 379–393, 1983.

[73] J. Kaiser and R. Schafer, "On the use of the I0-sinh window for spectrum analysis," *IEEE Trans. Acoust., Speech, Signal Proc.,*, vol. 28, no. 1, pp. 105–107, Feb. 1980.

[74] P. Halpern, "Optimum finite duration Nyquist signals," *IEEE Trans. Commun.*, vol. 27, no. 6, pp. 884–888, Jun. 1979.

[75] A. Vahlin and N. Holte, "Optimal finite duration pulses for OFDM," *IEEE Trans. Commun.*, vol. 44, no. 1, pp. 10–14, Jan. 1996.

[76] G. Walter and T. Soleski, "A new friendly method of computing prolate spheroidal wave functions and wavelets," *Applied and Computational Harmonic Analysis*, vol. 19, no. 3, pp. 432–443, 2005.

[77] I. C. Moore and M. Cada, "Prolate spheroidal wave functions, anintroduction to the Slepian series and its properties," *Applied and Computational Harmonic Analysis*, vol. 16, no. 3, pp. 208–230, 2004.

[78] K. W. Martin, "Small side-lobe filter design for multitone data-communication applications," *IEEE Trans. Circuits and Systems–II: Analog and Digital Signal Processing*, vol. 45, no. 8, pp. 1155–1161, Aug. 1998.

[79] M. Bellanger, "Specification and design of a prototype filter for filter bank based multicarrier transmission," in *Proc. IEEE Int. Conf. Acoustics, Speech, Sig. Proc. (ICASSP)*, vol. 4, Salt Lake City, UT, May 2001, pp. 2417–2420.

[80] S. Mirabbasi and K. Martin, "Design of prototype filter for near-perfect-reconstruction overlapped complex-modulated transmultiplexers," in *Proc. IEEE International Symposium on Circuits and Systems (ISCAS)*, vol. 1, 2002, pp. 821–824.

[81] R. Haas and J. Belfiore, "A time-frequency well-localized pulse for multiple carrier transmission," *Wireless Personal Commun.*, vol. 5, no. 1, pp. 1–18, July 1997.

[82] F. Harris, "On the use of windows for harmonic analysis with the discrete Fourier transform," *Proceedings of the IEEE*, vol. 66, no. 1, pp. 51–83, 1978.

[83] N. Geckinli and D. Yavuz, "Some novel windows and a concise tutorial comparison of window families," *IEEE Trans. Acoust., Speech, Signal*, vol. 26, no. 6, pp. 501–507, 1978.

[84] G. Nigam, R. Singh, and A. Chaturvedi, "Finite duration root Nyquist pulses with maximum in-band fractional energy," *IEEE Commun. Lett.*, vol. 14, no. 9, pp. 797 – 799, Sep. 2010.

[85] J. Du and S. Signell, "Pulse shape adaptivity in OFDM/OQAM systems," in *Proc. IEEE Int. Conf. Advanced Infocomm Technology (ICAIT)*, Shen Zhen, China, July 2008.

[86] C. Roche and P. Siohan, "A family of extended gaussian functions with a nearly optimal localization property," in *Multi-Carrier Spread-Spectrum*, K. Fazel and G. Fettweis, Eds. Springer US, 1997.

[87] P. Siohan and C. Roche, "Cosine-modulated filterbanks based on extended Gaussian functions," *IEEE Trans. Sig. Proc.*, vol. 48, no. 11, pp. 3052–3061, Nov. 2000.

[88] P. Singla and T. Singh, "Desired order continuous polynomial time window functions for harmonic analysis," *IEEE Trans. Instrum. Meas.*, vol. 59, no. 9, pp. 2475–2481, 2010.

[89] S. Mirabbasi and K. Martin, "Overlapped complex-modulated transmultiplexer filters with simplified design and superior stopbands," *IEEE Trans. Circuits Syst. II, Analog Digit. Signal Process.*, vol. 50, no. 8, pp. 456–469, 2003.

[90] F. Schaich, "Filterbank based multi carrier transmission (FBMC) evolving OFDM: FBMC in the context of WiMAX," in *Proc. European Wireless Conf. (EW)*, Lucca, Italy, Apr. 2010, pp. 1051–1058.

[91] M. Bellanger, "FBMC physical layer: A primer," *PHYDYAS FP7 Project Document*, Jan. 2010.

[92] S. Brandes, I. Cosovic, and M. Schnell, "Reduction of Out-of-Band Radiation in OFDM Systems by Insertion of Cancellation Carriers," *IEEE Communications Letters*, vol. 10, no. 6, pp. 420–422, 2006.

[93] P. Amini, C. Yuen, R. Chen, and B. Farhang-Boroujeny, "Isotropic filter design for MIMO filter bank multicarrier communications," in *Proc. IEEE Sensor Array and Multichannel Sig. Proc. Workshop (SAM)*, Israel, Oct. 2010, pp. 89–92.

[94] I. Trigui, M. Siala, S. Affes, A. Stéphenne, and H. Boujemâa, "Optimum pulse shaping for OFDM/BFDM systems operating in time varying multi-path channels," in *Proc. IEEE Global Telecommun. Conf. (GLOBECOM)*, Washington, D.C., Nov. 2007, pp. 3817–3821.

[95] D. Schafhuber, G. Matz, and F. Hlawatsch, "Pulse-shaping OFDM/BFDM systems for time-varying channels: ISI/ICI analysis, optimal pulse design, and efficient implementation," in *Proc. IEEE Int. Symp. Personal, Indoor and Mobile Radio Commun. (PIMRC)*, vol. 3, Lisboa, Portugal, Sep. 2002, pp. 1012–1016.

[96] H. Lin and P. Siohan, "Robust channel estimation for OFDM/OQAM," *IEEE Commun. Lett.*, vol. 13, no. 10, pp. 724–726, Oct. 2009.

[97] B. Farhang-Boroujeny, "A square-root nyquist (M) filter design for digital communication systems," *IEEE Trans. Sig. Proc.*, vol. 56, no. 5, pp. 2127–2132, May 2008.

[98] P. Bello, "Characterization of randomly time-variant linear channels," *IEEE Trans. Commun. Syst.*, vol. 11, no. 4, pp. 360–393, Dec. 1963.

[99] B. G. Molnar, I. Frigyes, Z. Bodnar, and Z. Herczku, "The WSSUS channel model: comments and a generalisation," in *Proc. IEEE Global Telecommun. Conf. (GLOBECOM)*, London, England, Nov. 1996, pp. 158–162.

[100] G. Matz, "Statistical characterization of non-WSSUS mobile radio channels," *e& i Elektrotechnik und Informationstechnik*, vol. 122, no. 3, pp. 80–84, Mar. 2005.

[101] W. Kozek and A. Molisch, "On the eigenstructure of underspread WSSUS channels," in *Proc. IEEE Workshop on Sig. Proc. Advances in Wireless Commun. (SPAWC)*, Apr. 1997.

[102] T. Rappaport, *Wireless Communications: Principles and Practice*, 2nd ed. Upper Saddle River, NJ, USA: Prentice Hall PTR, 2001.

[103] ITU Recommendation, "ITU-R M.1225 Guidelines for Evaluation of Radio Transmission Technologies for IMT-2000," 1997.

[104] A. Sahin and H. Arslan, "Edge windowing for OFDM based systems," *IEEE Commun. Lett.*, vol. 15, no. 11, pp. 1208–1211, 2011.

[105] ——, "The impact of scheduling on edge windowing," in *Proc. IEEE Global Telecommunications Conference (GLOBECOM)*, 2011, pp. 1–5.

[106] T. Weiss, J. Hillenbrand, A. Krohn, and F. Jondral, "Mutual interference in OFDM-based spectrum pooling systems," in *Proc. IEEE Vehic. Technol. Conf. (VTC)*, vol. 4, May. 2004, pp. 1873–1877.

[107] H. Mahmoud and H. Arslan, "Spectrum Shaping of OFDM-Based Cognitive Radio Signals," Jan. 2008, pp. 113 –116.

[108] ——, "Sidelobe Suppression in OFDM-Based Spectrum Sharing Systems Using Adaptive Symbol Transition," *IEEE Communications Letters*, vol. 12, no. 2, pp. 133–135, Feb. 2008.

[109] V. Erceg, D. Michelson, S. Ghassemzadeh, L. Greenstein, J. Rustako, A.J., P. Guerlain, M. Dennison, R. Roman, D. Barnickel, S. Wang, and R. Miller, "A model for the multipath delay profile of fixed wireless channels," *Selected Areas in Communications, IEEE Journal on*, vol. 17, no. 3, pp. 399 –410, Mar. 1999.

[110] L. Greenstein, V. Erceg, Y. Yeh, and M. Clark, "A new path-gain/delay-spread propagation model for digital cellular channels," *IEEE Trans. Vehic. Tech.*, vol. 46, no. 2, pp. 477–485, May 1997.

[111] A. Sahin and H. Arslan, "Multi-user aware frame structure for OFDMA based system," in *Proc. IEEE Veh. Technol. Conf. (VTC)*, Quebec City, Canada, Sep. 2012, pp. 1–5.

[112] S. Sesia, I. Toufik, and M. Baker, *The UMTS Long Term Evolution: From Theory to Practice*. Wiley Publishing, 2009.

[113] Z. Zhao-yang and L. Li-Feng, "A novel OFDM transmission scheme with length-adaptive cyclic prefix," *Journal of Zhejiang University SCIENCE A*, vol. 5, no. 11, pp. 1336–1342, 2004.

[114] S. D'Alessandro, A. Tonello, and L. Lampe, "Improving WLAN Capacity via OFDMA and Cyclic Prefix Adaptation," in *Proc. IEEE Wireless Days (WD)*, Dec. 2009, pp. 1–5.

[115] ——, "On Power Allocation in Adaptive Cyclic Prefix OFDM," in *Proc. IEEE International Symposium on Power Line Communications and Its Applications (ISPLC)*, Mar. 2010, pp. 183–188.

[116] A. M. Tonello, S. D'Alessandro, and L. Lampe, "Cyclic prefix design and allocation in bit-loaded OFDM over power line communication channels," *IEEE Trans. Commun.*, vol. 58, pp. 3265–3276, Nov. 2010.

[117] Y. Huang and B. Rao, "On Using a Priori Channel Statistics for Cyclic Prefix Optimization in OFDM," in *Proc. IEEE Wireless Communications and Networking Conference (WCNC)*, Mar. 2011, pp. 1460–1465.

[118] S. Das, E. De Carvalho, and R. Prasad, "Dynamically adaptive bandwidth for sub carriers in ofdm based wireless systems," in *Proc. IEEE Wireless Communications and Networking Conference (WCNC)*, Mar. 2007, pp. 1378–1383.

[119] D. H. Holma and D. A. Toskala, *LTE for UMTS - OFDMA and SC-FDMA Based Radio Access*. Wiley Publishing, 2009.

[120] A. Sahin, I. Guvenc, and H. Arslan, "A comparative study of fbmc prototype filters in doubly dispersive channels," in *Proc. IEEE Broadband Wireless Access Workshop (co-located with IEEE GLOBECOM 2012) (Accepted)*, Anaheim, California, Dec. 2012.

[121] T. Rappaport, *Wireless Communications: Principles and Practice*, 2nd ed. Upper Saddle River, NJ, USA: Prentice Hall, 2001.

[122] C. Bettstetter, H. Hartenstein, and X. Pérez-Costa, "Stochastic properties of the random waypoint mobility model," *Wireless Networks*, vol. 10, pp. 555–567, Sep. 2004.

[123] P. Bratanov and E. Bonek, "Mobility model of vehicle-borne terminals in urban cellular systems," *IEEE Trans. Vehic. Tech.*, vol. 52, no. 4, pp. 947–952, Jul. 2003.

[124] P. Dintchev, B. Perez-Quiles, and E. Bonek, "An improved mobility model for 2G and 3G cellular systems," *Proc. IEE International Conference on 3G Mobile Communication Technologies*, vol. 1, pp. 402–406, 2004.

[125] G. Paschos, E. Vagenas, and S. Kotsopoulos, "User Mobility Model Based on Street Pattern," in *Proc. IEEE Vehicular Technology Conference (VTC)*, vol. 4, May 2005, pp. 2123–2126.

[126] D. Shnidman, "The calculation of the probability of detection and the generalized Marcum Q-function," *IEEE Transactions on Information Theory*, vol. 35, no. 2, pp. 389–400, Mar. 1989.

[127] Y. Li and J. Cimini, L.J., "Bounds on the interchannel interference of OFDM in time-varying impairments," *IEEE Trans. Commun.*, vol. 49, no. 3, pp. 401–404, Mar. 2001.

[128] 3GPP TS 36.814 V9.0.0, "Evolved Universal Terrestrial Radio Access (E-UTRA); Further advancements for E-UTRA physical layer aspects V9.0.0," Mar. 2010.

[129] A. Sahin, I. Güvenç, and H. Arslan, "A survey on multicarrier communications: Prototype filters, lattice structures, and implementation aspects," *CoRR*, vol. abs/1212.3374v2, 2012.

[130] W. Kozek and A. Molisch, "Nonorthogonal pulseshapes for multicarrier communications in doubly dispersive channels," *IEEE J. Select. Areas Commun. (JSAC)*, vol. 16, no. 8, pp. 1579–1589, Oct. 1998.

[131] D. Lopez-Perez, I. Guvenc, G. De la Roche, M. Kountouris, T. Quek, and J. Zhang, "Enhanced intercell interference coordination challenges in heterogeneous networks," *IEEE Wireless Communications*, vol. 18, no. 3, pp. 22–30, 2011.

[132] J. Andrews, "Interference cancellation for cellular systems: a contemporary overview," *IEEE Wireless Communications*, vol. 12, no. 2, pp. 19–29, 2005.

[133] S. Verdu, *Multiuser Detection*. Cambridge University Press, 1998.

[134] V. Cadambe and S. Jafar, "Interference alignment and degrees of freedom of the k-user interference channel," *IEEE Trans. Information Theory,*, vol. 54, no. 8, pp. 3425–3441, 2008.

[135] A. Mishra, V. Shrivastava, S. Banerjee, and W. Arbaugh, "Partially overlapped channels not considered harmful," *SIGMETRICS Perform. Eval. Rev.*, vol. 34, no. 1, pp. 63–74, Jun. 2006.

[136] Y. Ding, Y. Huang, G. Zeng, and L. Xiao, "Channel assignment with partially overlapping channels in wireless mesh networks," in *Proceedings of the 4th Annual International Conference on Wireless Internet*, ser. WICON '08, ICST, Brussels, Belgium, 2008, pp. 38:1–38:9.

[137] Y. Cui, W. Li, and X. Cheng, "Partially overlapping channel assignment based on node orthogonality for 802.11 wireless networks," in *Proc. IEEE International Conference on Computer Communications (INFOCOM)*, 2011, pp. 361–365.

[138] O. Ileri, I. Hokelek, H. Arslan, and E. Ustunel, "Improving data capacity in cellular networks through utilizing partially overlapping channels," in *Proc. IEEE Conference on Signal Processing and Communications Applications (SIU),*, Apr. 2011, pp. 1121–1124.

[139] P. Duarte, Z. Fadlullah, A. Vasilakos, and N. Kato, "On the partially overlapped channel assignment on wireless mesh network backbone: A game theoretic approach," *IEEE J. Select. Areas Commun. (JSAC)*, vol. 30, no. 1, pp. 119–127, 2012.

[140] M. Fu, H. Crussiere and M. Helard, "Spectral efficiency optimization in overlapping channels using TR-MISO systems," in *Proc. IEEE Wireless Communications and Networking Conference (WCNC)*, Apr. 2013.

[141] V. Chandrasekhar, J. Andrews, and A. Gatherer, "Femtocell networks: a survey," *IEEE Commun. Mag.*, vol. 46, no. 9, pp. 59–67, Sep. 2008.

[142] M. Sahin, I. Guvenc, and H. Arslan, "Opportunity Detection for OFDMA-Based Cognitive Radio Systems with Timing Misalignment," *IEEE Trans. Wireless Commun.*, vol. 8, no. 10, pp. 5300–5313, Oct. 2009.

[143] A. Sahin, I. Guvenc, and H. Arslan, "Analysis of uplink inter-carrier-interference observed at femtocell networks," in *Proc. IEEE International Conference on Communications (ICC)*, 2011, pp. 1–6.

[144] K. Hamdi and Y. Shobowale, "Interference analysis in downlink OFDM considering imperfect intercell synchronization," *IEEE Trans. Veh. Tech.*, vol. 58, no. 7, pp. 3283–3291, Sep. 2009.

[145] Y. Medjahdi, M. Terre, D. L. Ruyet, D. Roviras, and A. Dziri, "Performance analysis in the downlink of asynchronous OFDM/FBMC based multi-cellular networks," *IEEE Trans. Wireless Commun.*, vol. 10, no. 8, pp. 2630–2639, Aug. 2011.

[146] A. Sahin, E. Guvenkaya, and H. Arslan, "User distance distribution for overlapping and coexisting cell scenarios," *IEEE Wireless Commun. Lett.*, vol. 1, no. 5, pp. 432–435, Oct. 2012.

[147] M. Win, P. Pinto, and L. Shepp, "A mathematical theory of network interference and its applications," *Proceedings of the IEEE*, vol. 97, no. 2, pp. 205–230, 2009.

[148] J. Andrews, F. Baccelli, and R. Ganti, "A tractable approach to coverage and rate in cellular networks," *IEEE Trans. Commun.*, vol. 59, no. 11, pp. 3122–3134, Nov. 2011.

[149] T. D. Novlan, H. S. Dhillon, and J. G. Andrews, "Analytical modeling of uplink cellular networks," *CoRR*, vol. abs/1203.1304, 2012.

[150] H. Dhillon, R. Ganti, F. Baccelli, and J. Andrews, "Modeling and analysis of K-tier downlink heterogeneous cellular networks," *IEEE J. Sel. Areas Commun.*, vol. 30, no. 3, pp. 550–560, Apr. 2012.

[151] P. Pinto and M. Win, "Communication in a Poisson field of interferers–part I: Interference distribution and error probability," *IEEE Trans. Wireless Commun.*, vol. 9, no. 7, pp. 2176–2186, 2010.

[152] X. Lin, J. G. Andrews, and A. Ghosh, "A comprehensive framework for device-to-device communications in cellular networks," *CoRR*, vol. abs/1305.4219, 2013.

[153] C. Tellambura and D. Senaratne, "Accurate computation of the MGF of the lognormal distribution and its application to sum of lognormals," *IEEE Trans. Commun.*, vol. 58, no. 5, pp. 1568–1577, May 2010.

[154] N. Mehta, J. Wu, A. Molisch, and J. Zhang, "Approximating a sum of random variables with a lognormal," *IEEE Trans. Wireless Commun.*, vol. 6, no. 7, pp. 2690–2699, Jul. 2007.

[155] M. Marey and H. Steendam, "Analysis of the narrowband interference effect on OFDM timing synchronization," *IEEE Trans. Sig. Proc.*, vol. 55, no. 9, pp. 4558–4566, 2007.

[156] M. Morelli and M. Moretti, "Robust frequency synchronization for OFDM-based cognitive radio systems," *IEEE Trans. Wireless Commun.*, vol. 7, no. 12, pp. 5346–5355, 2008.

[157] J. Anderson, F. Rusek, and V. Owall, "Faster-Than-Nyquist signaling," *Proceedings of the IEEE*, vol. 101, no. 8, pp. 1817–1830, 2013.

[158] K. Hamdi, "A useful technique for interference analysis in Nakagami fading," *IEEE Trans. Commun.*, vol. 55, no. 6, pp. 1120–1124, Jun. 2007.

[159] K. Cho and D. Yoon, "On the general BER expression of one- and two-dimensional amplitude modulations," *IEEE Trans. Commun.*, vol. 50, no. 7, pp. 1074–1080, 2002.

[160] K. Hamdi, "Precise interference analysis of OFDMA time-asynchronous wireless ad-hoc networks," *IEEE Trans. Wireless Commun.*, vol. 9, no. 1, pp. 134–144, Jan. 2010.

[161] Report ITU-R M.2135, "Guidelines for evaluation of radio interface technologies for IMA-Advanced."

[162] H. Arslan and E. Bottomley, "Channel estimation in narrowband wireless communication systems," *IEEE Trans. Commun. Technol.*, vol. 1, pp. 201–219, Apr. 2001.

[163] L. Baltar, A. Mezghani, and J. Nossek, "MLSE and MMSE subchannel equalization for filter bank based multicarrier systems: Coded and uncoded results," in *Proc. European Signal Processing Conf. (EUSIPCO)*, Aalborg, Denmark, Aug. 2010, pp. 2186–2190.

[164] G. Bottomley, *Channel Equalization for Wireless Communications: From Concepts to Detailed Mathematics*, ser. IEEE Series on Digital & Mobile Communication. Wiley, 2011.

[165] M. Wax and T. Kailath, "Detection of signals by information theoretic criteria," *IEEE Trans. Acoust., Speech, Signal Process. (19751990)*, vol. 33, no. 2, pp. 387–392, 1985.

[166] P. Stoica and Y. Selen, "Model-order selection: a review of information criterion rules," *IEEE Sig. Proc. Mag.*, vol. 21, no. 4, pp. 36–47, 2004.

[167] B. Yang, K. Letaief, R. Cheng, and Z. Cao, "Channel estimation for OFDM transmission in multipath fading channels based on parametric channel modeling," *IEEE Trans. Commun.*, vol. 49, no. 3, pp. 467–479, 2001.

[168] A. Ali, V. D. Nguyen, K. Kyamakya, and A. Omar, "Estimation of the channel-impulse-response length for adaptive OFDM systems based on information theoretic criteria," in *Proc. IEEE Vehicular Technology Conference (VTC)*, vol. 4, 2006, pp. 1888–1892.

[169] J.-H. Chen and Y. Lee, "Joint synchronization, channel length estimation, and channel estimation for the maximum likelihood sequence estimator for high speed wireless communications," in *Proc. IEEE Vehicular Technology Conference (VTC)*, vol. 3, 2002, pp. 1535–1539.

[170] V. D. Nguyen, H.-P. Kuchenbecker, and M. Patzold, "Estimation of the channel impulse response length and the noise variance for ofdm systems," in *Proc. IEEE Vehicular Technology Conference (VTC)*, vol. 1, 2005, pp. 429–433.

[171] A. Sahin, S. Aldırmaz, I. Güvenç, and H. Arslan, "An investigation on number of effective taps for multicarrier schemes," in *Proc. IEEE Vehicular Technology Conference (VTC)*, 2013.

[172] D. Chu, "Polyphase codes with good periodic correlation properties," *IEEE Trans. Inf. Theory*, vol. 18, no. 4, pp. 531–532, 1972.

[173] K. Burnham and D. Anderson, *Model selection and multi-model inference: a practical information-theoretic approach*. Springer, 2002.

[174] H. Akaike, "A new look at the statistical model identification," *IEEE Trans. on Automatic Control*, vol. 19, no. 6, pp. 716–723, Dec. 1974.

[175] C. M. Hurvich and C.-L. Tsai, "Regression and time series model selection in small samples," *Biometrika*, vol. 76, no. 2, pp. 297–307, 1989.

[176] J. Rissanen, "Modeling by shortest data description," *Automatica*, vol. 14, no. 5, pp. 465 – 471, 1978.

APPENDICES

Appendix A : Copyright Notice for Chapter 3

Thesis / Dissertation Reuse

The IEEE does not require individuals working on a thesis to obtain a formal reuse license, however, you may print out this statement to be used as a permission grant:

Requirements to be followed when using any portion (e.g., figure, graph, table, or textual material) of an IEEE copyrighted paper in a thesis:

1) In the case of textual material (e.g., using short quotes or referring to the work within these papers) users must give full credit to the original source (author, paper, publication) followed by the IEEE copyright line © 2011 IEEE.
2) In the case of illustrations or tabular material, we require that the copyright line © [Year of original publication] IEEE appear prominently with each reprinted figure and/or table.
3) If a substantial portion of the original paper is to be used, and if you are not the senior author, also obtain the senior author's approval.

Requirements to be followed when using an entire IEEE copyrighted paper in a thesis:

1) The following IEEE copyright/ credit notice should be placed prominently in the references: © [year of original publication] IEEE. Reprinted, with permission, from [author names, paper title, IEEE publication title, and month/year of publication]
2) Only the accepted version of an IEEE copyrighted paper can be used when posting the paper or your thesis on-line.
3) In placing the thesis on the author's university website, please display the following message in a prominent place on the website: In reference to IEEE copyrighted material which is used with permission in this thesis, the IEEE does not endorse any of [university/educational entity's name goes here]'s products or services. Internal or personal use of this material is permitted. If interested in reprinting/republishing IEEE copyrighted material for advertising or promotional purposes or for creating new collective works for resale or redistribution, please go to http://www.ieee.org/publications_standards/publications/rights/rights_link.html to learn how to obtain a License from RightsLink.

If applicable, University Microfilms and/or ProQuest Library, or the Archives of Canada may supply single copies of the dissertation.

BACK CLOSE WINDOW

Appendix A (Continued)

Title: The Impact of Scheduling on Edge Windowing
Conference Proceedings: Global Telecommunications Conference (GLOBECOM 2011), 2011 IEEE
Author: Sahin, A.; Arslan, H.
Publisher: IEEE
Date: 5-9 Dec. 2011

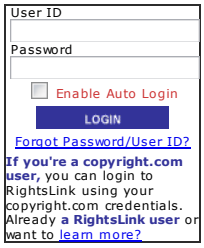

Thesis / Dissertation Reuse

The IEEE does not require individuals working on a thesis to obtain a formal reuse license, however, you may print out this statement to be used as a permission grant:

Requirements to be followed when using any portion (e.g., figure, graph, table, or textual material) of an IEEE copyrighted paper in a thesis:

1) In the case of textual material (e.g., using short quotes or referring to the work within these papers) users must give full credit to the original source (author, paper, publication) followed by the IEEE copyright line © 2011 IEEE.
2) In the case of illustrations or tabular material, we require that the copyright line © [Year of original publication] IEEE appear prominently with each reprinted figure and/or table.
3) If a substantial portion of the original paper is to be used, and if you are not the senior author, also obtain the senior author's approval.

Requirements to be followed when using an entire IEEE copyrighted paper in a thesis:

1) The following IEEE copyright/ credit notice should be placed prominently in the references: © [year of original publication] IEEE. Reprinted, with permission, from [author names, paper title, IEEE publication title, and month/year of publication]
2) Only the accepted version of an IEEE copyrighted paper can be used when posting the paper or your thesis on-line.
3) In placing the thesis on the author's university website, please display the following message in a prominent place on the website: In reference to IEEE copyrighted material which is used with permission in this thesis, the IEEE does not endorse any of [university/educational entity's name goes here]'s products or services. Internal or personal use of this material is permitted. If interested in reprinting/republishing IEEE copyrighted material for advertising or promotional purposes or for creating new collective works for resale or redistribution, please go to http://www.ieee.org/publications_standards/publications/rights/rights_link.html to learn how to obtain a License from RightsLink.

If applicable, University Microfilms and/or ProQuest Library, or the Archives of Canada may supply single copies of the dissertation.

Appendix B : Copyright Notice for Chapter 4

Thesis / Dissertation Reuse

The IEEE does not require individuals working on a thesis to obtain a formal reuse license, however, you may print out this statement to be used as a permission grant:

Requirements to be followed when using any portion (e.g., figure, graph, table, or textual material) of an IEEE copyrighted paper in a thesis:

1) In the case of textual material (e.g., using short quotes or referring to the work within these papers) users must give full credit to the original source (author, paper, publication) followed by the IEEE copyright line © 2011 IEEE.
2) In the case of illustrations or tabular material, we require that the copyright line © [Year of original publication] IEEE appear prominently with each reprinted figure and/or table.
3) If a substantial portion of the original paper is to be used, and if you are not the senior author, also obtain the senior author's approval.

Requirements to be followed when using an entire IEEE copyrighted paper in a thesis:

1) The following IEEE copyright/ credit notice should be placed prominently in the references: © [year of original publication] IEEE. Reprinted, with permission, from [author names, paper title, IEEE publication title, and month/year of publication]
2) Only the accepted version of an IEEE copyrighted paper can be used when posting the paper or your thesis on-line.
3) In placing the thesis on the author's university website, please display the following message in a prominent place on the website: In reference to IEEE copyrighted material which is used with permission in this thesis, the IEEE does not endorse any of [university/educational entity's name goes here]'s products or services. Internal or personal use of this material is permitted. If interested in reprinting/republishing IEEE copyrighted material for advertising or promotional purposes or for creating new collective works for resale or redistribution, please go to http://www.ieee.org/publications_standards/publications/rights/rights_link.html to learn how to obtain a License from RightsLink.

If applicable, University Microfilms and/or ProQuest Library, or the Archives of Canada may supply single copies of the dissertation.

BACK CLOSE WINDOW

Appendix C : Mean Square Error of Channel Estimation

Let $\mathbf{y_{T},_1}$ and $\mathbf{y_{T},_2}$ be the received signals exposed to the same channel but different noise components as

$$\mathbf{y_{T},_1} = \mathbf{\Phi_T h} + \omega_1 \ ,$$
$$\mathbf{y_{T},_2} = \mathbf{\Phi_T h} + \omega_2$$

where ω_1 and ω_2 are the noise vectors. Consider that the channel estimation is performed based on $\mathbf{y_{T},_1}$ using (6.17). Then, expected LS error based on $\mathbf{y_{T},_1}$, MSE of the channel estimation, expected RSS based on $\mathbf{y_{T},_2}$ are given as

$$\begin{aligned}
&\mathrm{E}\left[(\mathbf{y_{T},_1} - \tilde{\mathbf{y}}_{\mathbf{T},1})^*(\mathbf{y_{T},_1} - \tilde{\mathbf{y}}_{\mathbf{T},1})\right] \\
&= \mathrm{E}\left[(\mathbf{Q}^{(L)}\mathbf{y_{T},_1})^*\mathbf{Q}^{(L)}\mathbf{y_{T,1}}\right] \\
&\overset{a}{=} \mathrm{E}\left[\mathbf{h}^*\mathbf{\Phi}^*\mathbf{Q}^{(L)^*}\mathbf{Q}^{(L)}\mathbf{\Phi h}\right] + \mathrm{E}\left[{\omega_1}^*\mathbf{Q}^{(L)^*}\mathbf{Q}^{(L)}\omega_1\right] \\
&\overset{b}{=} \mathrm{E}\left[\mathbf{h}^*\mathbf{\Phi}^*\mathbf{Q}^{(L)}\mathbf{\Phi h}\right] + \mathrm{E}\left[{\omega_1}^*\mathbf{Q}^{(L)}\omega_1\right] \\
&\overset{c}{=} \mathrm{E}\left[\mathrm{tr}\left\{\mathbf{h}^*\mathbf{\Phi}^*\mathbf{Q}^{(L)}\mathbf{\Phi h}\right\}\right] + \mathrm{E}\left[\mathrm{tr}\left\{[{\omega_1}^*\mathbf{Q}^{(L)}\omega_1\right\}\right] \\
&\overset{d}{=} \mathrm{E}\left[\mathrm{tr}\left\{\mathbf{Q}^{(L)}\mathbf{\Phi h h}^*\mathbf{\Phi}^*\right\}\right] + \mathrm{E}\left[\mathrm{tr}\left\{\mathbf{Q}^{(L)}\omega_1{\omega_1}^*\right\}\right] \\
&\overset{e}{=} \mathrm{tr}\left\{\mathbf{Q}^{(L)}\mathbf{\Phi}\mathrm{E}\left[\mathbf{h h}^*\right]\mathbf{\Phi}^*\right\} + \mathrm{tr}\left\{\mathbf{Q}^{(L)}\mathrm{E}\left[\omega_1{\omega_1}^*\right]\right\} \\
&\overset{f}{=} N_o\sigma^2_{\tilde{\mathrm{R}}^{(\mathrm{L})}} + (N_o - L)\sigma^2_{\mathrm{n}} \ ,
\end{aligned} \tag{C.1}$$

$$\begin{aligned}
&\mathrm{E}\left[(\mathbf{h} - \tilde{\mathbf{h}}^{(L)})^*(\mathbf{h} - \tilde{\mathbf{h}}^{(L)})\right] \\
&= \mathrm{E}\left[(\mathbf{h} - \Psi^{(L)}\mathbf{y_{T,1}})^*(\mathbf{h} - \Psi^{(L)}\mathbf{y_{T,1}})\right] \\
&\overset{a}{=} \mathrm{E}\left[\mathbf{h}^*(\mathbf{I} - \Psi^{(L)})^*(\mathbf{I} - \Psi^{(L)})\mathbf{h}\right] + \mathrm{E}\left[\omega_1^*\Psi^{(L)^*}\Psi^{(L)}\omega_1\right] \\
&\overset{c}{=} \mathrm{E}\left[\mathrm{tr}\left\{\mathbf{h}^*(\mathbf{I} - \Psi^{(L)})^*(\mathbf{I} - \Psi^{(L)})\mathbf{h}\right\}\right] + \mathrm{E}\left[\mathrm{tr}\left\{\omega_1^*\Psi^{(L)^*}\Psi^{(L)}\omega_1\right\}\right] \\
&\overset{d}{=} \mathrm{E}\left[\mathrm{tr}\left\{(\mathbf{I} - \Psi^{(L)})^*(\mathbf{I} - \Psi^{(L)})\mathbf{h h}^*\right\}\right] + \mathrm{E}\left[\mathrm{tr}\left\{\Psi^{(L)^*}\Psi^{(L)}\omega_1\omega_1^*\right\}\right] \\
&\overset{e}{=} \mathrm{tr}\left\{(\mathbf{I} - \Psi^{(L)})^*(\mathbf{I} - \Psi^{(L)})\mathrm{E}\left[\mathbf{h h}^*\right]\right\} + \mathrm{tr}\left\{\Psi^{(L)^*}\Psi^{(L)}\mathrm{E}\left[\omega_1\omega_1^*\right]\right\} \\
&= \sigma^2_{\tilde{\mathrm{R}}^{(\mathrm{L})}} + \frac{L}{N_o^2}\mathbf{I}\mathrm{tr}\left\{\mathrm{E}\left[\omega_1\omega_1^*\right]\right\} \\
&= \sigma^2_{\tilde{\mathrm{R}}^{(\mathrm{L})}} + \frac{L}{N_o}\sigma^2_{\mathrm{n}} \ ,
\end{aligned} \tag{C.2}$$

and

$$
\begin{aligned}
&\mathrm{E}\left[(\mathbf{y}_2-\tilde{\mathbf{y}}_1)^*(\mathbf{y}_2-\tilde{\mathbf{y}}_1)\right] \\
&= \mathrm{E}\left[(\mathbf{Q}^{(L)}\mathbf{\Phi}\mathbf{h}+\mathbf{P}^{(L)}\boldsymbol{\omega}_1+\boldsymbol{\omega}_2)^*(\mathbf{Q}^{(L)}\mathbf{\Phi}\mathbf{h}+\mathbf{P}^{(L)}\boldsymbol{\omega}_1+\boldsymbol{\omega}_2)\right] \\
&\overset{a}{=} \mathrm{E}\left[\mathbf{h}^*\mathbf{\Phi}^*\mathbf{Q}^{(L)^*}\mathbf{Q}^{(L)}\mathbf{\Phi}\mathbf{h}\right]+\mathrm{E}\left[\boldsymbol{\omega}_1{}^*\mathbf{P}^{(L)^*}\mathbf{P}^{(L)}\boldsymbol{\omega}_1\right]+\mathrm{E}\left[\boldsymbol{\omega}_2{}^*\boldsymbol{\omega}_2\right] \\
&\overset{b}{=} \mathrm{E}\left[\mathbf{h}^*\mathbf{\Phi}^*\mathbf{Q}^{(L)}\mathbf{\Phi}\mathbf{h}\right]+\mathrm{E}\left[\boldsymbol{\omega}_1{}^*\mathbf{P}^{(L)}\boldsymbol{\omega}_1\right]+N_o\sigma_{\mathrm{n}}^2 \\
&\overset{c}{=} \mathrm{E}\left[\mathrm{tr}\left\{\mathbf{h}^*\mathbf{\Phi}^*\mathbf{Q}^{(L)}\mathbf{\Phi}\mathbf{h}\right\}\right]+\mathrm{E}\left[\mathrm{tr}\left\{\boldsymbol{\omega}_1{}^*\mathbf{P}^{(L)}\boldsymbol{\omega}_1\right\}\right]+N_o\sigma_{\mathrm{n}}^2 \\
&\overset{d}{=} \mathrm{E}\left[\mathrm{tr}\left\{\mathbf{Q}^{(L)}\mathbf{\Phi}\mathbf{h}\mathbf{h}^*\mathbf{\Phi}^*\right\}\right]+\mathrm{E}\left[\mathrm{tr}\left\{\mathbf{P}^{(L)}\boldsymbol{\omega}_1\boldsymbol{\omega}_1{}^*\right\}\right]+N_o\sigma_{\mathrm{n}}^2 \\
&\overset{e}{=} \mathrm{tr}\left\{\mathbf{Q}^{(L)}\mathbf{\Phi}\mathrm{E}\left[\mathbf{h}\mathbf{h}^*\right]\mathbf{\Phi}^*\right\}+\mathrm{tr}\left\{\mathbf{P}^{(L)}\mathrm{E}\left[\boldsymbol{\omega}_1\boldsymbol{\omega}_1{}^*\right]\right\}+N_o\sigma_{\mathrm{n}}^2 \\
&\overset{f}{=} N_o\sigma_{\overline{\mathrm{R}}^{(\mathrm{L})}}^2+(N_o+L)\sigma_{\mathrm{n}}^2
\end{aligned}
\tag{C.3}
$$

respectively, where

$$
\mathbf{Q}^{(L)}=\mathbf{I}-\mathbf{P}^{(L)}=\mathbf{I}-\mathbf{\Phi}^{(L)}(\mathbf{\Phi}^{(L)^*}\mathbf{\Phi}^{(L)})^{-1}\mathbf{\Phi}^{(L)^*}\,.
$$

In (C.1), (C.2), and (C.3), (a) follows from being independent variables of symbols and noise, (b) is because of the features of the projection matrices, i.e., $\mathbf{P}^{(L)^*}=\mathbf{P}^{(L)}$, $\mathbf{Q}^{(L)^*}=\mathbf{Q}^{(L)}$, $\mathbf{P}^{(L)^2}=\mathbf{P}^{(L)}$, and $\mathbf{Q}^{(L)^2}=\mathbf{Q}^{(L)}$, (c) is because of having 1×1 matrix in the argument of expected value operation (i.e., 1×1 matrix is equal to its own trace), (d) is due to the circulant property of the trace operation, (e) is due to the linear operations of expected value and trace, and (f) follows that the rank of $\mathbf{P}^{(L)}$ is L, the rank of $\mathbf{Q}^{(L)}$ is N_o-L, and $\mathbf{\Phi}$ has orthogonal column vectors, i.e., training sequence has perfect auto-correlation and cross-correlation properties.

ABOUT THE AUTHOR

Alphan Şahin received his B.S. degrees in Electrical Engineering and Telecommunication Engineering from Istanbul Technical University in June 2005 and June 2006 respectively. He received his M.S degree in Electrical Engineering from Istanbul Technical University in June 2008. From June 2006 to December 2009, he was with the Scientific and Technological Research Council of Turkey - National Research Institute of Electronics and Cryptology (TUBITAK-UEKAE) and he involved with the several projects related to the hardware design as a researcher. He is expecting his Ph.D. degree in December 2013 from University of South Florida in Electrical Engineering. His research interests are related to advanced signal processing techniques on communications systems. Current research interests are waveform design, multicarrier systems, and time-frequency analysis.